NASA TN D-582

TECHNICAL NOTE

D-582

PERFORMANCE CHARTS FOR MULTISTAGE ROCKET BOOSTERS

By John S. MacKay and Richard J. Weber

Lewis Research Center
Cleveland, Ohio

NATIONAL AERONAUTICS AND SPACE ADMINISTRATION

WASHINGTON

January 1961

NATIONAL AERONAUTICS AND SPACE ADMINISTRATION

TECHNICAL NOTE D-582

PERFORMANCE CHARTS FOR MULTISTAGE ROCKET BOOSTERS

By John S. MacKay and Richard J. Weber

SUMMARY

Charts relating the stage propellant fractions are given for two- and three-stage rockets launching payloads into nominal low-altitude circular orbits about the earth. A simple method is described for extending these data to higher orbit or escape missions. Various combinations of stages using RP - liquid-oxygen and hydrogen - liquid-oxygen propellants are considered. However, the results can be generalized with little error to any other propellant combination.

Examples are given to illustrate how the charts may be applied to the preliminary design of booster vehicles.

INTRODUCTION

Optimal design of a multistage rocket vehicle for any particular mission involves a complicated compromise among such factors as mass-ratio requirements, structural weights, guidance, operational characteristics, and so forth. Of these, estimation of the needed stage mass ratios (or, equivalently, the stage propellant fractions) is ordinarily the primary design requirement, inasmuch as the propellant comprises the greatest volume and weight of most chemically fueled vehicles.

Simplified methods for such estimations are usually inadequate for vehicles operating in the vicinity of the earth because of the need to account properly for aerodynamic effects, gravity losses, varying thrust-weight ratios, and so forth. On the other hand, accurate calculations for each particular case are quite time-consuming because of the nonlinearity of the differential equations of motion and the necessity for selecting an efficient flight path. To fill the need for a rapid, yet reasonably accurate technique, this report presents a group of charts for estimating the stage propellant fractions of booster vehicles that carry out orbital or escape missions. The accuracy of these generalized charts is adequate for preliminary design purposes.

The two missions for which results are specifically given are flights under continuous power from the earth's surface into circular orbits at

altitudes of 75 and 150 nautical miles. As discussed later, optimum trajectories for more energetic missions usually pass through approximately orbital conditions. Since the required superorbital maneuvers can be closely approximated by impulsive-thrust equations, the presented data can be easily extended to cover any higher orbit or escape missions.

The propellants considered are RP - liquid-oxygen and hydrogen - liquid-oxygen, used both throughout all stages and in various combinations. A simple method is given for modifying the data for propellants having other specific impulses. A range of thrust-weight ratios is covered that is typical of liquid-fueled rockets.

E-799

SYMBOLS

A	area, sq ft
a	$\tan \psi_0$
b	$d(\tan \psi)/dt$, sec^{-1}
C_D	drag coefficient, based on cross-sectional area
D	drag, lb
F	thrust, lb
g	local acceleration due to gravity, ft/sec^2
g_c	weight-to-mass conversion factor, 32.174 lb/slug
h	altitude, ft
I	specific impulse, lb-sec/lb
P	ambient pressure, lb/sq ft
R	radius, ft
r_i	stage weight ratio, $(W_0/W_f)_i$
t	time measured from ignition of i^{th} stage, sec
V	velocity, ft/sec
ΔV	characteristic velocity increment, ft/sec
W	weight, lb

$w_{p,i}$ propellant fraction, $(W_p/W_0)_i$

x x-coordinate of fig. 16, ft

y y-coordinate of fig. 16, ft

α angle of attack, deg (see fig. 1)

β angle between velocity vector and a normal to the radius vector (see fig. 1), rad (unless otherwise specified)

θ angle between instantaneous and initial radius vector, (see fig. 1), rad (unless otherwise specified)

μ gravitational constant, 1.4077×10^{16}, ft^3/sec^2

ρ ambient density, slugs/cu ft

ψ angle between thrust vector and x-axis, deg (see fig. 16)

Subscripts:

cs cross-sectional

d evaluated at design altitude (h_d = 20,000 ft)

E evaluated at surface of earth

e evaluated at rocket nozzle exit

en engine

f evaluated at burnout of i^{th} stage

i stage number

L payload

p propellant

s structure

t total

0 evaluated at stage ignition (t = 0)

Superscripts:

$\bar{}$ evaluated at $t = W_0/\dot{W}$

' relates to impulsive velocity addition

" conditions after change of specific impulse

ANALYSIS

Assumptions

The following assumptions were made in the calculations. Unless otherwise specified, the discussion relates to three-stage vehicles.

Flight path. - As shown in figure 1, the vehicle takes off and climbs vertically for 10 seconds and is then turned for 10 seconds at a constant angle of attack α. A gravity turn ($\alpha = 0$) is followed thereafter until burnout of the first stage. During the next two stages the engine-thrust vector is directed according to the relation

$$\tan \psi = a - bt$$

This "linear-tangent" form of steering has been shown to result in approximately minimum propellant consumption for satellite launchings (refs. 1, 2, and 3).

Drag coefficient. - A constant value of 0.4, which is typical of current vehicles, was used for the drag coefficient during first-stage flight. For the class of large boosters considered this corresponds to a value for $C_D A_{cs}/W_0$ of 1.6×10^{-4} square foot per pound and gives a conservative estimate of the drag losses. No drag was included during flight of the upper stages, which operate only at high altitudes where drag is negligible. (A typical first-stage burnout altitude for the cases considered is 180,000 ft.)

Engine performance. - The propellant flow rate was maintained constant during each stage of flight. The specific impulse at sea level was taken as 267 seconds for RP-oxygen propellant and 358 seconds for hydrogen-oxygen; the assumed variation with altitude is given in figure 2. These values are typical of engines having chamber pressures on the order of 800 to 1000 pounds per square inch and nozzle expansion ratios of 15 to 20.

Equations of Motion

The first-stage trajectories were calculated using a fourth-order Runge-Kutta numerical integration. Rotation of the earth was ignored so that the data, as presented, apply to polar orbits. However, a method

for including earth rotation will be presented. The upper-stage linear-tangent paths were calculated with an approximate closed-form solution that is considerably faster than numerical integration.

Details of the equations are given in appendix A.

Procedure

A number of first-stage trajectories were studied to obtain burnout conditions (altitude, velocity, path angle) as functions of $w_{p,1}$, $F/W_{0,1}$, and α. These are shown in figures 3 and 4 for RP-oxygen and hydrogen-oxygen, respectively. Using values obtained from figures 3 and 4 as initial conditions, the upper-stage trajectories were calculated for various combinations of F/W_0 in each stage and w_p in stages one and two. Automatic iteration was used on the steering parameters a and b and on third-stage burning time in order to achieve a circular orbit at 75 or 150 nautical miles. The output of each calculation is the required third-stage propellant fraction $w_{p,3}$. Each point was repeated for several values of α to find the minimum $w_{p,3}$. The calculations were performed on an IBM 704 digital computer and took approximately 25 hours of machine time.

Conditions along a representative flight path are shown in figure 5.

RESULTS AND DISCUSSION

Propellant-Loading Charts

The minimum values of $w_{p,3}$ have been plotted as functions of $w_{p,1}$ and $w_{p,2}$. These basic data are given in figures 6 to 10 as indicated in the following table:

Figure	Fuel in stage -			Orbit altitude, naut. miles
	One	Two	Three	
6	RP	RP	RP	150
7	H_2	H_2	H_2	150
8	RP	RP	H_2	150
9	RP	H_2	H_2	150
10	RP	H_2	H_2	75

For each case, all combinations of the following initial thrust-weight ratios are presented:

Stage	F/W_0		
First	1.20	1.30	1.40
Second	1.00	1.25	1.50
Third	0.50	1.00	1.50

Each point on the propellant-loading charts represents a three-stage vehicle capable of achieving the specified orbit. In general, higher orbits or escape energy is desired, and a correction must be made in the propellant requirements. This is discussed in a later section. After making any necessary corrections, the determination of actual payload capabilities requires the incorporation of structural weights. Simplified examples of such calculations are given in appendix B to illustrate how the charts may be applied.

Thrust-weight ratio. - From the trajectory viewpoint high acceleration (thrust-weight ratio) is ordinarily thought to be desirable. This is because velocity is increased rapidly at low altitudes, and one saves the work required to lift propellants against gravity. However, the charts show that, for the 150-mile orbits, high acceleration tends to increase $w_{p,3}$ in some cases (e.g., fig. 6(c)). The explanation lies in the requirement of the present analysis for continuous acceleration until a circular orbit is established. High-acceleration vehicles tend to build up too much velocity at low altitudes. Therefore, a less efficient boost path must be utilized in order not to exceed orbital velocity at burnout of the third stage. This problem is diminished if low orbits are desired, since the high velocities at low altitudes are then usually advantageous. Thus, it is seen that high thrust-weight ratios are more beneficial in the case of the 75-mile orbit.

In any event, of course, no conclusions can be made about optimum thrust-weight ratios without including their effect on the weight of both the engines and the other thrust-sensitive structure.

Drag coefficient. - A first-stage drag coefficient of 0.4 has been used in the charts. In order to indicate the importance of this parameter, figure 11 shows the change in propellant consumption when the drag is taken as zero. It is seen that the results are quite insensitive to variations in the selected value.

Extension of the Charts

The charts as they are drawn apply to two specific missions, neither of which necessarily corresponds to the actual desired mission. This section describes how the charts may be applied to a much broader range of uses.

Except for very low orbit missions, flight paths incorporating a coast period are usually more efficient than those that continuously apply thrust. An example of this is shown in figure 12 for the 150-mile-orbit mission. The upper part of the figure reproduces the data from figure 8(c) for a $w_{p,2}$ of 0.70. The lower part of the figure presents the result of optimum trajectory calculations that employed coasting between the second and third stages. It is seen that $w_{p,3}$ is improved by this procedure. (The crossover in the thrust-weight-ratio lines is also eliminated by including a coast period, for the reasons discussed in a previous section.) The benefits of coasting are noticeable even for this comparatively low altitude of 150 nautical miles. They become more substantial as the final altitude is increased.

Study of optimum trajectories that employ coast periods reveals the fortunate fact that the flight path prior to the start of coasting is usually nearly horizontal. Also, the velocity at that point is super-orbital. This means that very nearly optimum results would be obtained by achieving a circular orbit and continuing to accelerate until the proper velocity is reached, after which the vehicle coasts to its final altitude where it is injected into orbit. Calculations also show that the propellant consumption during both acceleration out of the low circular orbit and injection into a higher energy orbit can be obtained with negligible error by the simple impulsive-thrust equations. The significance of these two facts is that, if data are given for achieving one initial low circular orbit, the total propellant consumption for achieving any higher orbit is readily derived.

The choice of the best altitude for the initial circular orbit still remains. To show the effect of this selection, results are shown in figure 13(a) for a final circular orbit altitude of 500 nautical miles. In the range shown, the lower the initial altitude, the better. This is a result of the greater gravity loss when carrying fuel to high altitudes, the somewhat higher efficiency of departure from low orbits, and the interaction of altitude and thrust as previously discussed.

Because of the presence of the earth's atmosphere, it is not practical to lower the altitude indefinitely. Reducing the altitude requires the vehicle to achieve greater velocities while still in the denser portions of the atmosphere. The attendant greater drag penalties would eventually limit performance. Even more serious are the effects of aerodynamic loads and heating. These structural factors lie outside the scope of this analysis, but it must be recognized that they exist and serve to limit the orbit altitude to some minimum value. For preliminary design purposes it is felt that the two orbit altitudes considered herein provide a range of trajectories which includes those of practical interest. (In addition, 150-mile orbits are high enough to be of some interest in themselves, such as for refueling or assembly purposes, yet are low enough to make continuous acceleration a reasonable practice if coasting should be undesirable, e.g., to avoid prolonged zero-g conditions or engine restarts.)

The previous discussion has emphasized orbital missions, but the same argument applies to escape missions. The only difference is that enough velocity is imparted when leaving the initial orbit to achieve escape energy. Of course, no injection into orbit at the end of coasting is required in this case. Figure 13(b) shows that the orbital-departure technique is a good approximation to the optimum direct-escape trajectory. (However, this good agreement is true only for the case of escape at approximately zero flight-path angle. Nonhorizontal escape may be occasionally desired, but specific trajectory calculations must then be made for that case.)

The charts discussed thus far have used three stages to gain the initial orbit. Another method of operation is to employ only two stages to reach the orbital condition. Two-stage data may be obtained from the charts (figs. 6 to 10) by extrapolating the curves down to the horizontal axis. For convenience, however, a chart specifically for this case has been prepared in figure 14 (which corresponds to an extrapolation of fig. 10).

Procedure for extension. - As previously explained, the propellant consumption for more energetic missions is obtained by assuming the additional velocity beyond the initial orbit is gained impulsively. It has been found that for top-stage thrust-weight ratios of 0.5 or higher, there is small error in this assumption.

Figure 15 shows the propellant fraction w_p' required for various characteristic velocity increments ΔV added beyond the nominal orbital condition. This is merely a plot of the simple impulsive relation

$$\Delta V = -Ig_c \ln(1 - w_p') \tag{1}$$

Also indicated in the figure are the required values of total ΔV for various typical missions starting from initial circular orbits of 75 and 150 nautical miles. Minimum-energy (Hohmann) transfer ellipses are assumed for the orbital missions.

The values of w_p' in figure 15 are based on the weight of the stage when in the initial orbit. If this stage (the third stage, say) has been already used in reaching the low orbit, its weight in the orbit is different from its initial, fully loaded weight. The total stage propellant fraction after allowing for this difference is given by

$$(w_{p,3})_t = w_{p,3} + w_p'(1 - w_{p,3}) \tag{2a}$$

where $w_{p,3}$ (which is the propellant used prior to the impulsive maneuver) is taken from the appropriate chart and $(w_{p,3})_t$ is based on the initial third-stage gross weight.

Earth rotation. - Rotation of the earth was ignored when integrating the equations of motion. The presented data may therefore be interpreted as applying to launch azimuths of 0° or 180°. For nonpolar launchings, calculations showed that the charts may be applied with little error, if the additional ΔV used in figure 15 or equation (1) is reduced by the component of the earth's surface velocity lying in the launch direction. For example, an eastward firing from Cape Canaveral, Florida (latitude, 28.5°) yields a benefit of 1350 feet per second.

If no transfer to a higher orbit is to be made, the corrected $w_{p,3}$ is given by

$$(w_{p,3})_t \cong w_{p,3} - w'_p(1 - w_{p,3}) \tag{2b}$$

where w'_p corresponds to a ΔV equal to the surface velocity.

Other propellants. - It was purely for the sake of convenience that the two propellant combinations considered herein have been designated RP - liquid oxygen and hydrogen - liquid oxygen. As far as the trajectory calculations are concerned, only the value of specific impulse is of direct interest. The charts may therefore be applied to any propellant combination yielding specific impulses identical to those of figure 2.

In addition, it is possible to modify the presented data to obtain results for propellants having other values of specific impulse. This method depends on the fact that the stage ΔV is approximately independent of the specific impulse of that stage. (This is not exactly true because varying the specific impulse changes the variation of stage gross weight during flight.) Assuming ΔV_i does not change and applying equation (1) give the following expression for the new $w_{p,i}$ after changes in the specific impulse of the stage (no change being made in the thrust-weight ratio):

$$w''_{p,i} = \left[1 - (1 - w_p)^{I/I''}\right]_i \tag{3}$$

When using I_1 in this equation, it should be an average value, which may be taken as one-third the sea-level value plus two-thirds the vacuum value. This gives 292 and 393 seconds for the RP and hydrogen data, respectively.

Equation (3) is generally accurate to within 3 percent if I_1 is varied, 2 percent if I_2 is varied, and 1 percent if I_3 is varied. When several or all values of I are changed, the combined error seldom exceeds the error for variations of I_1.

Comparison with Mathematical Optimization

Mathematical techniques for optimizing multistage vehicles have been discussed by many authors (e.g., refs. 4, 5, and 6). In general, these methods seek to find the stage propellant fractions that extremize a selected criterion (e.g., gross weight, empty weight, cost, etc.) subject to various constraints, such as burnout velocity, stage specific impulse, and so forth.

For booster vehicles, the effects of drag, gravity, and turning losses are usually included by either increasing the required burnout velocity or by depreciating the specific impulse of each stage in appropriate amounts. Since, however, these losses are themselves functions of the propellant fractions, such corrections are mathematically invalid. Hence, it is not surprising that the numerical results of these techniques are usually in gross error. (A typical conclusion is that there should be no first stage, since the upper stages are more efficient.)

The deficiencies of the earlier techniques have been remedied in a more recent paper (ref. 7). In this paper the trajectory and the vehicle are analyzed concurrently to find a true system optimum. However, the method requires first calculating the flight performance of a series of representative vehicles. Unless the optimum vehicle is fairly accurately known in advance, the amount of trajectory data that must be calculated is quite substantial - equivalent to generating one of the charts of the present report.

If desired, the charts may be used in conjunction with the method of reference 7. However, direct calculations of the form shown in appendix B are probably simpler to carry out.

CONCLUDING REMARKS

Propellant-loading charts have been presented for multistage rockets launching payloads into nominal low-altitude circular orbits. Optimum trajectories for more energetic missions usually pass approximately through such orbital conditions. Since the required superorbital maneuvers can be closely approximated by impulsive equations, the presented data for the nominal mission can be easily extended to cover any higher orbit or escape missions. Various combinations of stages using RP - liquid-oxygen and hydrogen - liquid-oxygen propellants are considered. However, the results can be generalized with little error to any other propellant combination.

The data are based on trajectories that minimize propellant consumption. For real vehicles some of these optimum trajectories may engender excessive aerodynamic heating or structural loads. However, the

presented data are useful for preliminary design purposes even if the trajectories must be modified for some purpose. By incorporating structural weight assumptions, the charts permit the approximate optimum design of multistage chemical booster vehicles for either orbital or escape missions. The final optimization may be based on any desired criterion (e.g., maximum payload, minimum cost, etc.); that is, the presented data do not restrict the optimization procedure.

Lewis Research Center
National Aeronautics and Space Administration
Cleveland, Ohio, September 28, 1960

APPENDIX A

METHOD OF CALCULATION

Machine Trajectory Calculations

First stage. - The first-stage trajectories were computed by numerical integration of the equations of motion using the Runge-Kutta technique.

In solving the equations of motion, the following simplifications were made:

(a) Nonrotating earth

(b) Constant drag coefficient ($C_D = 0.4$)

(c) No lift.

The two-dimensional equations in polar coordinates then are

$$\dot{V} = \frac{g_c(F \cos \alpha - D)}{W} - g \sin \beta$$

$$V\dot{\beta} = \left(\frac{V^2}{R_E + h} - g\right) \cos \beta + \frac{g_c F \sin \alpha}{W}$$

$$\dot{h} = V \sin \beta$$

$$\dot{\theta} = \frac{V \cos \beta}{R_E + h}$$

where

$$F = I\dot{W}$$

$$D = \frac{\rho V^2 C_D A_{cs}}{2}$$

$$g = \frac{\mu}{(R_E + h)^2}$$

The specific-impulse variations shown in figure 2 are given by

$$I = I_d + \frac{A_e}{\dot{W}} (P_d - P)$$

in which the design altitude is taken as 20,000 feet and no nozzle separation is assumed.

During the integration process, the required values of P and ρ were found from a series of curve fits for the ICAO standard atmosphere.

Each case was computed using a step size of 10 seconds and continued until the fuel consumption was such that $w_{p,1} = 0.95$.

Second and third stages. - Neglecting drag and using $\tan \psi = a - bt$, the equations of motion, written for the rectangular coordinate system of figure 16, are

$$\left.\begin{aligned} \ddot{x} + \frac{\mu x}{R^3} &= \frac{g_c F}{W\sqrt{(a - bt)^2 + 1}} = f_x \\ \ddot{y} + \frac{\mu y}{R^3} &= \frac{g_c F(a - bt)}{W\sqrt{(a - bt)^2 + 1}} = f_y \end{aligned}\right\} \tag{A1}$$

Assuming that the magnitude of R does not change during one stage of powered flight, equations (A1) become

$$\left.\begin{aligned} \ddot{x} + \frac{\mu x}{R_0^3} &= f_x \\ \ddot{y} + \frac{\mu y}{R_0^3} &= f_y \end{aligned}\right\} \tag{A2}$$

where R_0 is the radius at the beginning of powered flight of the stage under consideration.

By using the method of variation of parameters, equations (A2) can be solved in the form

$$\left.\begin{aligned} y_f &= (y_0 + S) \cos \omega t_f + \left(\frac{\dot{y}_0}{\omega} + B\right) \sin \omega t_f \\ x_f &= (x_0 + U) \cos \omega t_f + \left(\frac{\dot{x}_0}{\omega} + E\right) \sin \omega t_f \end{aligned}\right\} \tag{A3}$$

where

$$\omega = \sqrt{\frac{\mu}{R_0^3}}$$

$$\left.\begin{aligned} S &= -\int_0^{t_f} \frac{f_y \sin \omega t \, dt}{\omega}; \qquad B = \int_0^{t_f} \frac{f_y \cos \omega t \, dt}{\omega} \\ U &= -\int_0^{t_f} \frac{f_x \sin \omega t \, dt}{\omega}; \qquad E = \int_0^{t_f} \frac{f_x \cos \omega t \, dt}{\omega} \end{aligned}\right\} \quad (A4)$$

Unfortunately, there is no apparent way to integrate equations (A4) without some additional assumption. Considering the magnitude of ω, it can be seen that it will never exceed $\sqrt{\mu/R_E^3} = 1.2398 \times 10^{-3}$ radian per second. Consequently, if $t < 200$ seconds, which is a typical burning time for one stage, ωt will always be less than 15°. For such small angles, it is reasonable to assume

$$\left.\begin{aligned} \sin \omega t &\cong \omega t \\ \cos \omega t &\cong 1.0 \end{aligned}\right\} \quad (A5)$$

Using equations (A5), equations (A4) can be integrated to give

$$S = V_e \left[\bar{t}(G - J \sin \bar{\psi}) + \frac{H}{b}\right]$$

$$B = \frac{V_e}{\omega} (J \sin \bar{\psi} - G)$$

$$U = -V_e \left(\bar{t} J \cos \bar{\psi} - \frac{G}{b}\right)$$

$$E = \frac{V_e}{\omega} J \cos \bar{\psi}$$

where

$$J = \ln \left\{ r \left[\frac{1 + \cos (\psi_f - \bar{\psi})}{1 + \cos (\psi_0 - \bar{\psi})} \frac{\cos \psi_0}{\cos \bar{\psi}} \right] \right\}$$

$$G = \ln \left[\frac{(\sin \psi_f + 1) \cos \psi_0}{(\sin \psi_0 + 1) \cos \bar{\psi}} \right]$$

$$H = \frac{\cos \psi_f - \cos \psi_0}{\cos \psi_0 \cos \psi_f}$$

By using the fact that the method of variation of parameters assumes

$$\dot{S} \cos \omega t + \dot{B} \sin \omega t = \dot{U} \cos \omega t + \dot{E} \sin \omega t = 0$$

the velocity components can be written as

$$\dot{y}_f = -\omega(y_0 + S) \sin \omega t_f + \omega \left(\frac{\dot{y}_0}{\omega} + B \right) \cos \omega t_f$$

$$\dot{x}_f = -\omega(x_0 + U) \sin \omega t_f + \omega \left(\frac{\dot{x}_0}{\omega} + E \right) \cos \omega t_f$$

Because of the assumptions made in equations (A5), the error of this approximate solution will increase with t_f. An indication of how this error behaves is shown by the upper curve in figure 17, where the percent error in r_3 is given as a function of $t_{f,2} + t_{f,3}$ for several vehicles. The scatter in the points shown is due to other differences in the vehicles chosen, but the essential feature to be noted is the rapid increase in error after $t_{f,2} + t_{f,3} = 400$ seconds (about 200 sec per stage). Consequently, it was necessary to use a modified solution for stages in which $t_f > 200$. This modification consists of adding another term to the truncated series given in equation (A5). Thus,

$$\left.\begin{aligned} \sin \omega t &\cong \omega t - \frac{(\omega t)^3}{3!} \\ \cos \omega t &\cong 1 - \frac{(\omega t)^2}{2!} \end{aligned}\right\} \qquad \text{(A6)}$$

After substitution of equations (A6) into equations (A4), subsequent integration gives

$$S = V_e \left\{ \bar{t} J \left(\frac{\omega^2 \bar{t}^2}{6} - 1 \right) \sin \bar{\psi} + \left[\bar{t} \left(1 + \frac{\omega^2}{4b^2} \right) + \frac{\omega^2}{6} \left(\frac{\tan \bar{\psi}}{b^3} - \bar{t}^3 \right) \right] G \right.$$
$$+ \left[\frac{1}{b} \left(\frac{\omega^2 \bar{t}^2}{2} - 1 \right) + \frac{\omega^2}{6b^3} (\tan^2 \bar{\psi} - 1) + \frac{\omega^2 \bar{t} \tan \bar{\psi}}{2b^2} \right] H$$
$$\left. - \frac{\omega^2}{4b^2} \left(\bar{t} + \frac{2 \tan \bar{\psi}}{3b} \right) K + \frac{\omega^2 L}{6b^3} \right\}$$

$$B = V_e \left\{ \frac{\sin \bar{\psi}}{\omega} \left(1 - \frac{\omega^2 \bar{t}^2}{2} \right) J + \left[\left(\frac{\omega^2 \bar{t}^2}{2} - 1 \right) - \frac{\omega^2}{4b^2} \right] \frac{G}{\omega} - \frac{\omega}{b} \left(\bar{t} + \frac{\tan \bar{\psi}}{2b} \right) H + \frac{\omega K}{4b^2} \right\}$$

$$U = V_e \left\{ \bar{t} \cos \bar{\psi} \left(\frac{\omega^2 \bar{t}^2}{6} - 1 \right) J + \left[\frac{1}{b} \left(\frac{\omega^2 \bar{t}^2}{2} - 1 \right) + \frac{\omega^2}{6b^3} (2 \tan^2 \bar{\psi} - 1) + \frac{\omega^2 \bar{t} \tan \bar{\psi}}{2b^2} \right] G - \frac{\omega^2}{2b^2} \left(\bar{t} + 2 \frac{\tan \bar{\psi}}{3b} \right) H + \frac{\omega^2 K}{12b^3} \right\}$$

$$E = V_e \left\{ \frac{\cos \bar{\psi}}{\omega} \left(1 - \frac{\omega^2 \bar{t}^2}{2} \right) J - \frac{\omega}{b} \left(\bar{t} + \frac{\tan \bar{\psi}}{2b} \right) G + \frac{\omega H}{2b^2} \right\}$$

where

$$K = \frac{\tan \psi_f \cos \psi_0 - \tan \psi_0 \cos \psi_f}{\cos \psi_0 \cos \psi_f}$$

$$L = \frac{\cos^3 \psi_0 - \cos^3 \psi_f}{(\cos \psi_0 \cos \psi_f)^3}$$

With these expressions for S, B, U, and E, the error is reduced to that shown by the lower curve in figure 17.

Calculation of Impulsive Transfer Velocities

Since energy and angular momentum are conserved along the path I-II (see fig. 18),

$$\frac{V_I^2}{2} - \frac{\mu}{R_I} = \frac{V_{II}^2}{2} - \frac{\mu}{R_{II}} \tag{A7}$$

$$R_I V_I = R_{II} V_{II} \tag{A8}$$

Using equations (A7) and (A8), V_I and V_{II} can be solved for as

$$V_I = V_{c,I} \sqrt{\frac{2\varphi}{\varphi + 1}}$$

$$V_{II} = V_{c,I} \sqrt{\frac{2}{\varphi(\varphi + 1)}}$$

where $V_{c,I} = \sqrt{\mu/R_I}$ (25,700 ft/sec for $R_I - R_E$ = 75 naut. miles, and 25,400 for $R_I - R_E$ = 150 naut. miles) and $\varphi = R_{II}/R_I$. Consequently, the required velocity increments (added at points I and II) are

$$\Delta V_I = V_I - V_{c,I} = V_{c,I}\left(\sqrt{\frac{2\varphi}{\varphi + 1}} - 1\right)$$

$$\Delta V_{II} = V_{c,II} - V_{II} = V_{c,I}\left[\frac{1}{\sqrt{\varphi}} - \sqrt{\frac{2}{\varphi(\varphi + 1)}}\right]$$

Note that as $\varphi \to \infty$, $\Delta V_I \to 0.414\ V_{c,I}$, which is the velocity increment required for escape.

APPENDIX B

ILLUSTRATIVE EXAMPLES

This section illustrates, by means of several highly simplified examples, how the charts may be applied to vehicle design.

Example 1. - Design a three-stage vehicle to place a 10,000-pound payload into a 1000-nautical-mile orbit. Use the thrust-weight ratios and the simple weight relations given in the following table:

	Stage		
	One	Two	Three
Fuel	RP	H_2	H_2
F/W_0	1.3	1.0	1.0
W_s/W_p	.08	.10	.11
W_{en}/F	.010	.012	.012

Assume that the vehicle is capable of withstanding the stresses incurred in trajectories that pass through orbital conditions at 75 nautical miles. As a start, pick $w_{p,1}$ and $w_{p,2}$ as 0.7 and 0.6, respectively. From figure 10(e), $w_{p,3} = 0.395$. From figure 15, the ΔV beyond orbit is 2850 feet per second. If we reduce this value by 1350 feet per second because of an eastward launch from Cape Canaveral, the corresponding propellant fraction from figure 15 (or eq. (1)) is 0.10. The total third-stage propellant fraction is given by equation (2) as

$$w_{p,3} = 0.395 + 0.10(1 - 0.395) = 0.456$$

Now sum the component weights of the third stage:

$$W_{0,3} = W_s + W_p + W_{en} + W_L$$

$$= W_0 w_p \left(1 + \frac{W_s}{W_p}\right) + W_0 \left(\frac{F}{W_0}\right)\left(\frac{W_{en}}{F}\right) + W_L$$

$$= \frac{W_L}{1 - w_p\left(1 + \frac{W_s}{W_p}\right) - \left(\frac{F}{W_0}\right)\left(\frac{W_{en}}{F}\right)}$$

$$W_{0,3} = \frac{10,000}{1 - 0.456(1.11) - (1.0)(0.012)} = 20,750 \text{ lb}$$

Similarly, for the second and first stages (where the payload of each stage is the stage above it),

$$W_{0,2} = \frac{20,750}{1 - 0.6(1.10) - (1.0)(0.012)} = 63,270 \text{ lb}$$

$$W_{0,1} = \frac{63,270}{1 - 0.7(1.08) - (1.3)(0.010)} = 273,900 \text{ lb}$$

The component weights can now be computed also.

To find the optimum staging, the previous calculations must be repeated for other $w_{p,1}$ and $w_{p,2}$ until $W_{0,1}$ (or any other selected parameter) is minimized. And finally, the entire optimization should be repeated for different values of thrust-weight ratios.

Example 2. - Find the third-stage propellant fraction to escape from the earth if no coasting is permitted below 150 nautical miles. Use the data of example 1, but take the specific impulse of the hydrogen - liquid-oxygen engines as 400 seconds.

From figure 9(e), $w_{p,3} = 0.430$. Applying equation (3), the corrected values are

$$w''_{p,3} = 1 - (1 - 0.430)^{425/400} = 0.450$$

$$w''_{p,2} = 1 - (1 - 0.60)^{425/400} = 0.622$$

Figure 15 shows that an additional ΔV of 10,500 feet per second is required for escape. Using equation (1),

$$10,500 = -(400)(32.174)\ln(1 - w'_p)$$

$$w'_p = 0.557$$

Finally, from equation (2a)

$$w_{p,3} = 0.450 + 0.557(1 - 0.450) = 0.756$$

A weight analysis can now be made, as in example 1.

Example 3. - Determine the optimum method of staging for a 24-hour satellite mission.

The mathematics for this problem is of the same nature as in the previous examples. The purpose of this paragraph is to point out the different methods of carrying out a mission that are possible using the charts. The following table lists how the various stages might be alternatively employed for this single mission:

CE-3 back

Application	Stage							
	I	II	III	IV	V	VI	VII	VIII
Boost into low orbit	1, 2	1, 2	1, 2	1, 2	1, 2, 3	1, 2, 3	1, 2, 3	1, 2, 3
Depart from low orbit	2	2	3	3	3	3	4	4
Inject into high oribt	2	3	3	4	3	4	4	5

No implication is intended that each of these eight alternatives is equally feasible. It is merely desired to emphasize the flexibility of the presented charts.

REFERENCES

1. Fried, Burton D.: On the Powered Flight Trajectory of an Earth Satellite. Jet Prop., vol. 27, no. 6, June 1957, pp. 641-643.

2. Okhotsimskii, D. E., and Eneev, T. M.: Some Variation Problems Connected with the Launching of Artificial Satellites of the Earth. Uspekhi Fizicheskikh Nauk, vol. 63, no. 1, Sept. 1957. (In Russian.) (See also Jour. Brit. Interplanetary Soc., vol. 16, no. 5, Jan.-Feb. 1958, pp. 263-294.)

3. Ross, Stanley: Composite Trajectories Yielding Maximum Coasting Apogee Velocity. ARS Jour., vol. 29, no. 11, Nov. 1959, pp. 843-848.

4. Vertregt, M.: A Method for Calculating the Mass Ratios of Step-Rockets. Jour. Brit. Interplanetary Soc., vol. 15, no. 2, Mar.-Apr. 1956, pp. 95-97.

5. Malina, Frank J., and Summerfield, Martin: The Problem of Escape from the Earth by Rocket. Jour. Aero. Sci., vol. 14, no. 8, Aug. 1947, pp. 471-480.

6. Builder, Carl H.: General Solution for Optimization of Staging of Multistaged Boost Vehicles. ARS Jour., vol. 29, no. 7, July 1959, pp. 497-499.

7. Chase, Ramon L.: Multistage Rocket Staging Optimization. Preprint 60-41, Am. Astron. Soc., 1960.

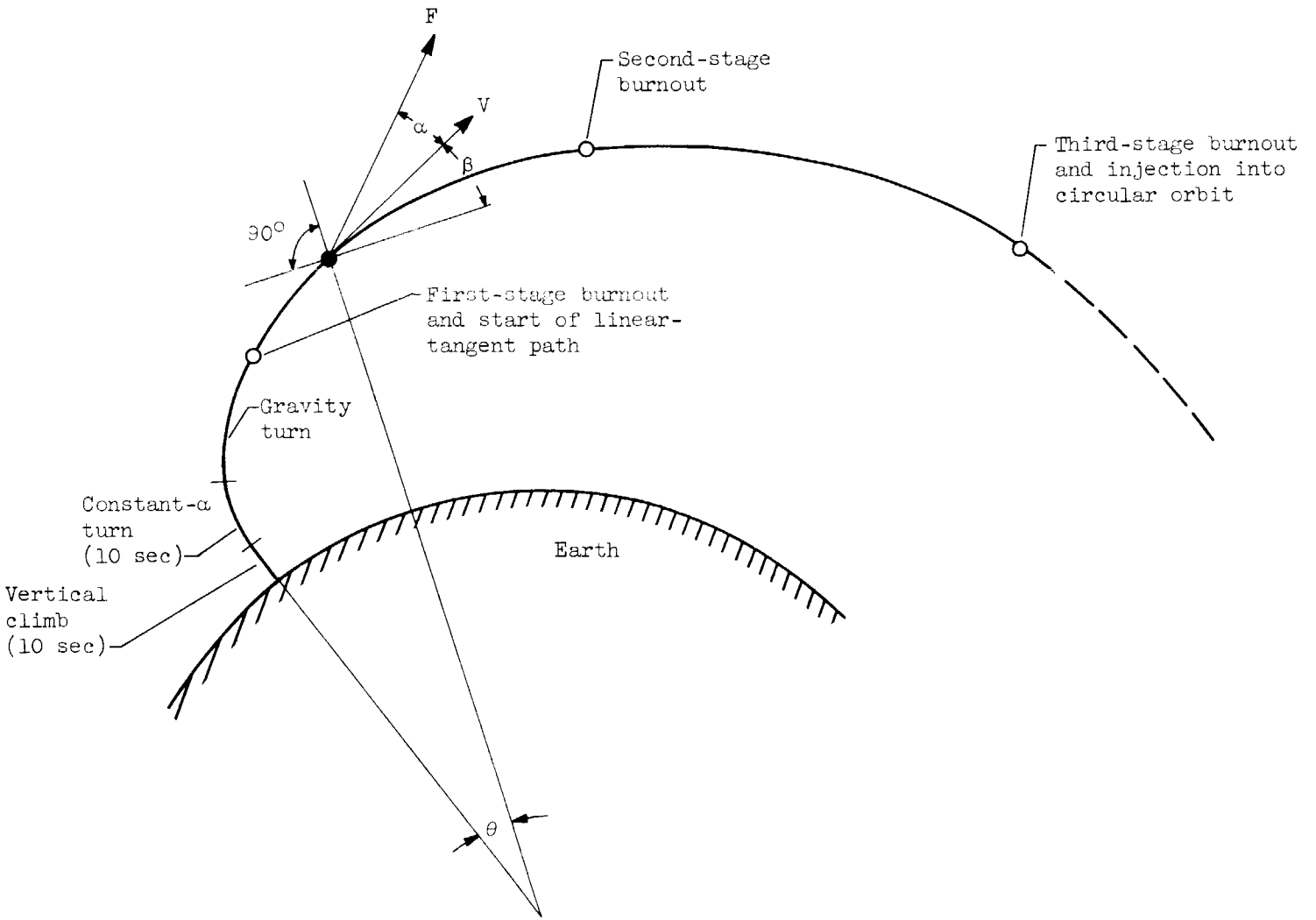

Figure 1. - Schematic diagram of flight path.

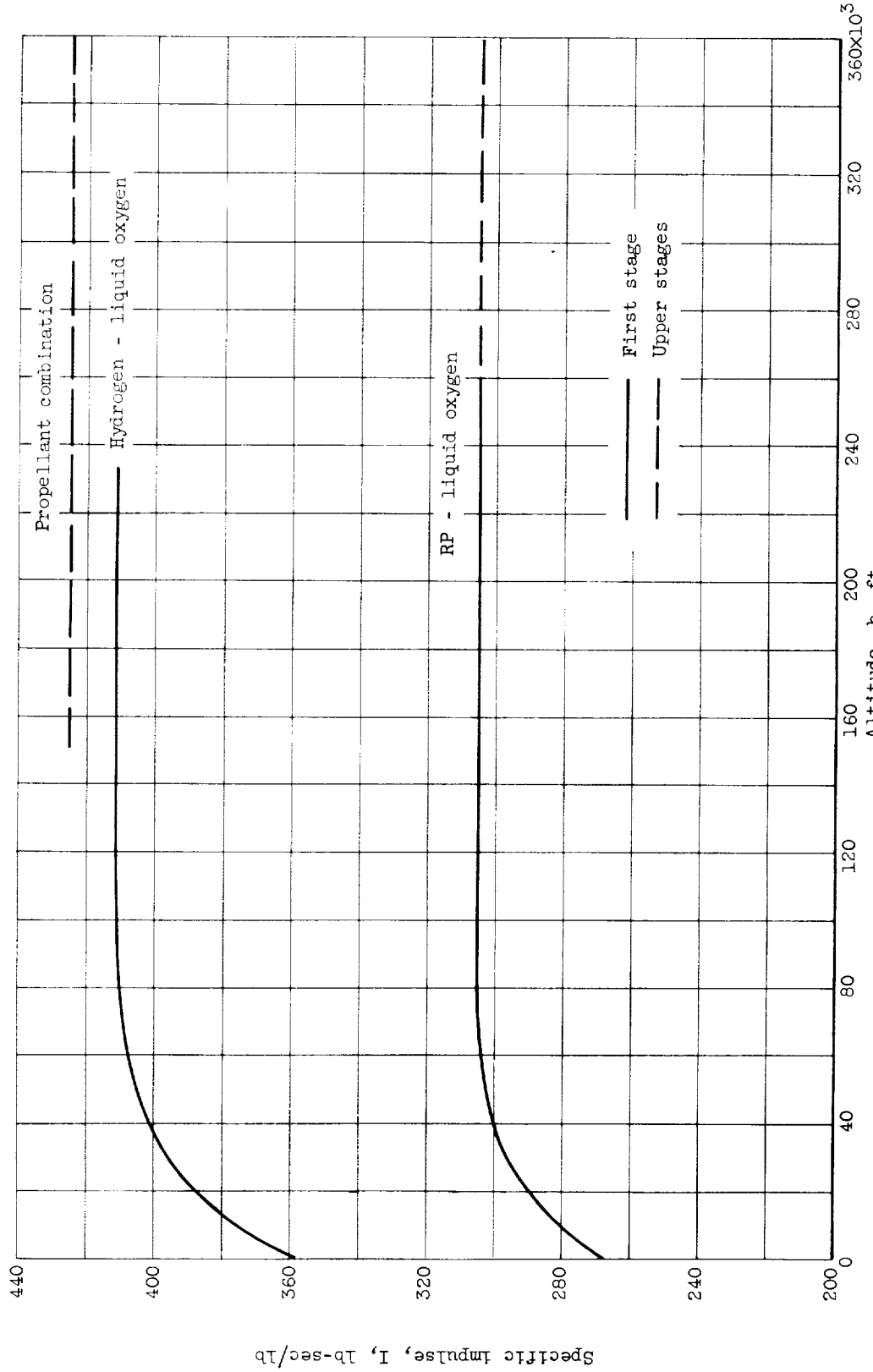

Figure 2. - Assumed variation of engine specific impulse with altitude.

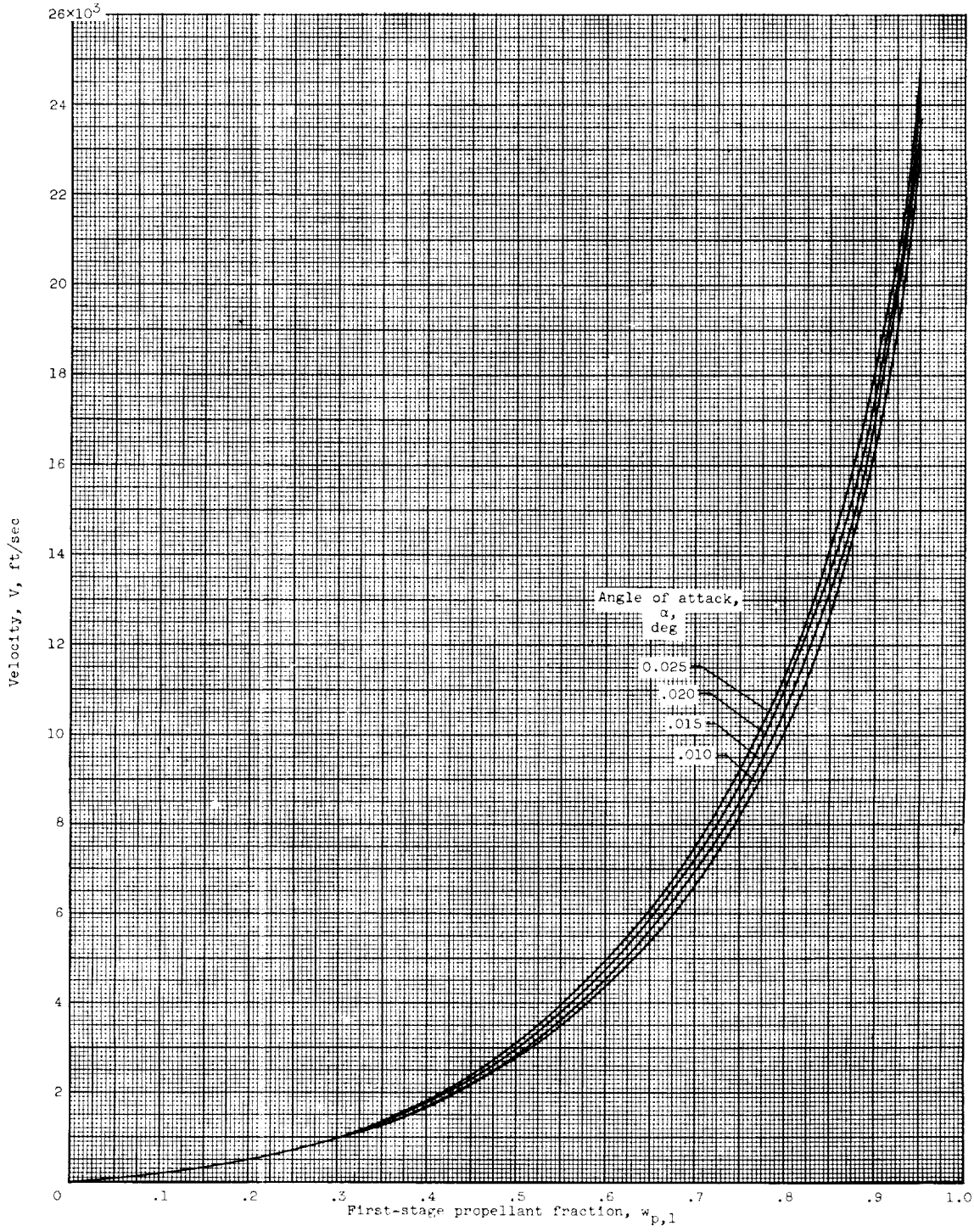

(a) Velocity; $F/W_{0,1} = 1.20$.

Figure 3. - First-stage burnout conditions. $I_1 = 292$ (av.); $C_D A_{cs}/W_{0,1} = 1.6 \times 10^{-4}$.

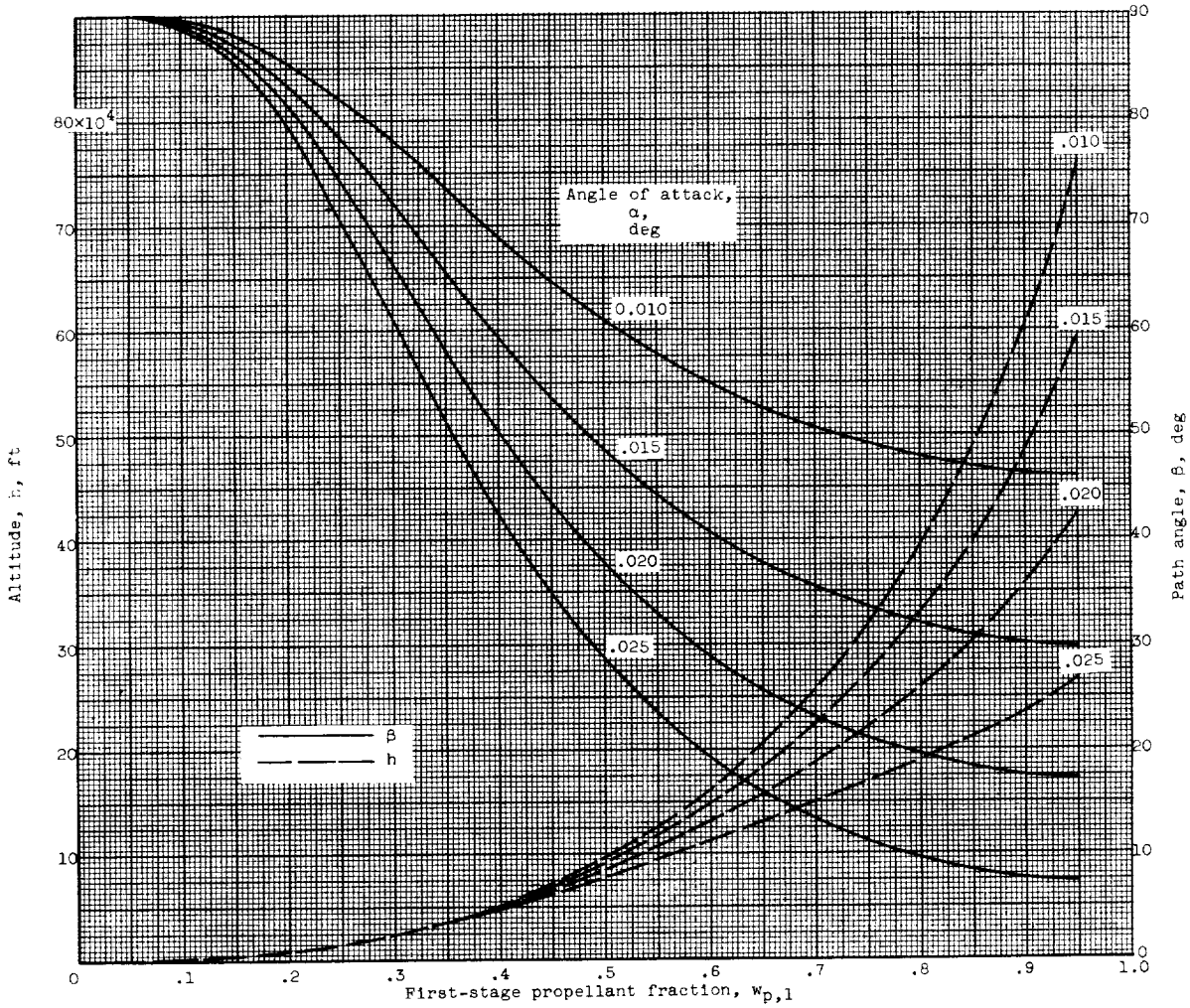

(b) Altitude and path angle; $F/W_{O,1} = 1.20$.

Figure 3. - Continued. First-stage burnout conditions. $I_1 = 292$ (av.); $C_D A_{cs}/W_{O,1} = 1.6 \times 10^{-4}$.

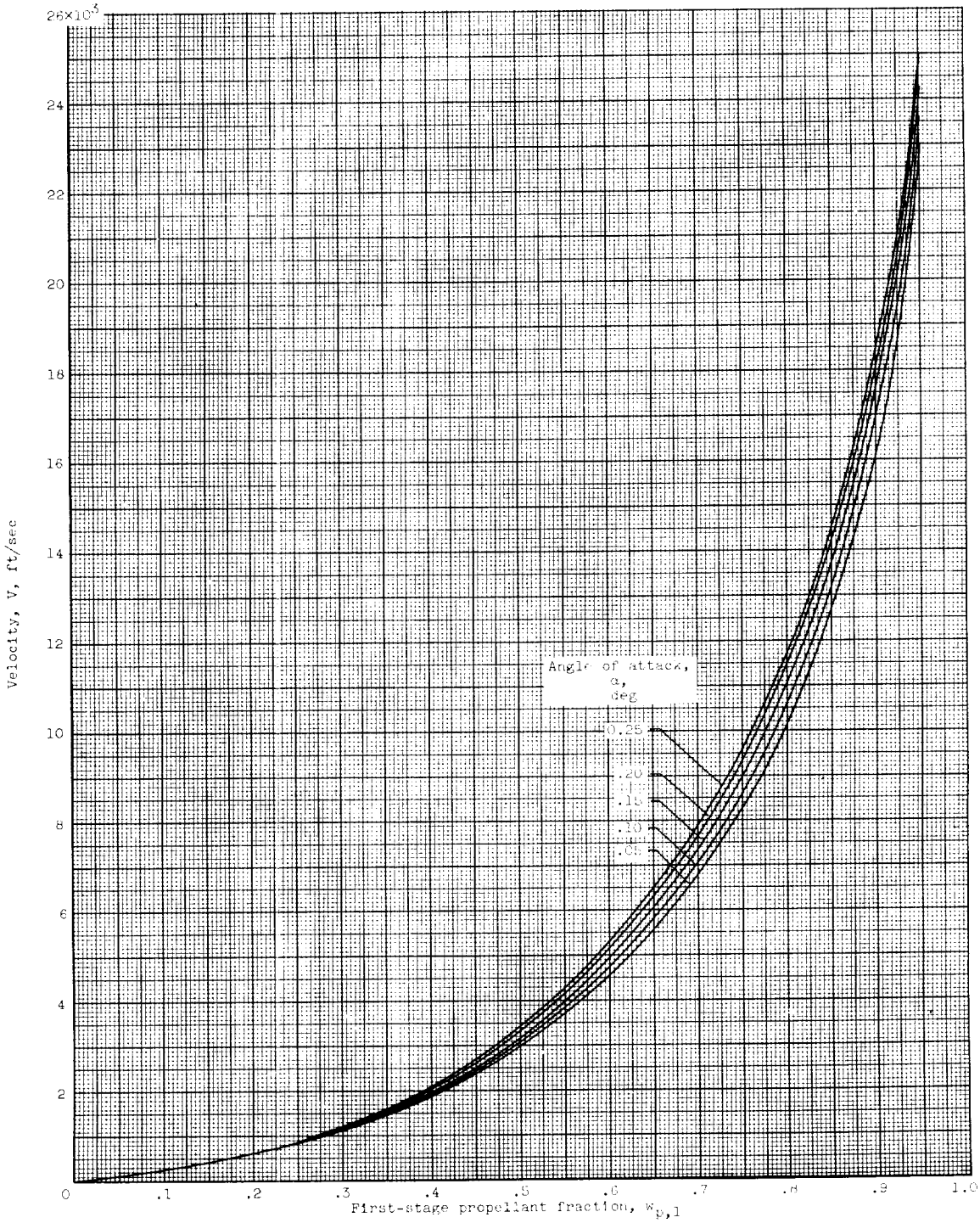

(c) Velocity; $F/W_{0,1} = 1.30$.

Figure 3. - Continued. First-stage burnout conditions. $I_1 = 292$ (av.); $C_D A_{cs}/W_{0,1} = 1.8 \times 10^{-4}$.

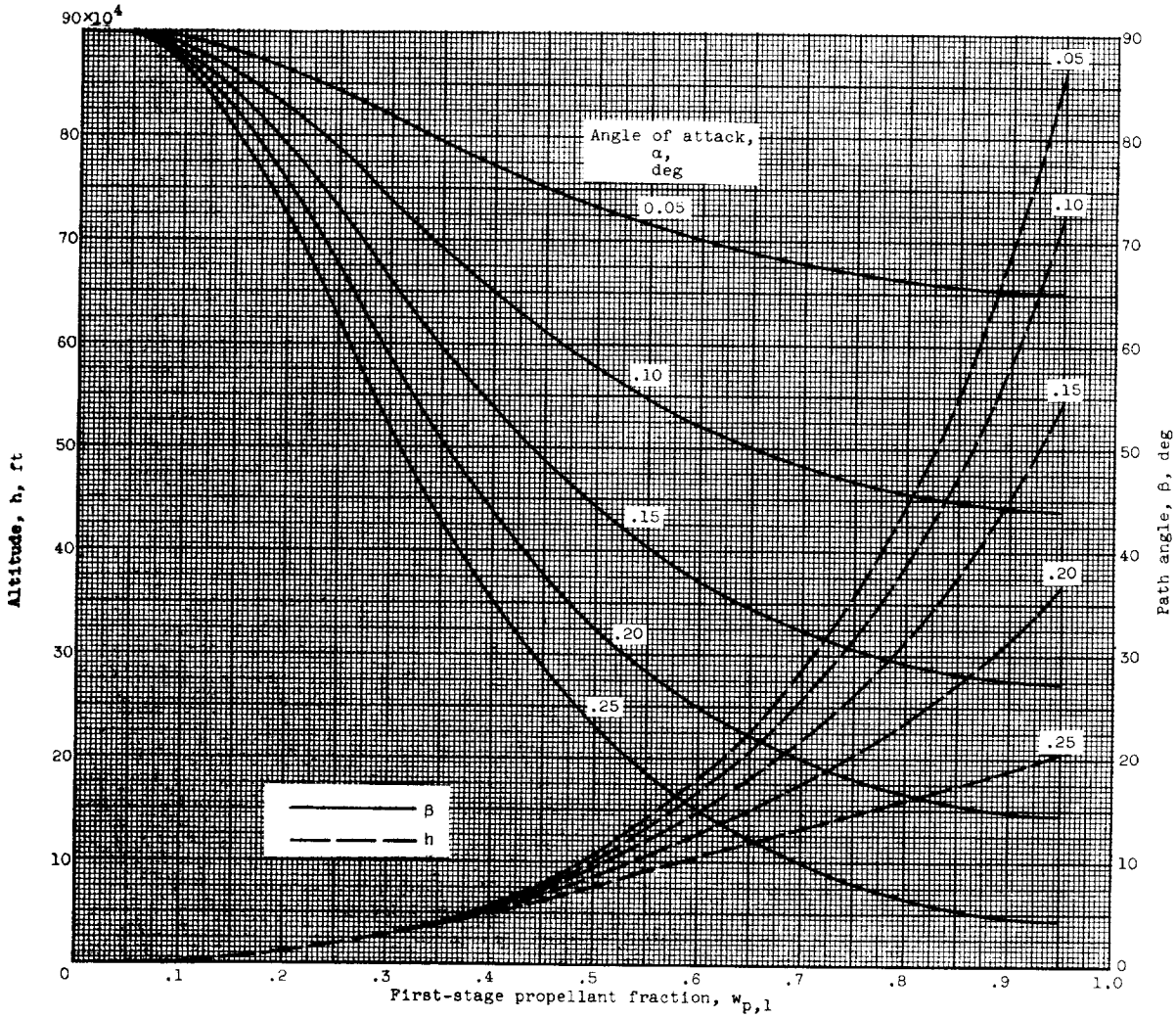

(d) Altitude and path angle; $F/W_{0,1} = 1.30$.

Figure 3. - Continued. First-stage burnout conditions. $I_1 = 292$ (av.); $C_D A_{cs}/W_{0,1} = 1.6 \times 10^{-4}$.

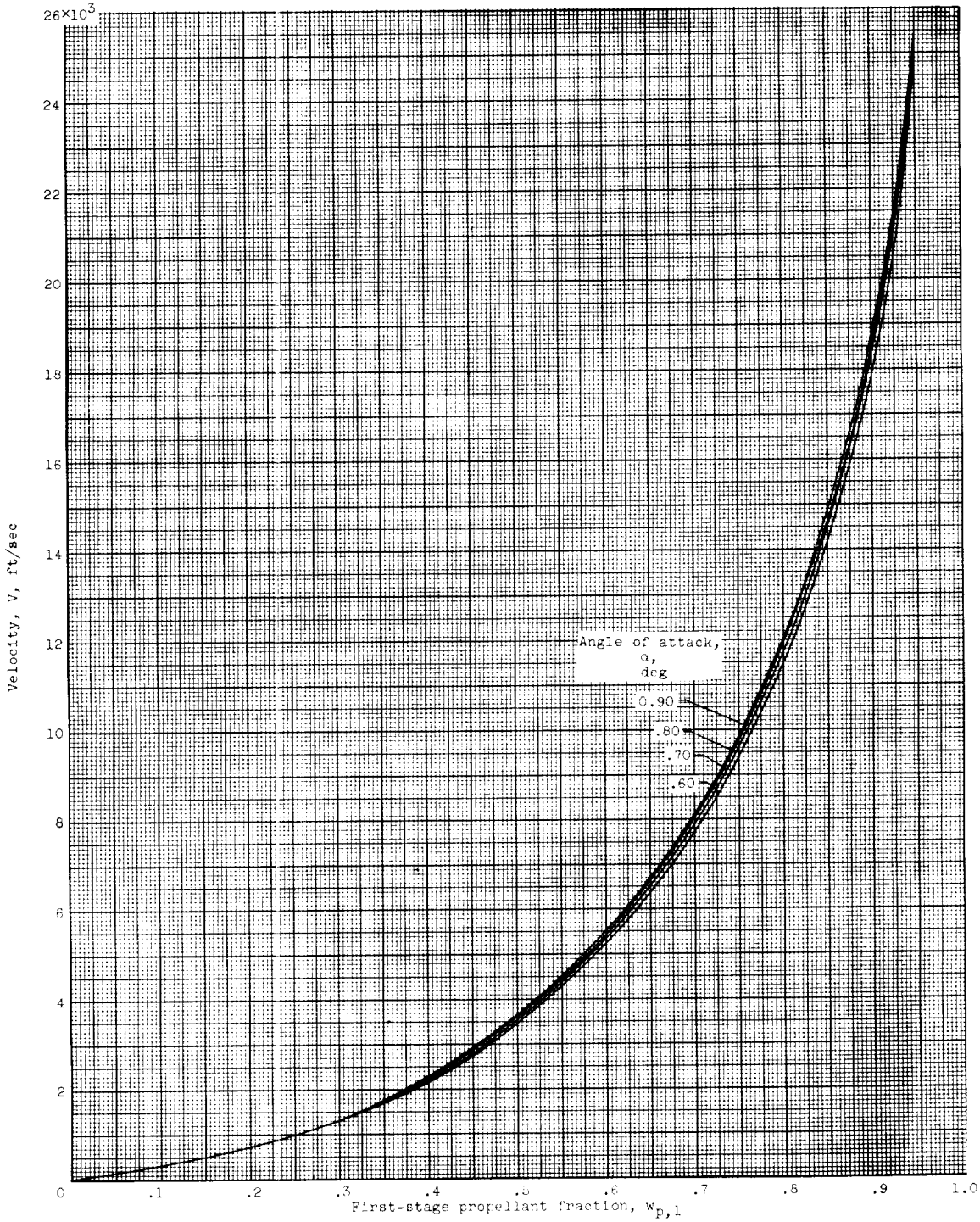

(e) Velocity; $F/W_{0,1} = 1.40$.

Figure 3. - Continued. First-stage burnout conditions. $I_i = 292$ (av.); $C_D A_{cs}/W_{0,1} = 1.6 \times 10^{-4}$.

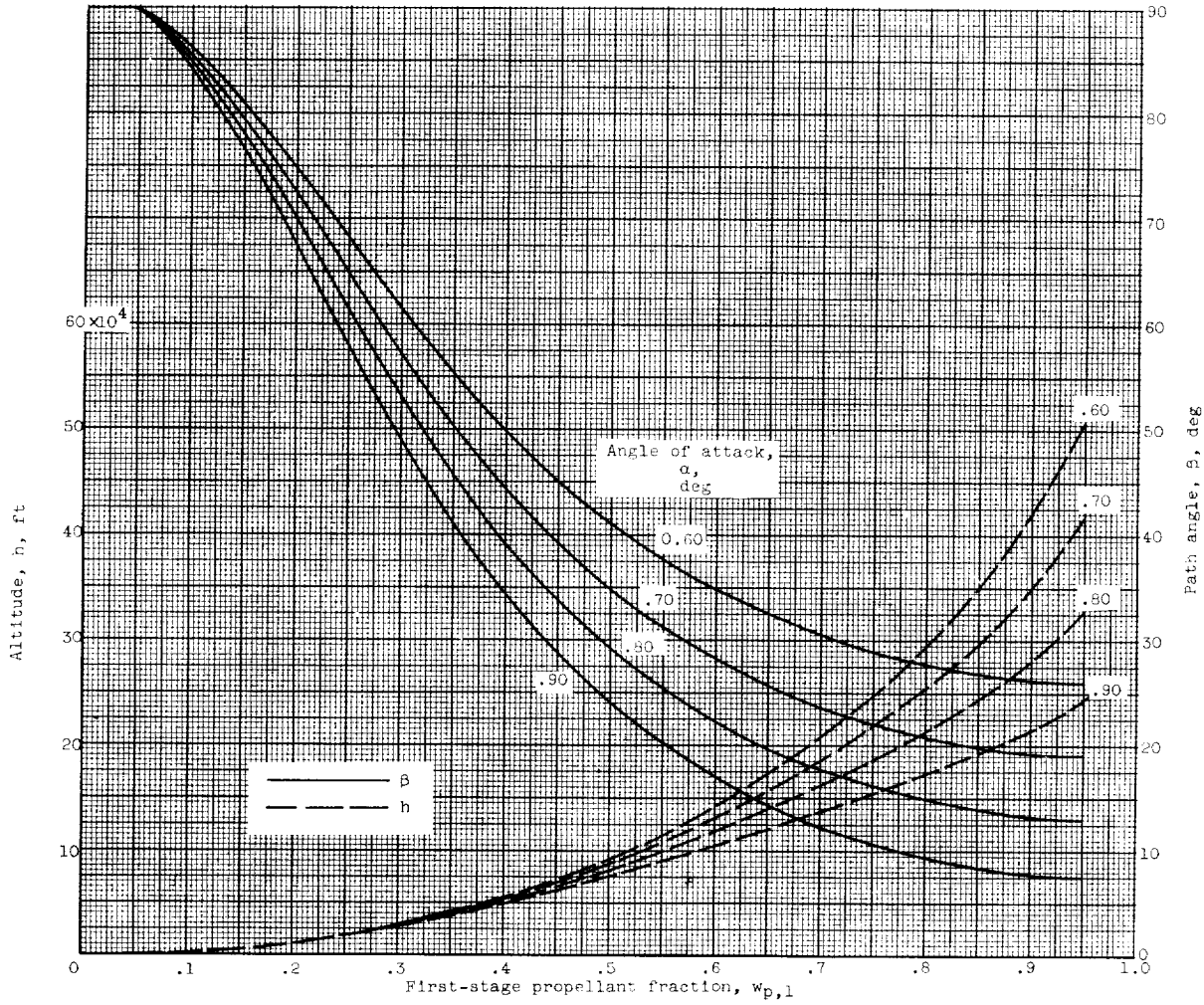

(f) Altitude and path angle; $F/W_{0,1} = 1.40$.

Figure 3. - Concluded. First-stage burnout conditions. $I_1 = 292$ (av.); $C_D A_{cs}/W_{0,1} = 1.6 \times 10^{-4}$.

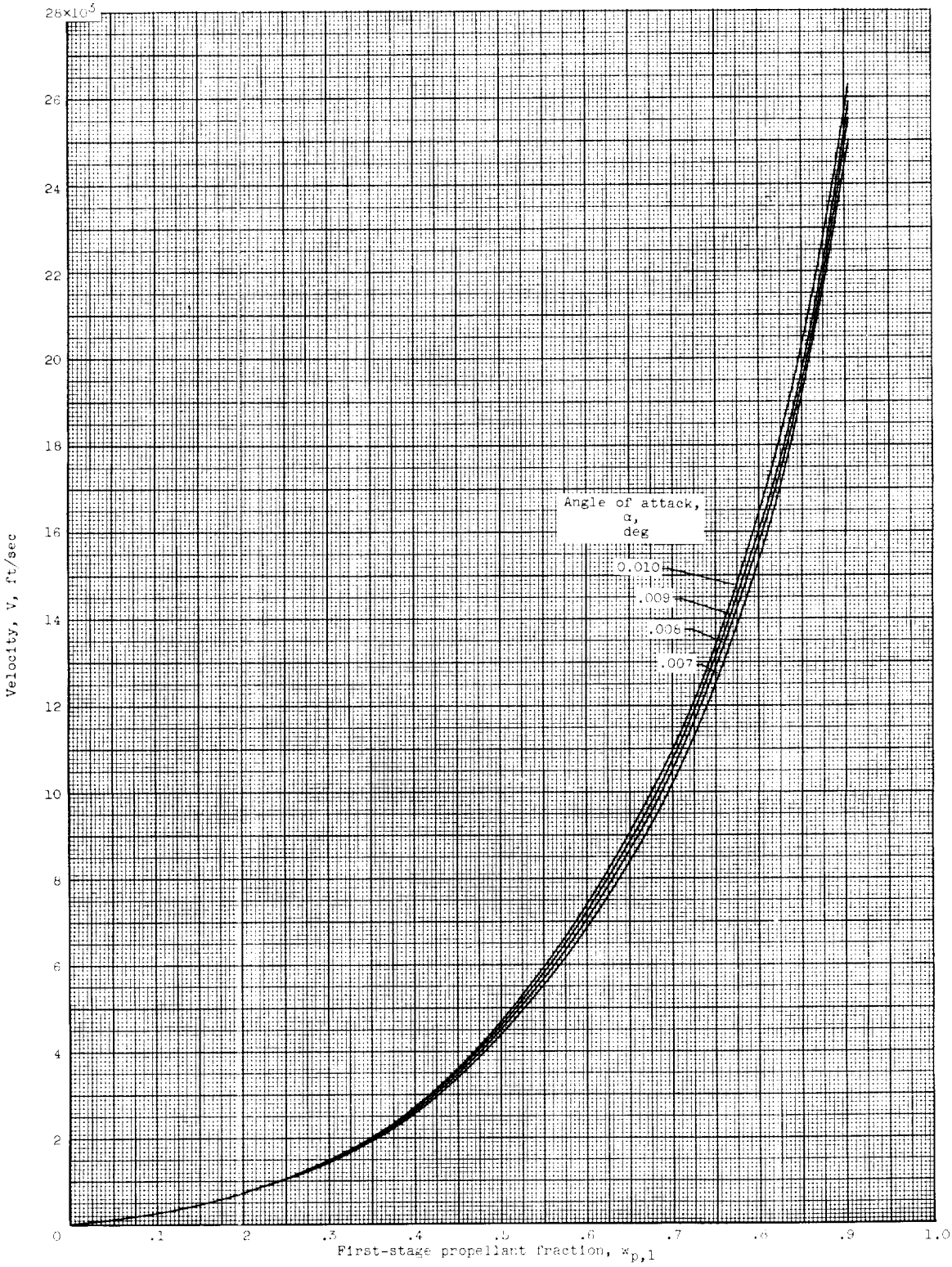

(a) Velocity; $F/W_{0,1} = 1.20$.

Figure 4. - First-stage burnout conditions. $I_1 = 288$ (av.); $C_D A_{cs}/W_{0,1} = 1.6 \times 10^{-4}$.

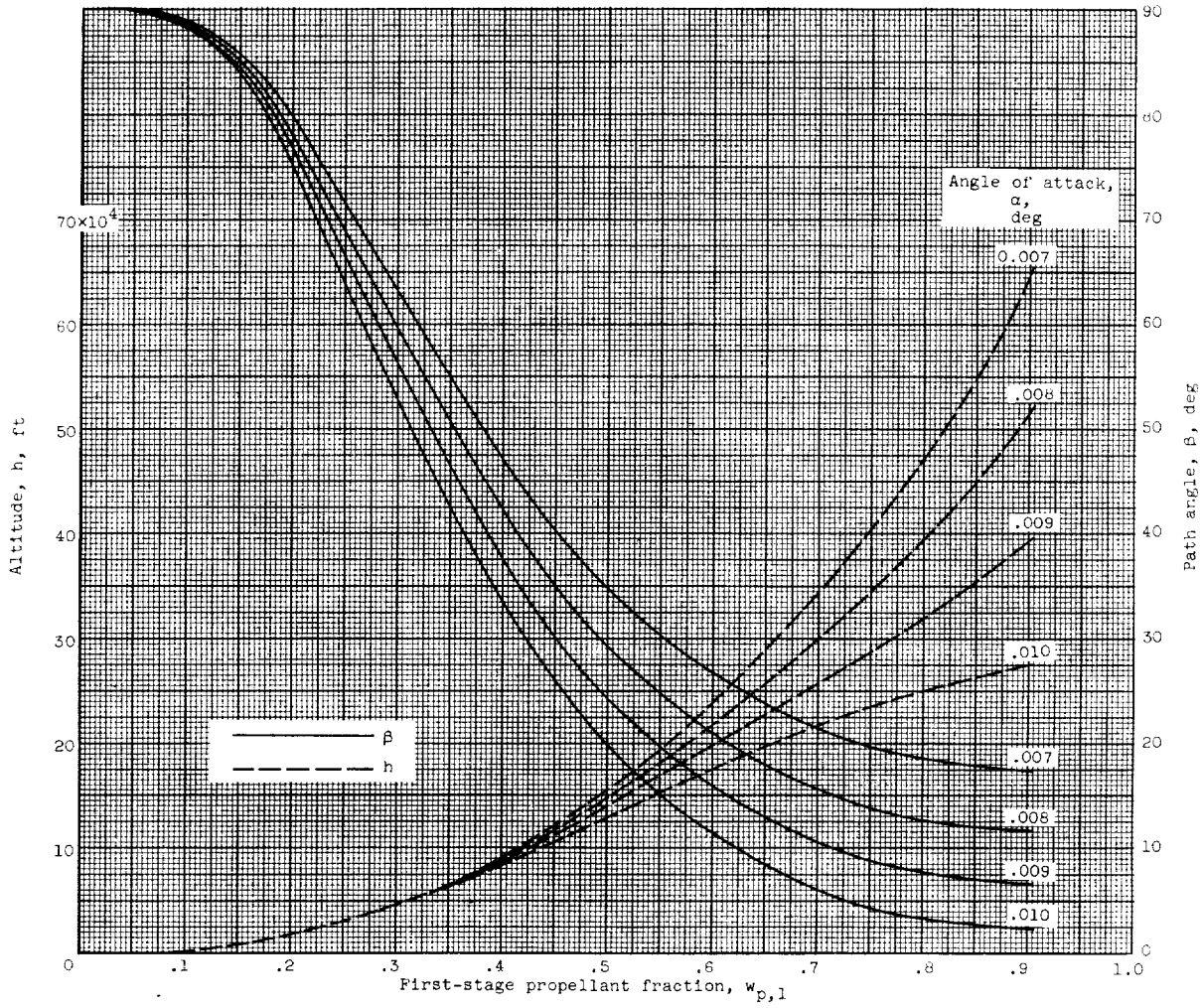

(b) Altitude and path angle; $F/W_{0,1} = 1.20$.

Figure 4. - Continued. First-stage burnout conditions. $I_1 = 393$ (av.); $C_D A_{cs}/W_{0,1} = 1.6 \times 10^{-4}$.

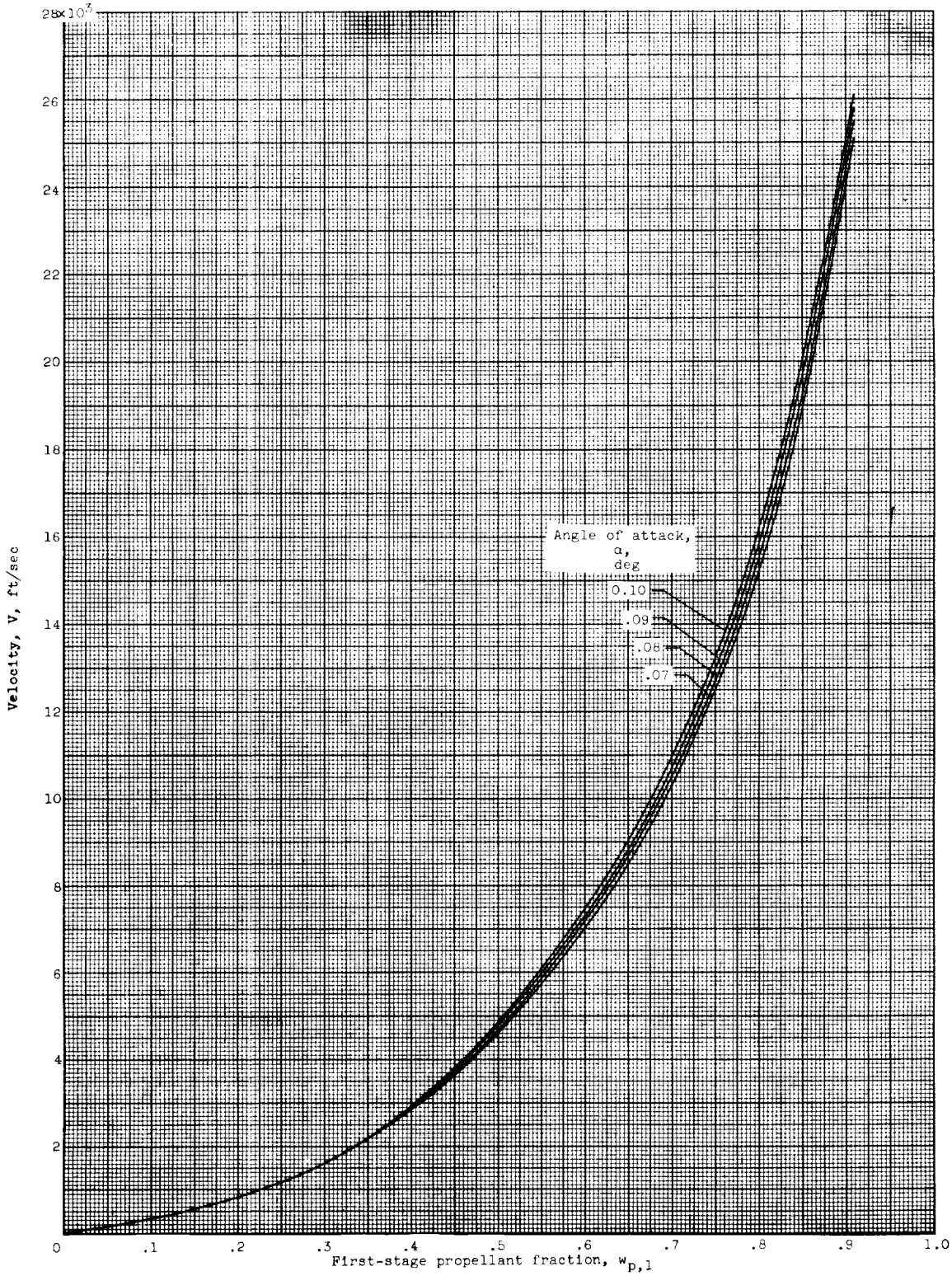

(c) Velocity; $F/W_{0,1} = 1.30$.

Figure 4. - Continued. First-stage burnout conditions. $I_1 = 393$ (av.); $C_D A_{cs}/W_{0,1} = 1.6 \times 10^{-4}$.

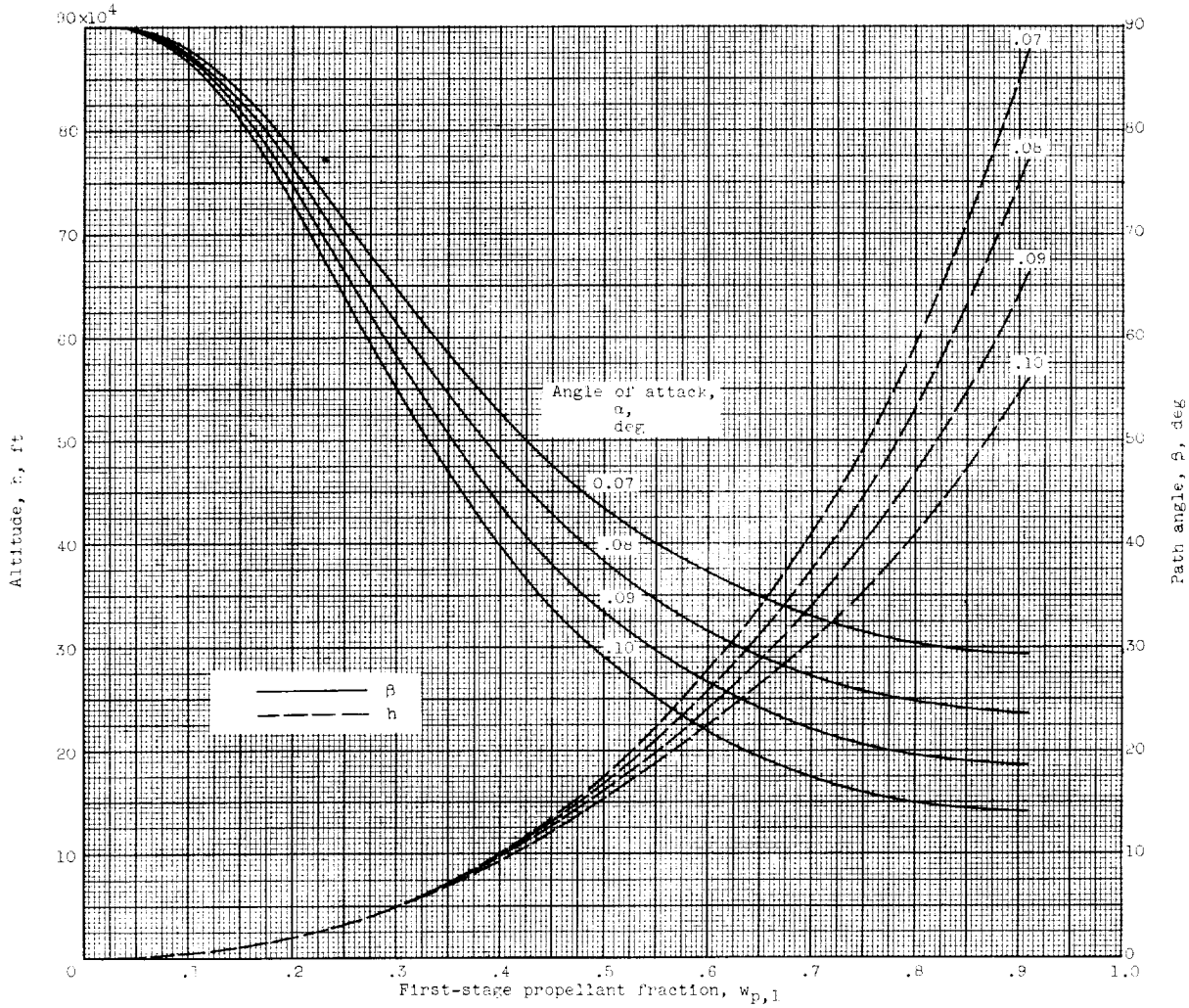

(d) Altitude and path angle; $F/W_{0,1} = 1.30$.

Figure 4. - Continued. First-stage burnout conditions. $I_1 = 393$ (av.); $C_D A_{cs}/W_{0,1} = 1.6 \times 10^{-4}$.

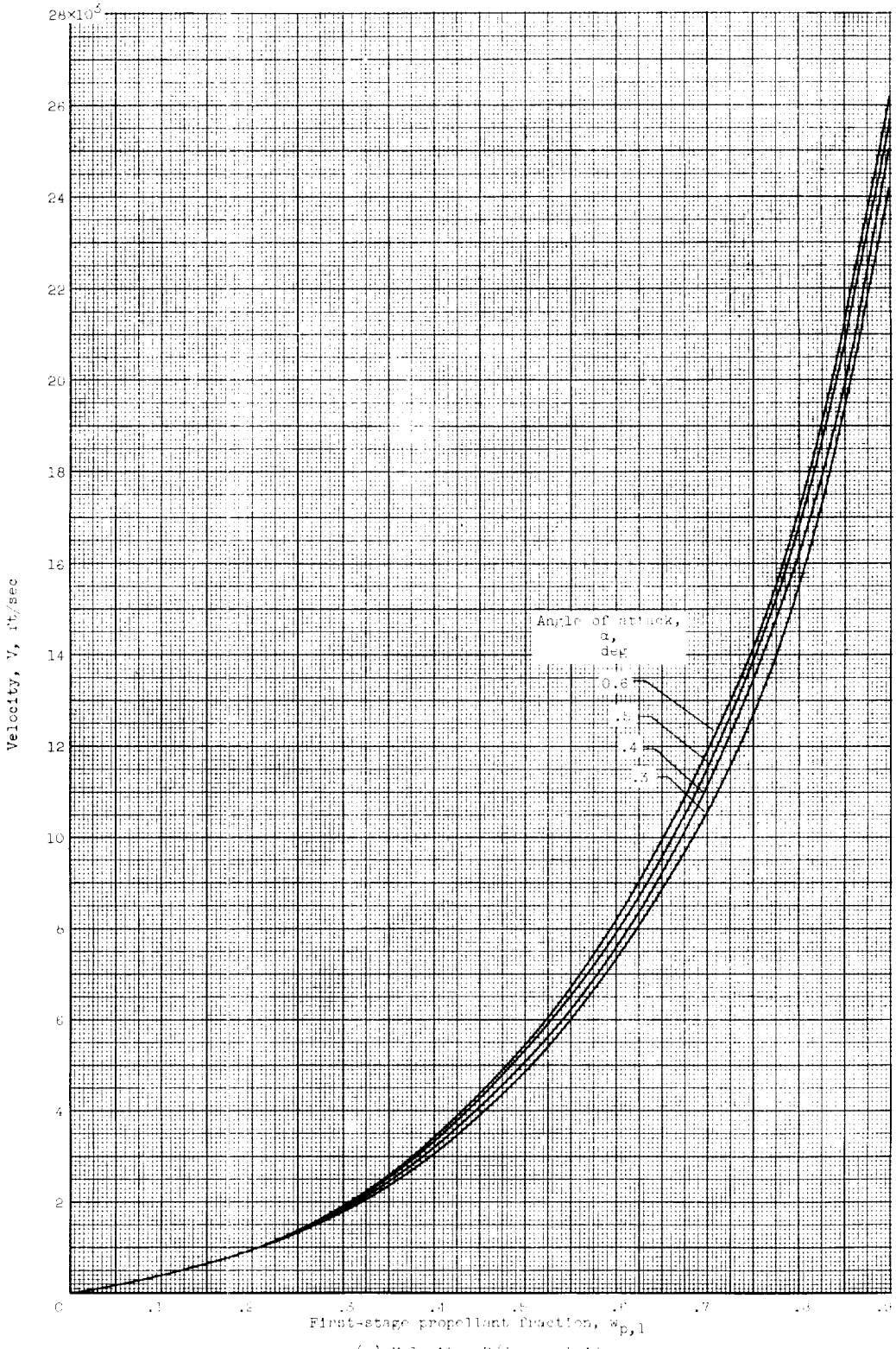

(e) Velocity; $F/W_{0,1} = 1.40$.

Figure 4. - Continued. First-stage burnout conditions. I_{sp} = 296 (av.); $C_D A_{ref}/W_{0,1}$ = [illegible] ft^2/lb.

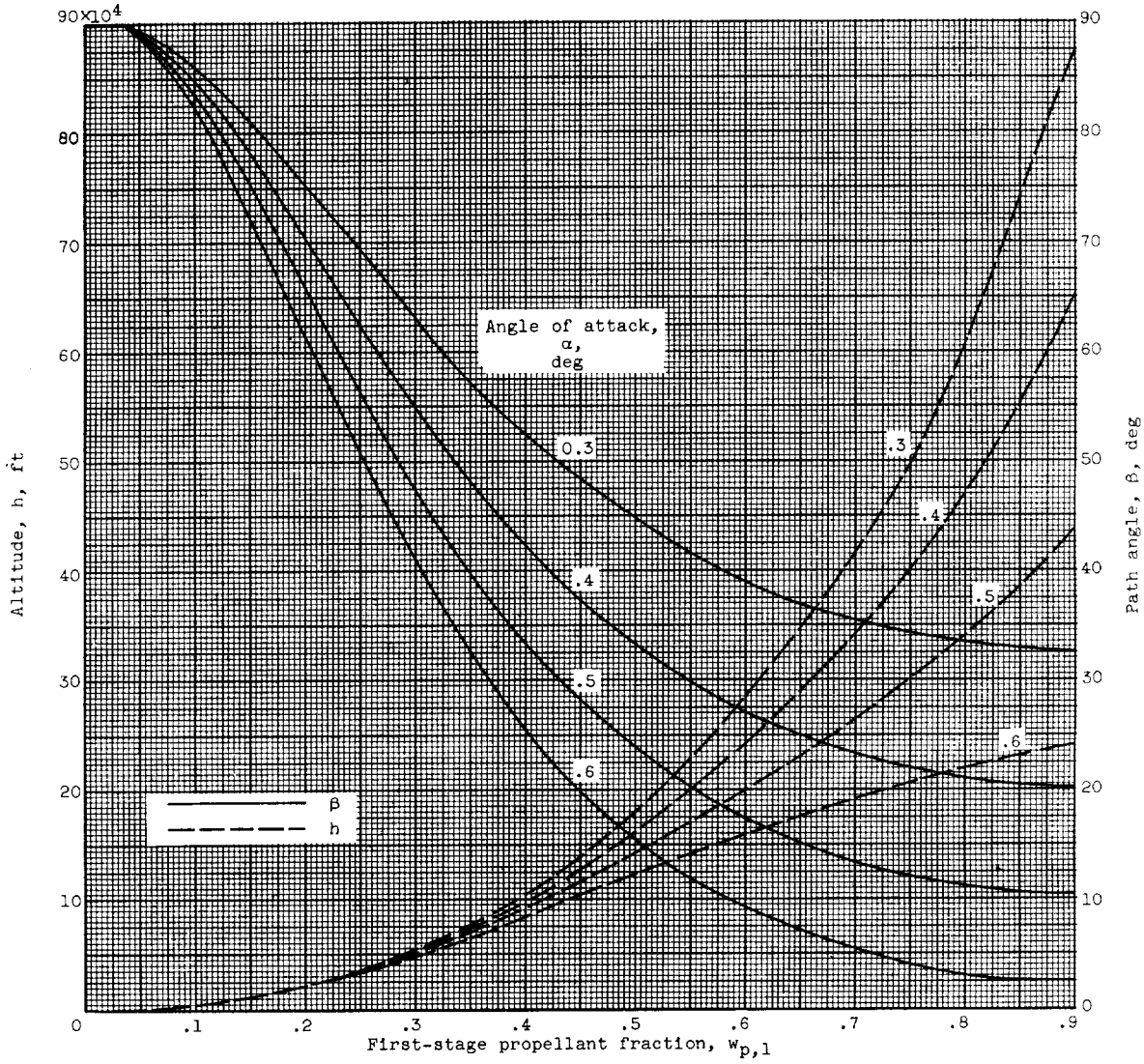

(f) Altitude and path angle; $F/W_{0,1} = 1.4$.

Figure 4. - Concluded. First-stage burnout conditions. $I_1 = 393$ (av.); $C_D A_{cs}/W_{0,1} = 1.6 \times 10^{-4}$.

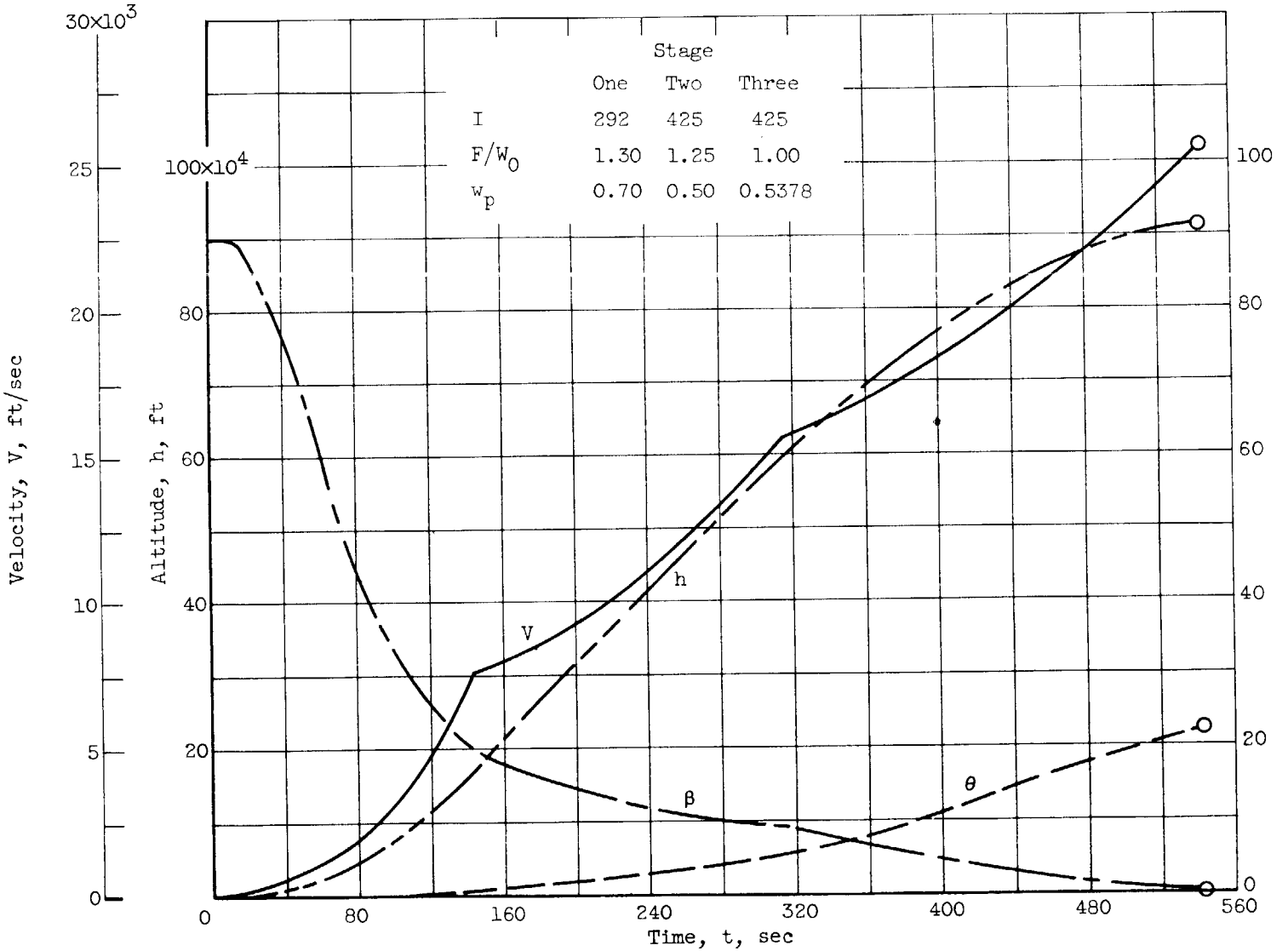

Figure 5. - Typical variation of flight path parameters.

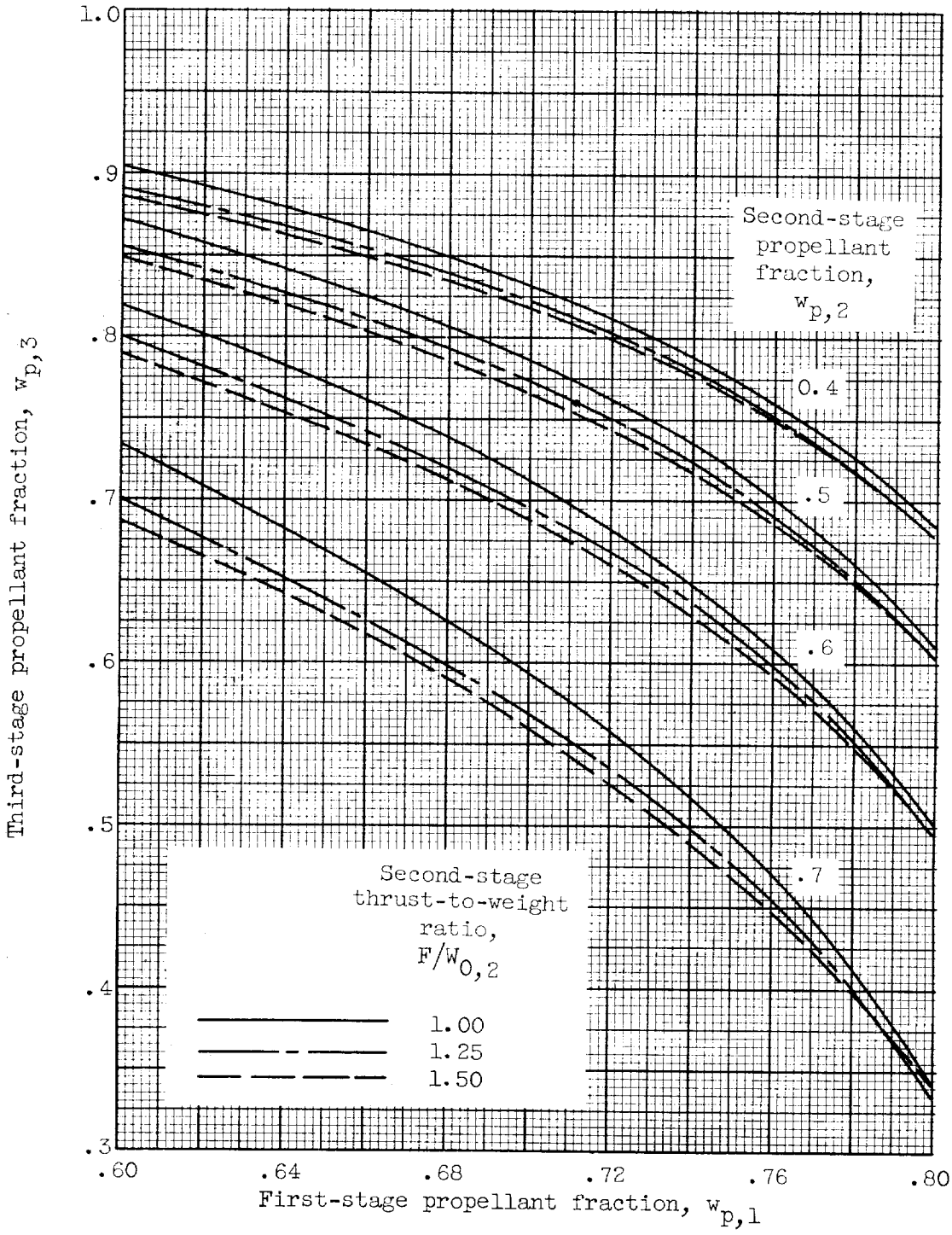

(a) $F/W_{0,1} = 1.20$; $F/W_{0,3} = 0.50$.

Figure 6. - Three-stage propellant-loading chart. 150-Nautical-mile orbit; $I_1 = 292$ (av.); $I_2 = 305$; $I_3 = 305$.

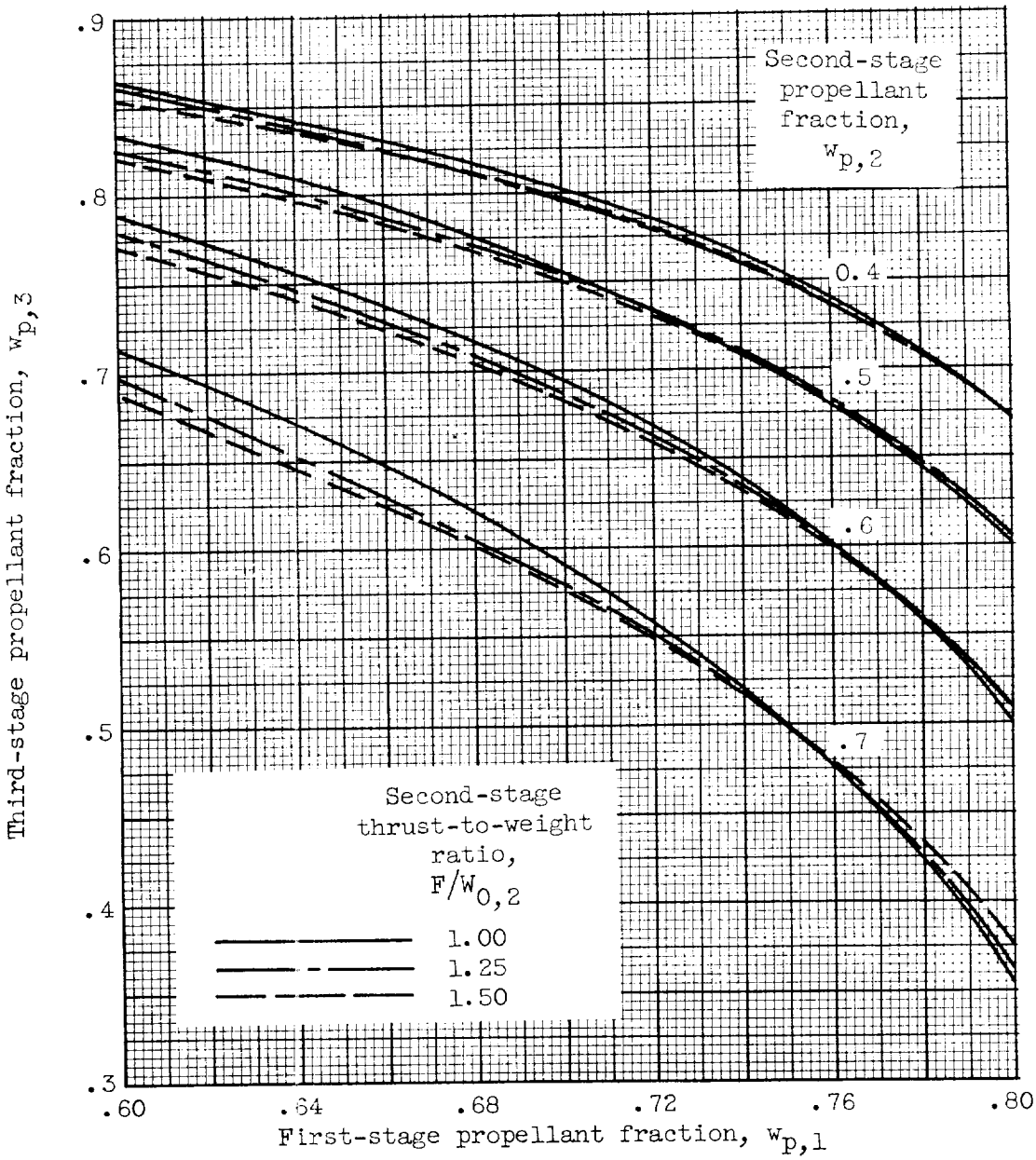

(b) $F/W_{0,1} = 1.20$; $F/W_{0,3} = 1.00$.

Figure 6. - Continued. Three-stage propellant-loading chart. 150-Nautical-mile orbit; $I_1 = 292$ (av.); $I_2 = 305$; $I_3 = 305$.

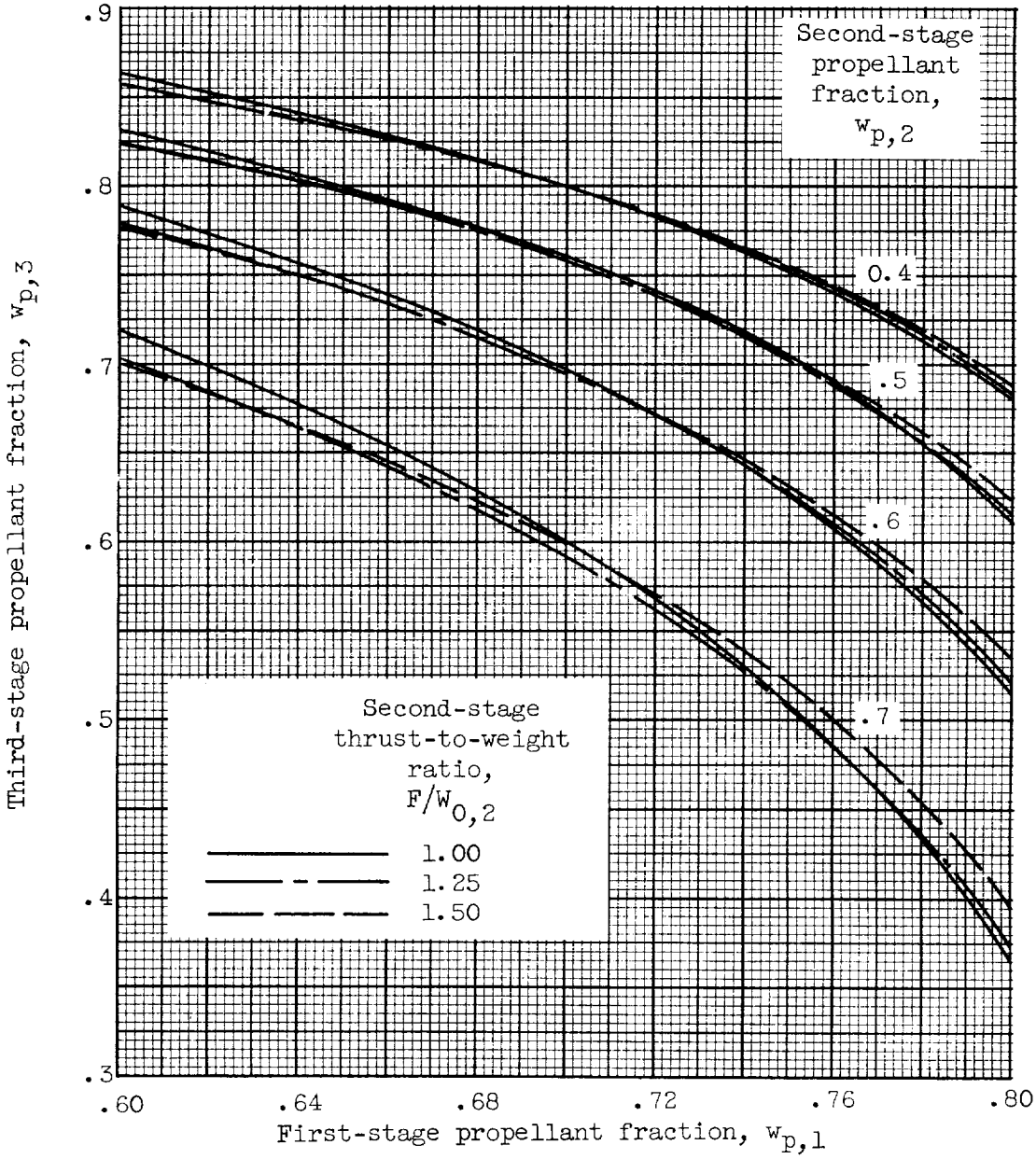

(c) $F/W_{0,1} = 1.20$; $F/W_{0,3} = 1.50$.

Figure 6. - Continued. Three-stage propellant-loading chart. 150-Nautical-mile orbit; $I_1 = 292$ (av.); $I_2 = 305$; $I_3 = 305$.

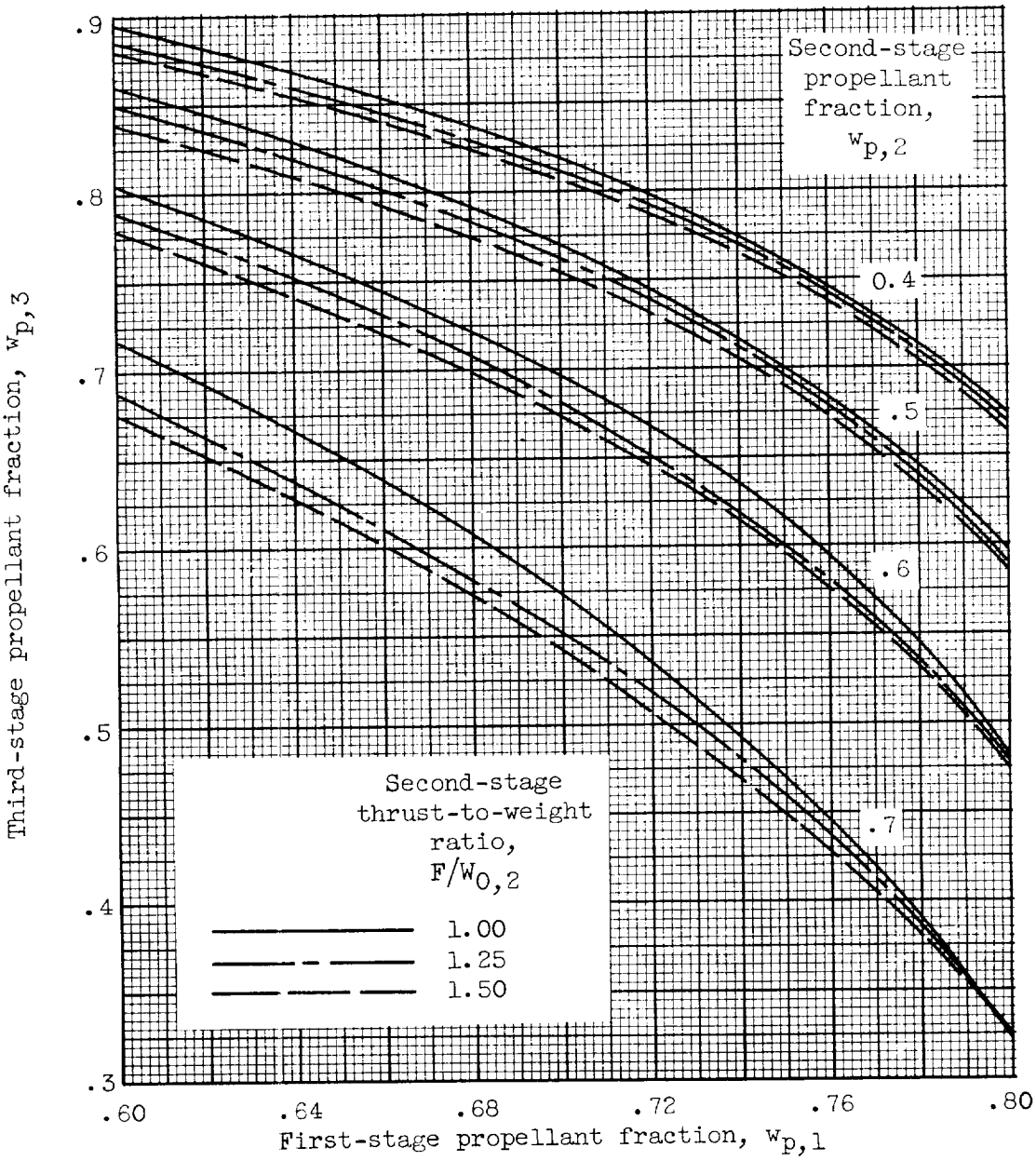

(d) $F/W_{0,1} = 1.30$; $F/W_{0,3} = 0.50$.

Figure 6. - Continued. Three-stage propellant-loading chart. 150-Nautical-mile orbit; $I_1 = 292$ (av.); $I_2 = 305$; $I_3 = 305$.

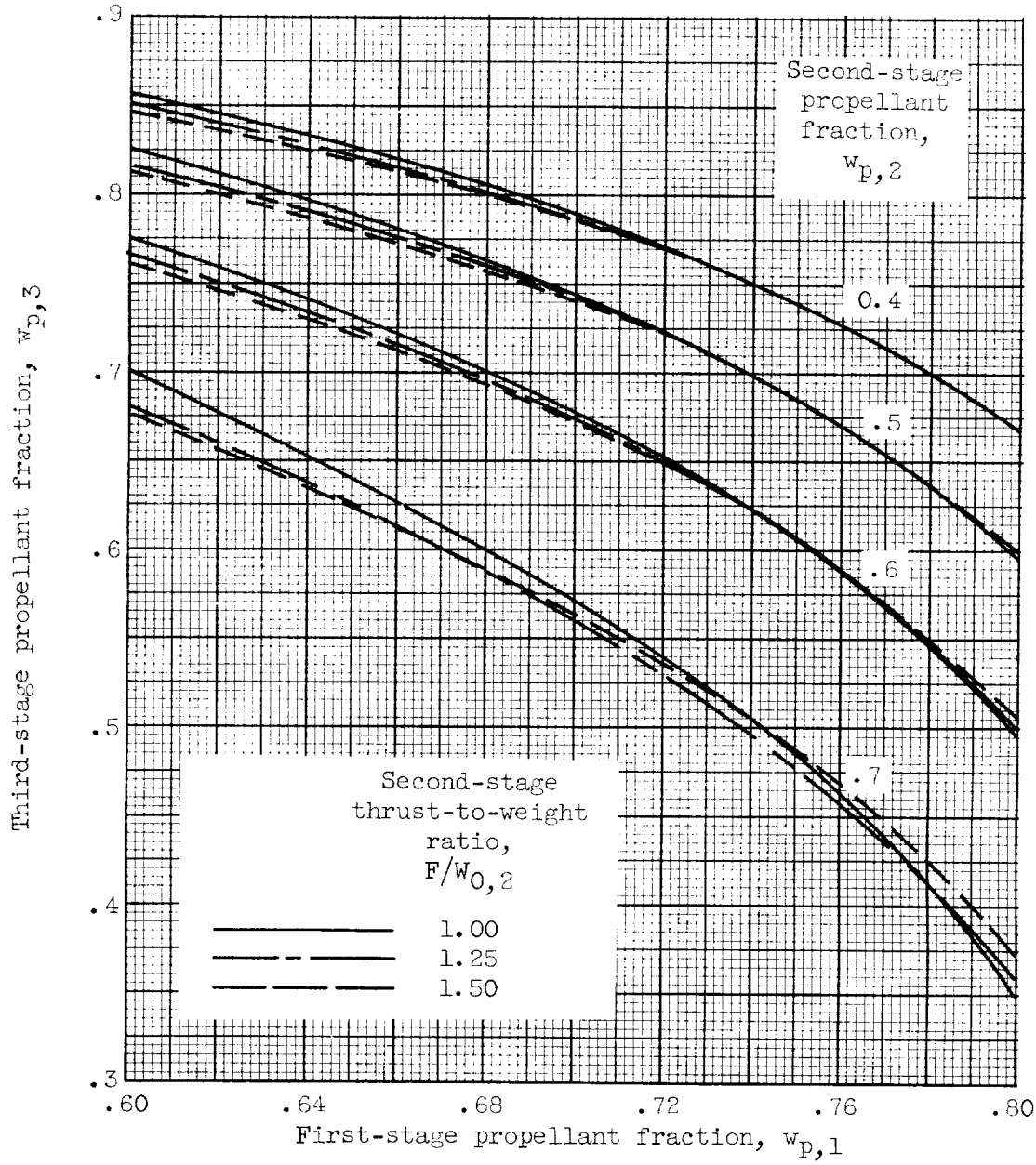

(e) $F/W_{0,1} = 1.30$; $F/W_{0,3} = 1.00$.

Figure 6. - Continued. Three-stage propellant-loading chart. 150-Nautical-mile orbit; $I_1 = 292$ (av.); $I_2 = 305$; $I_3 = 305$.

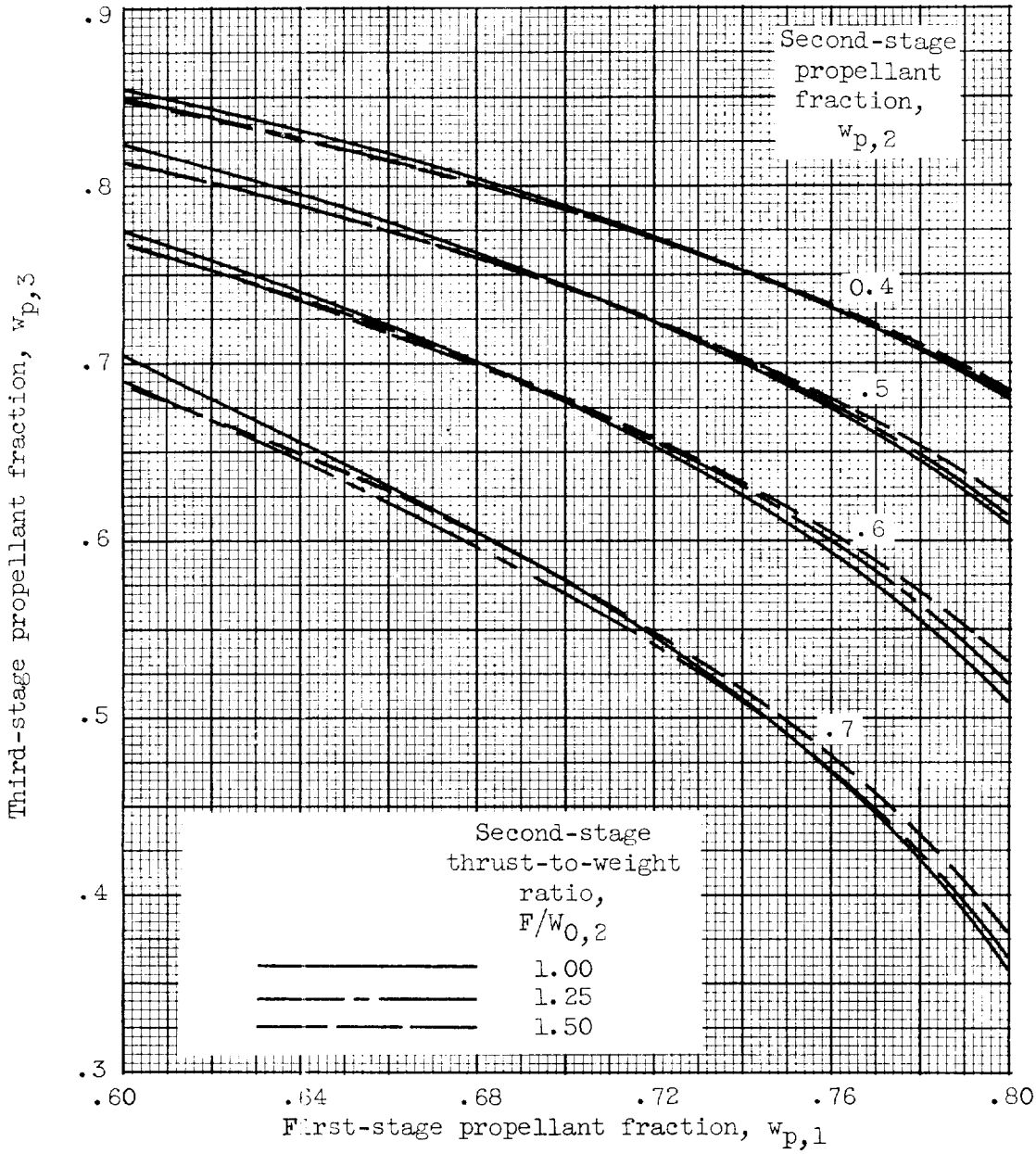

(f) $F/W_{0,1} = 1.30$; $F/W_{0,3} = 1.50$.

Figure 6. - Continued. Three-stage propellant-loading chart. 150-Nautical-mile orbit; $I_1 = 292$ (av.); $I_2 = 305$; $I_3 = 305$.

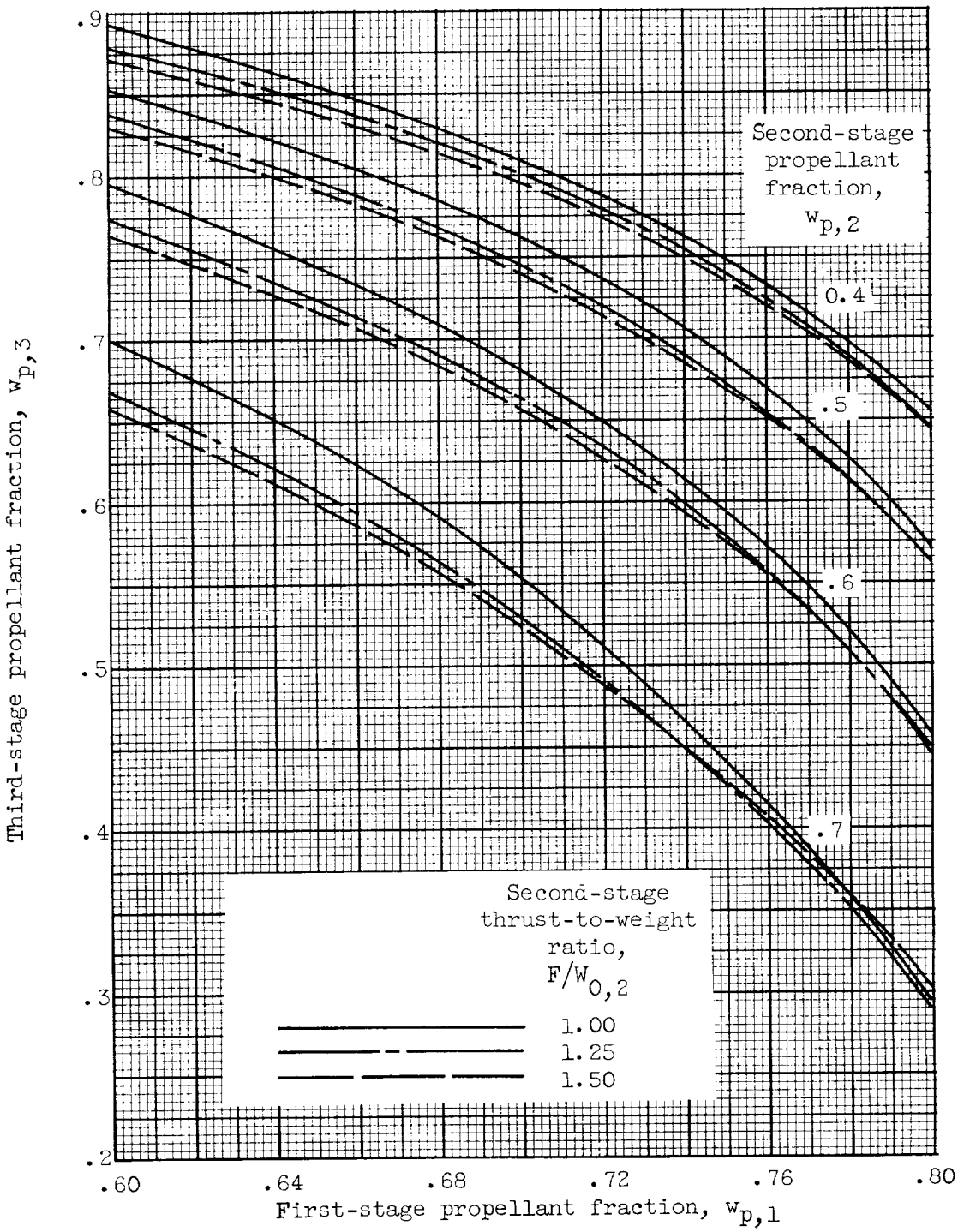

(g) $F/W_{0,1} = 1.40$; $F/W_{0,3} = 0.50$.

Figure 6. - Continued. Three-stage propellant-loading chart. 150-Nautical-mile orbit; $I_1 = 292$ (av.); $I_2 = 305$; $I_3 = 305$.

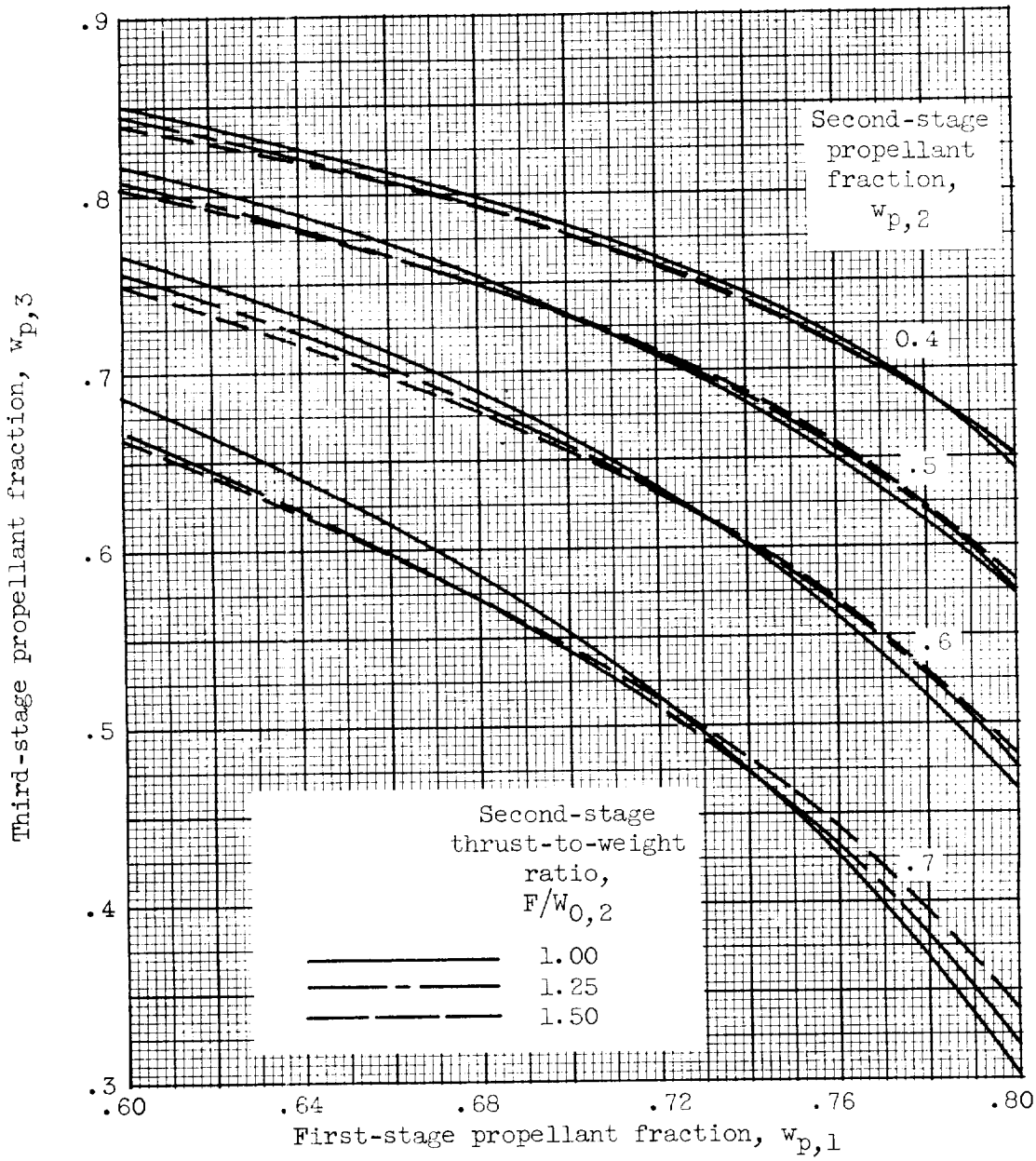

(h) $F/W_{0,1} = 1.40$; $F/W_{0,3} = 1.00$.

Figure 6. - Continued. Three-stage propellant-loading chart. 150-Nautical-mile orbit; $I_1 = 292$ (av.); $I_2 = 305$; $I_3 = 305$.

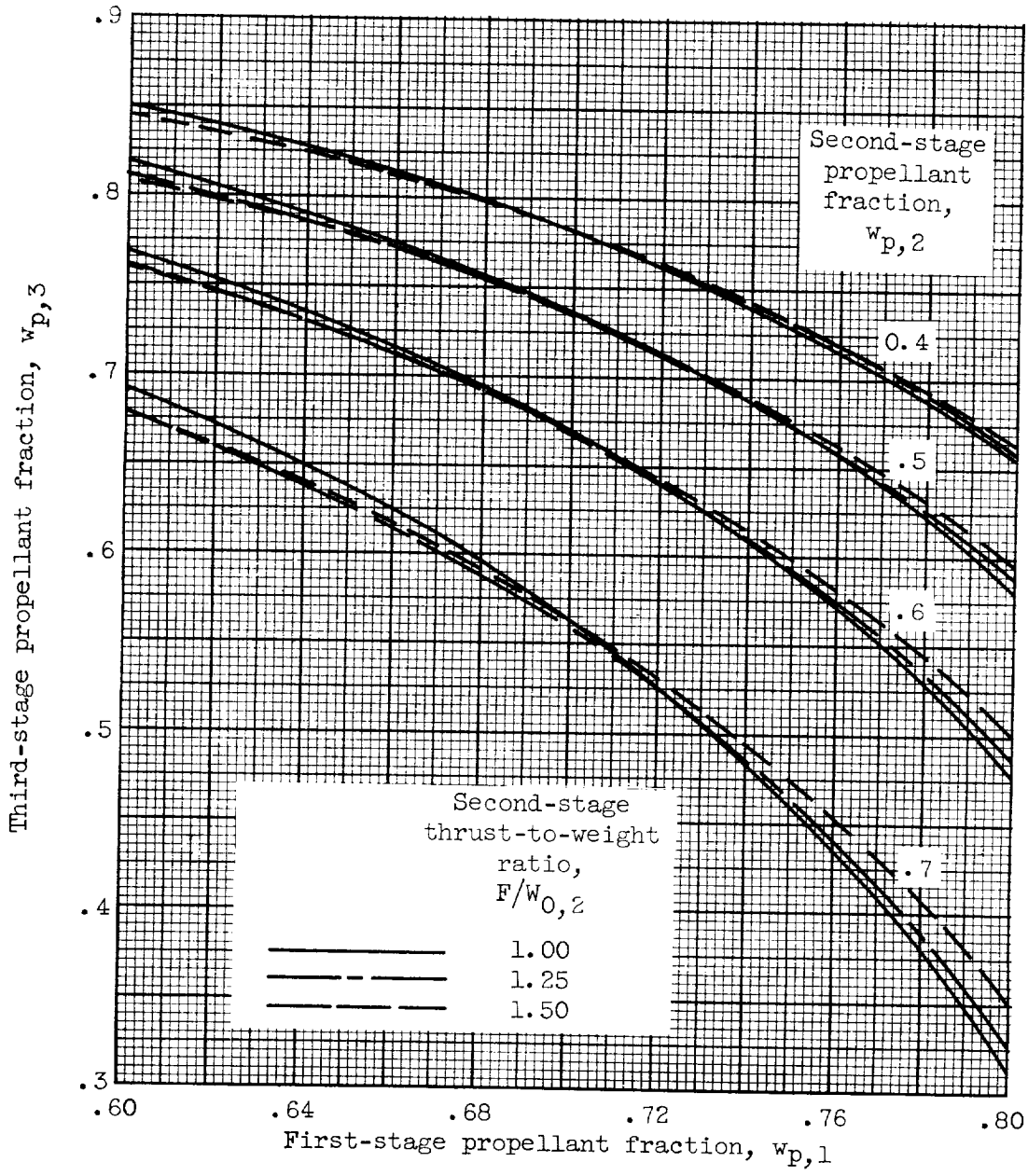

(i) $F/W_{0,1} = 1.40$; $F/W_{0,3} = 1.50$.

Figure 6. - Concluded. Three-stage propellant-loading chart. 150-Nautical-mile orbit; $I_1 = 292$ (av.); $I_2 = 305$; $I_3 = 305$.

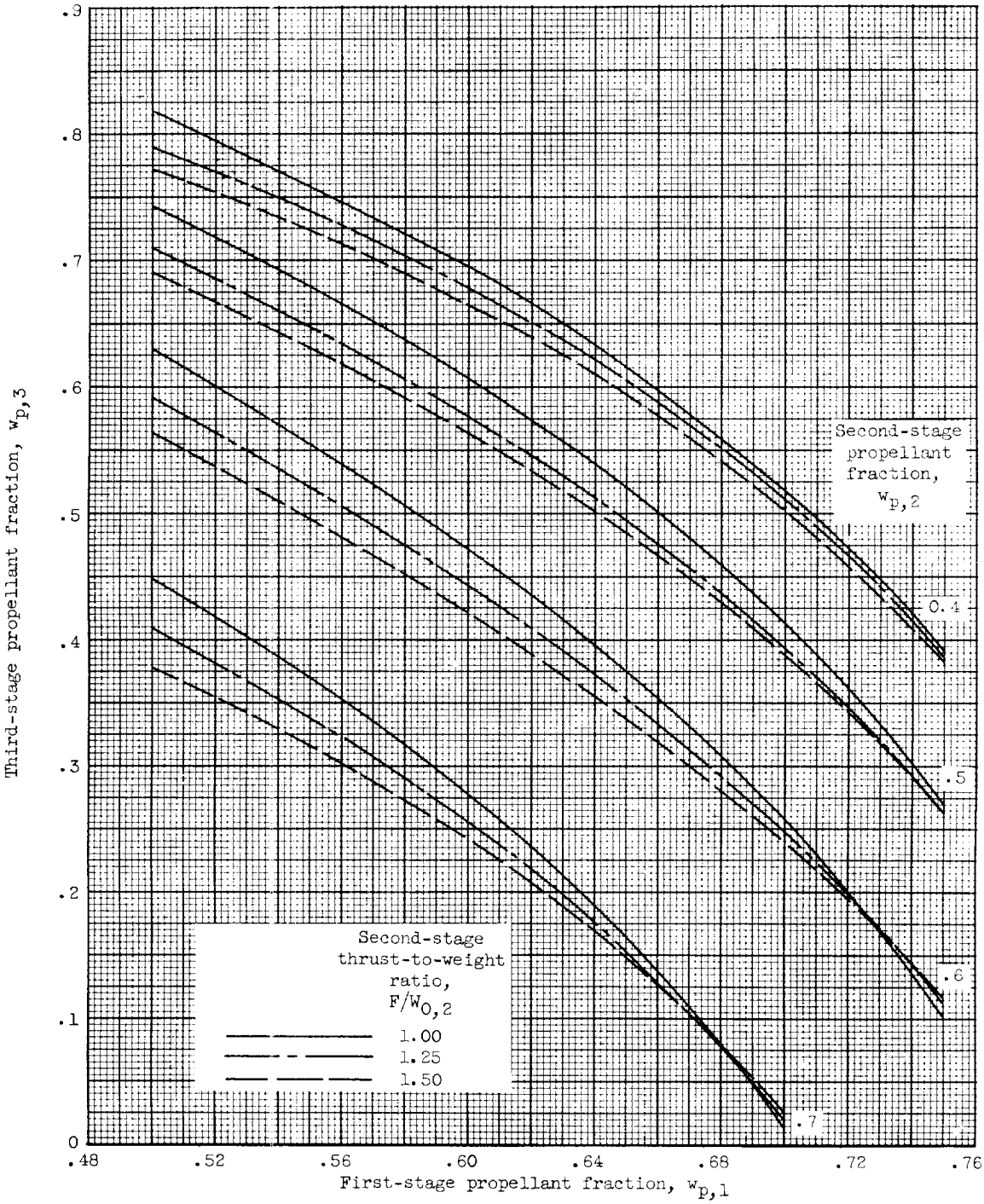

(a) $F/W_{0,1} = 1.20$; $F/W_{0,3} = 0.50$.

Figure 7. - Three-stage propellant-loading chart. 150-Nautical-mile orbit; I_1 = 393 (av.); I_2 = 425; I_3 = 425.

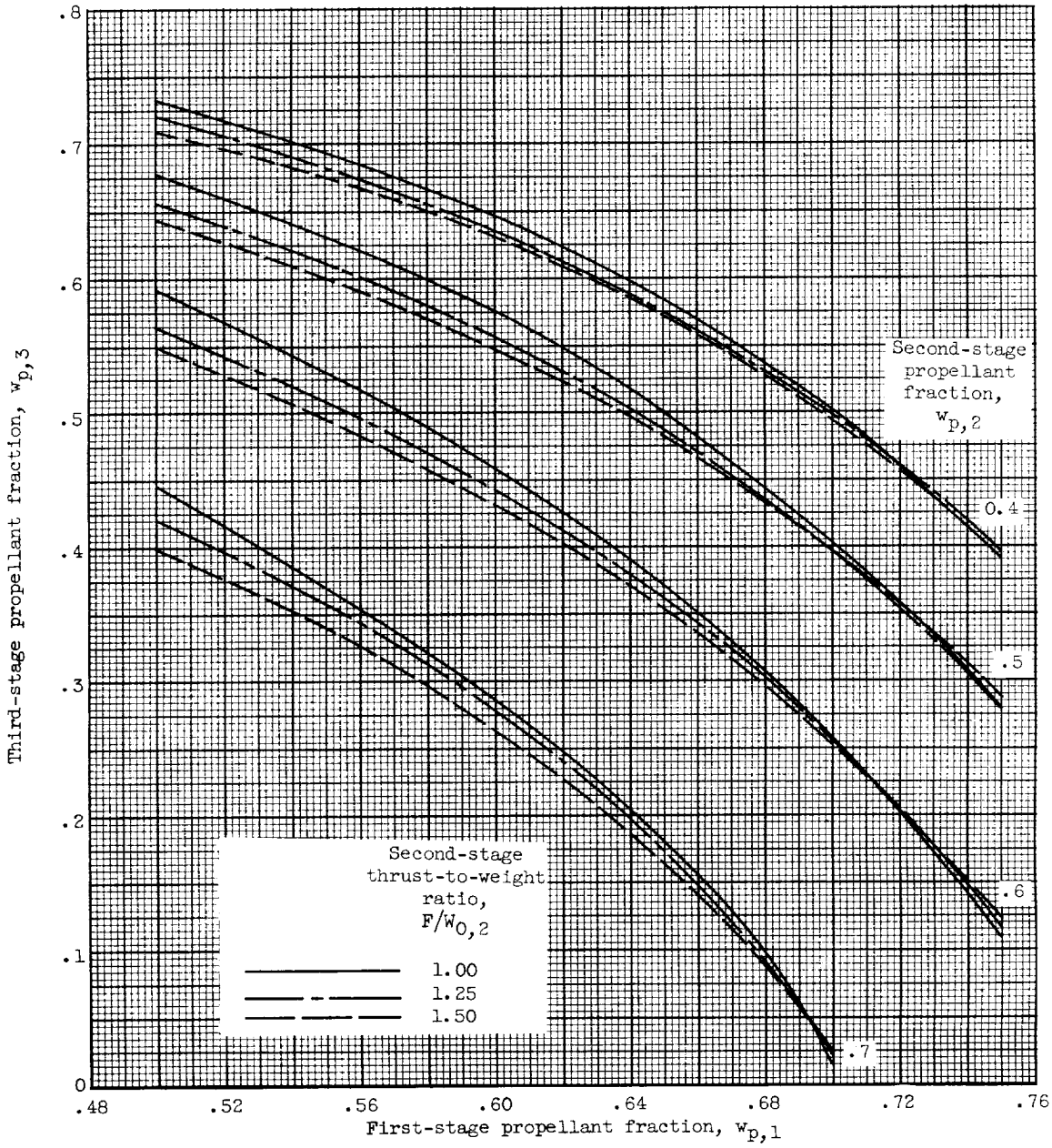

(b) $F/W_{0,1} = 1.20$; $F/W_{0,3} = 1.00$.

Figure 7. - Continued. Three-stage propellant-loading chart. 150-Nautical-mile orbit; $I_1 = 393$ (av.); $I_2 = 425$; $I_3 = 425$.

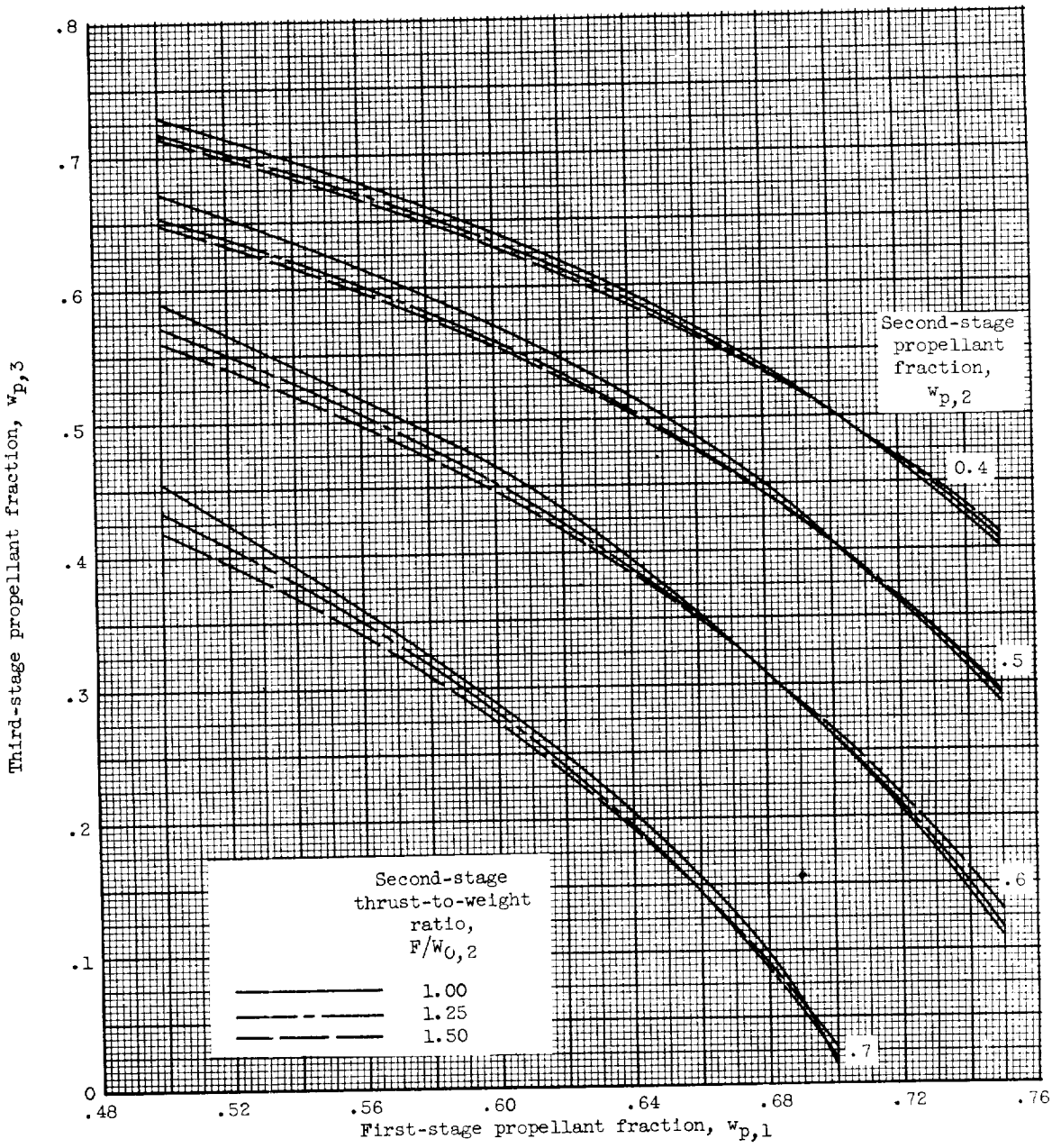

(c) $F/W_{0,1} = 1.20$; $F/W_{0,3} = 1.50$.

Figure 7. - Continued. Three-stage propellant-loading chart. 150-Nautical-mile orbit; $I_1 = 393$ (av.); $I_2 = 425$; $I_3 = 425$.

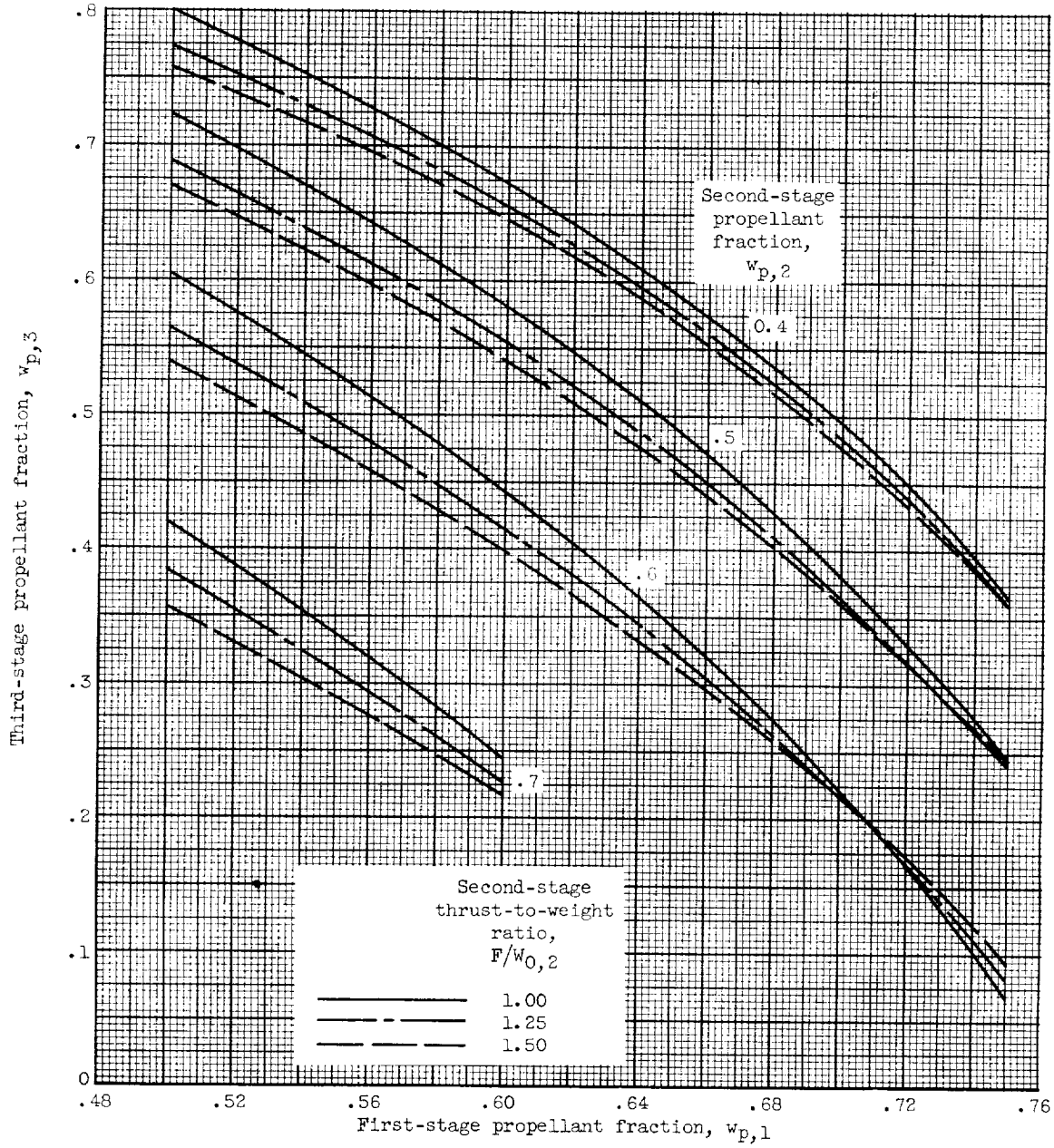

(d) $F/W_{0,1} = 1.30$; $F/W_{0,3} = 0.50$.

Figure 7. - Continued. Three-stage propellant-loading chart. 150-Nautical-mile orbit; $I_1 = 393$ (av.); $I_2 = 425$; $I_3 = 425$.

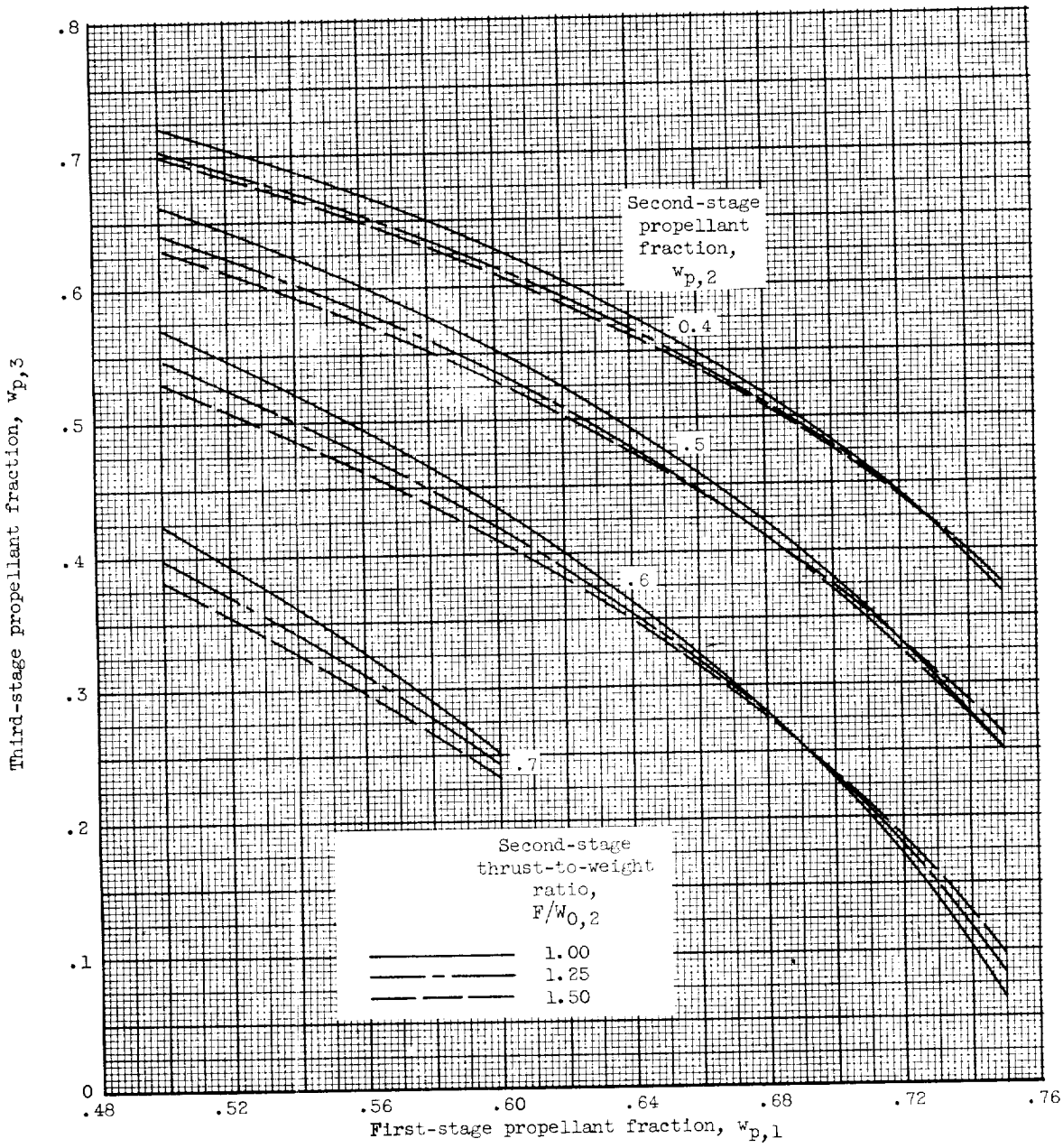

(e) $F/W_{0,1} = 1.30$; $F/W_{0,3} = 1.00$.

Figure 7. - Continued. Three-stage propellant-loading chart. 150-Nautical-mile orbit; $I_1 = 393$ (av.); $I_2 = 425$; $I_3 = 425$.

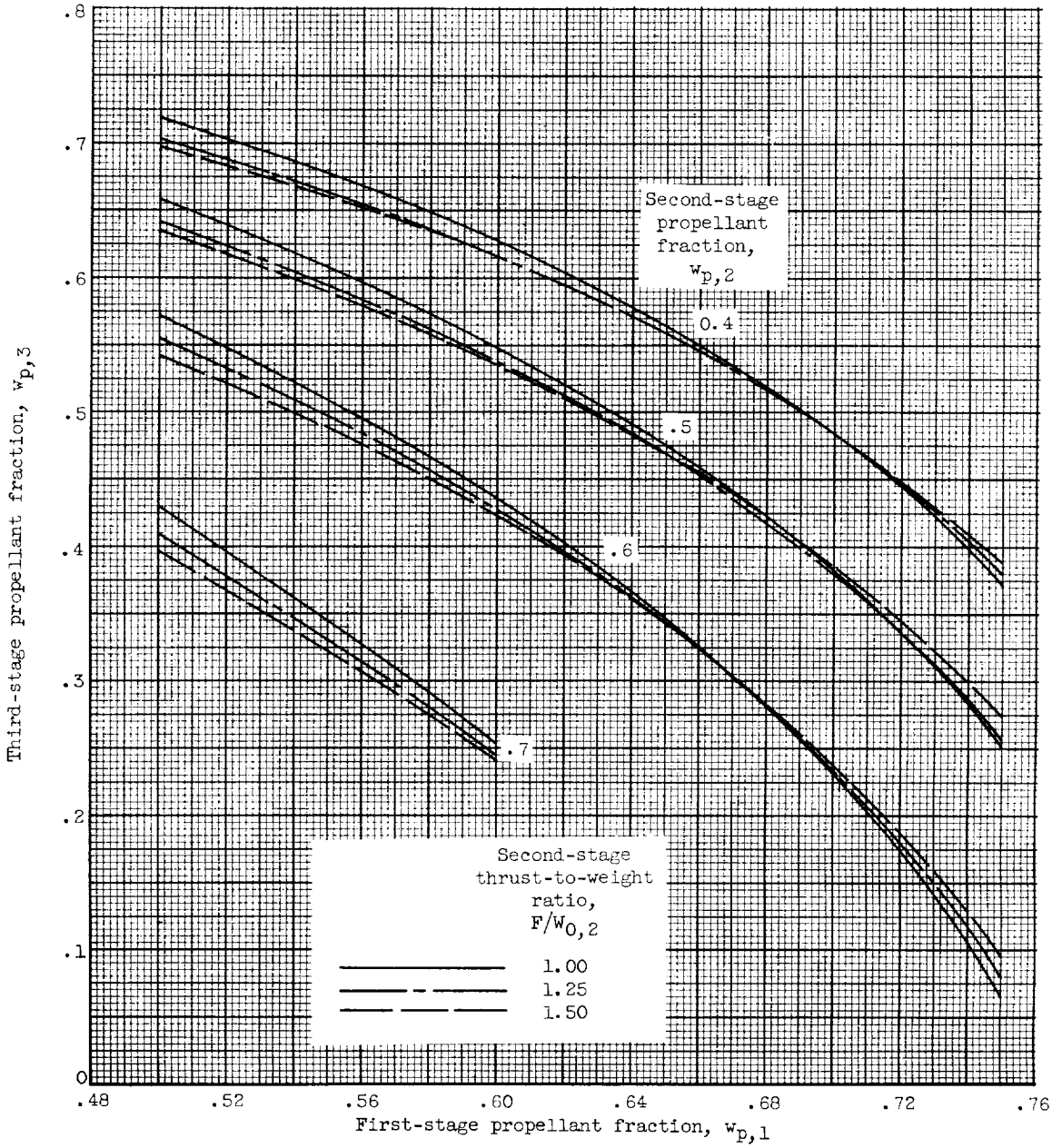

(f) $F/W_{0,1} = 1.30$; $F/W_{0,3} = 1.50$.

Figure 7. - Continued. Three-stage propellant-loading chart. 150-Nautical-mile orbit; $I_1 = 393$ (av.); $I_2 = 425$; $I_3 = 425$.

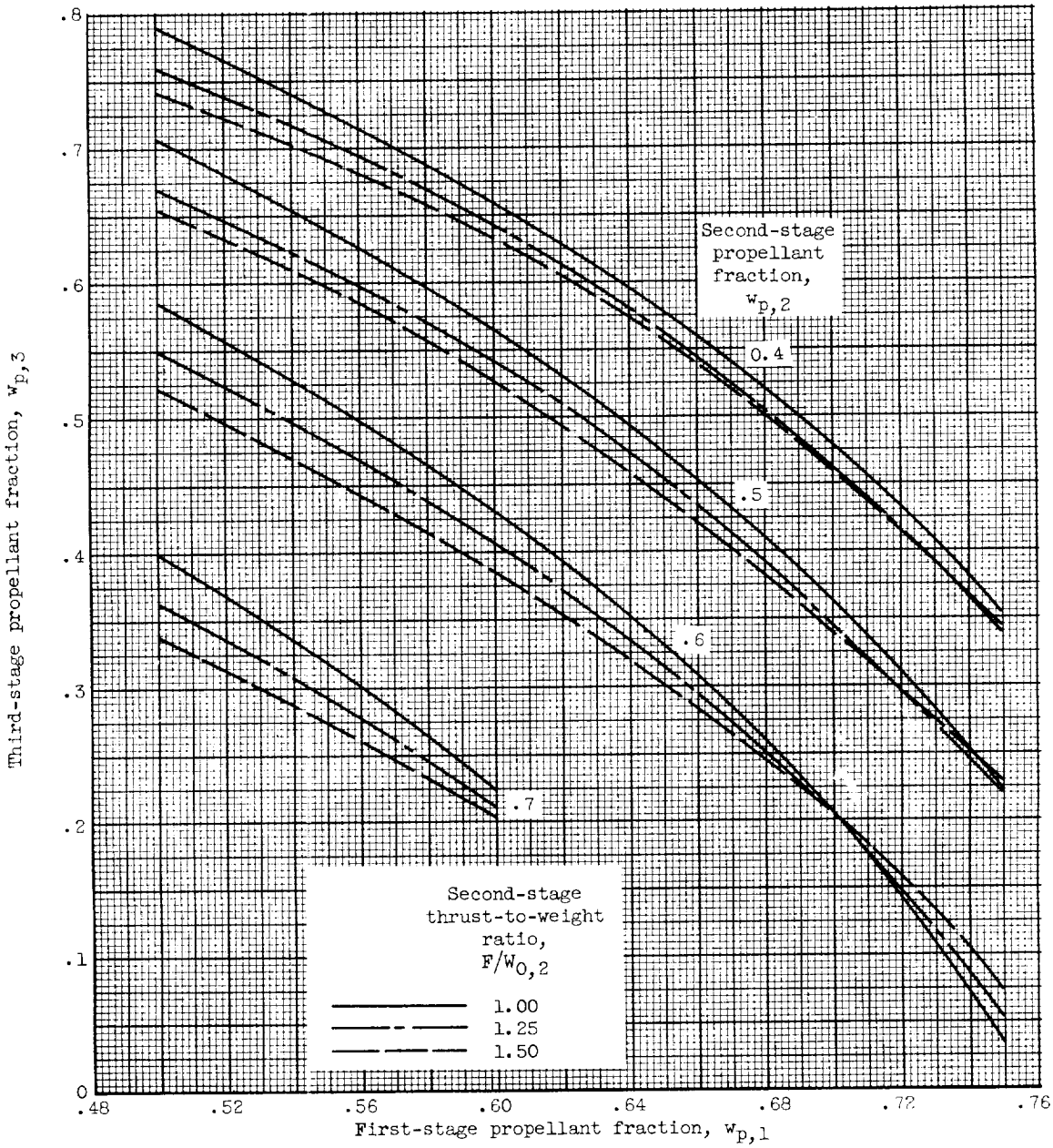

(g) $F/W_{0,1} = 1.40$; $F/W_{0,3} = 0.50$.

Figure 7. - Continued. Three-stage propellant-loading chart. 150-Nautical-mile orbit; $I_1 = 393$ (av.); $I_2 = 425$; $I_3 = 425$.

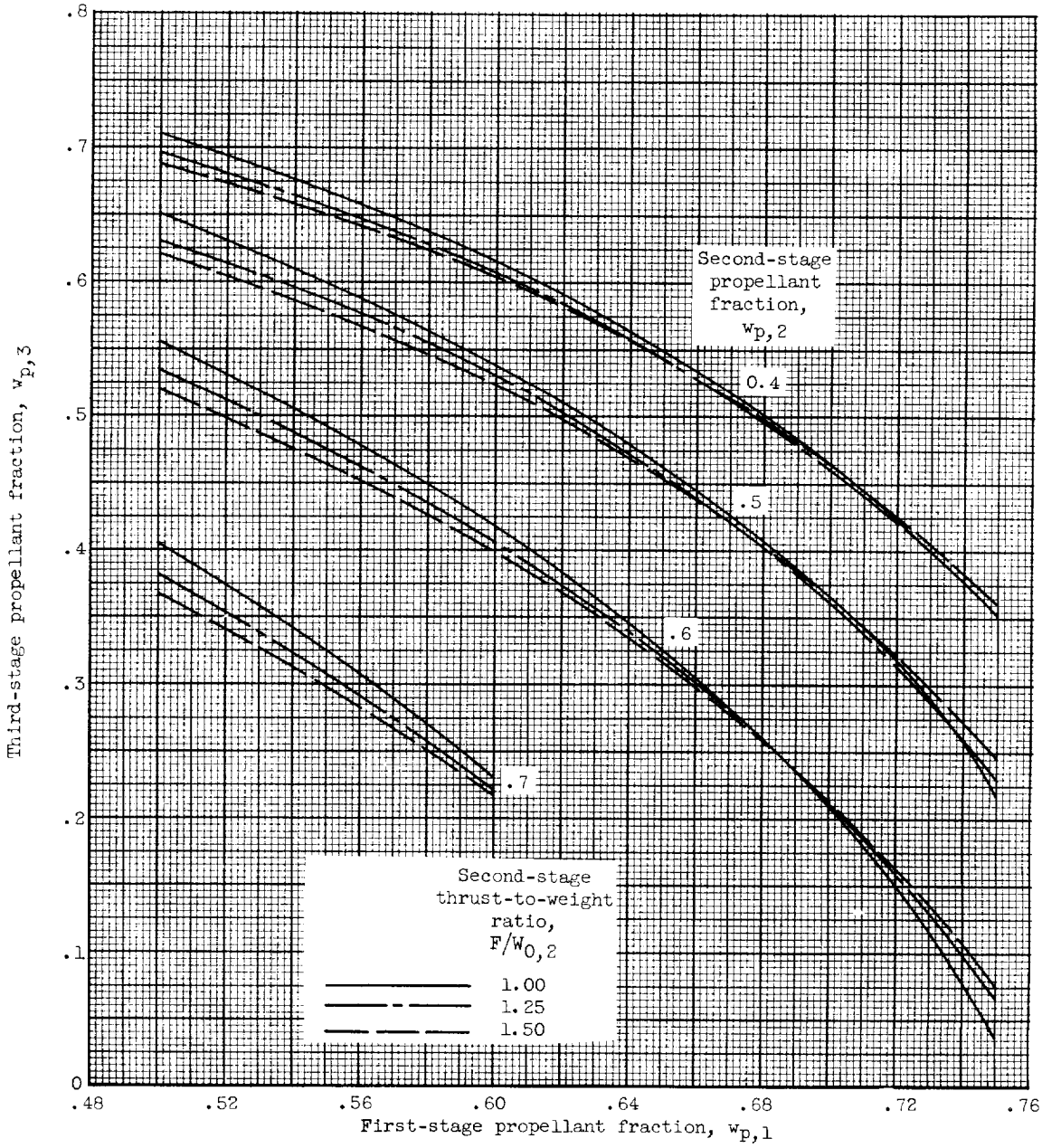

(h) $F/W_{0,1} = 1.40$; $F/W_{0,3} = 1.00$.

Figure 7. - Continued. Three-stage propellant-loading chart. 150-Nautical-mile orbit; $I_1 = 393$ (av.); $I_2 = 425$; $I_3 = 425$.

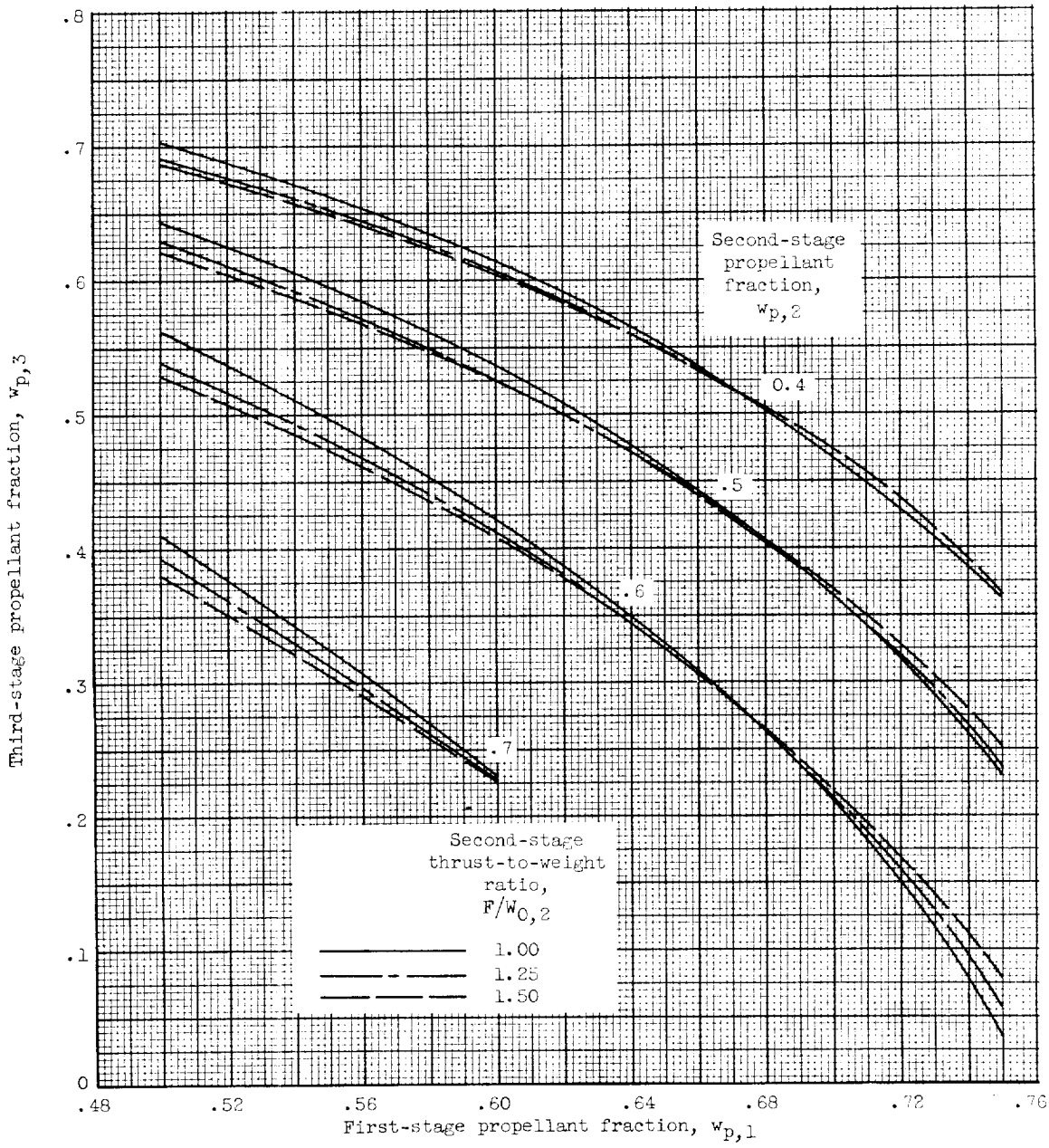

(i) $F/W_{0,1} = 1.40$; $F/W_{0,3} = 1.50$.

Figure 7. - Concluded. Three-stage propellant-loading chart. 150-Nautical-mile orbit; $I_1 = 393$ (av.); $I_2 = 425$; $I_3 = 425$.

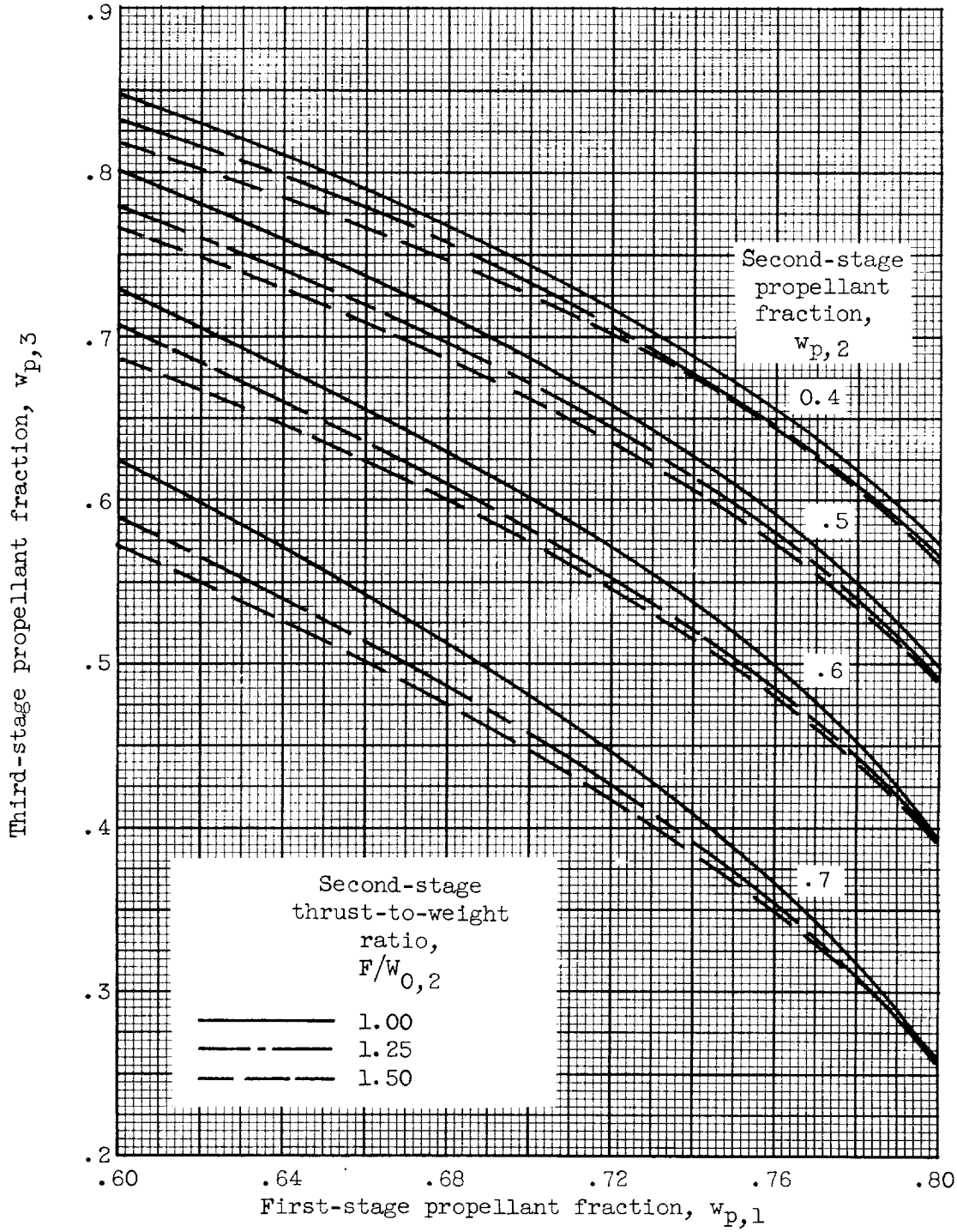

(a) $F/W_{0,1} = 1.20$; $F/W_{0,3} = 0.50$.

Figure 8. - Three-stage propellant-loading chart. 150-Nautical-mile orbit; $I_1 = 292$ (av.); $I_2 = 305$; $I_3 = 425$.

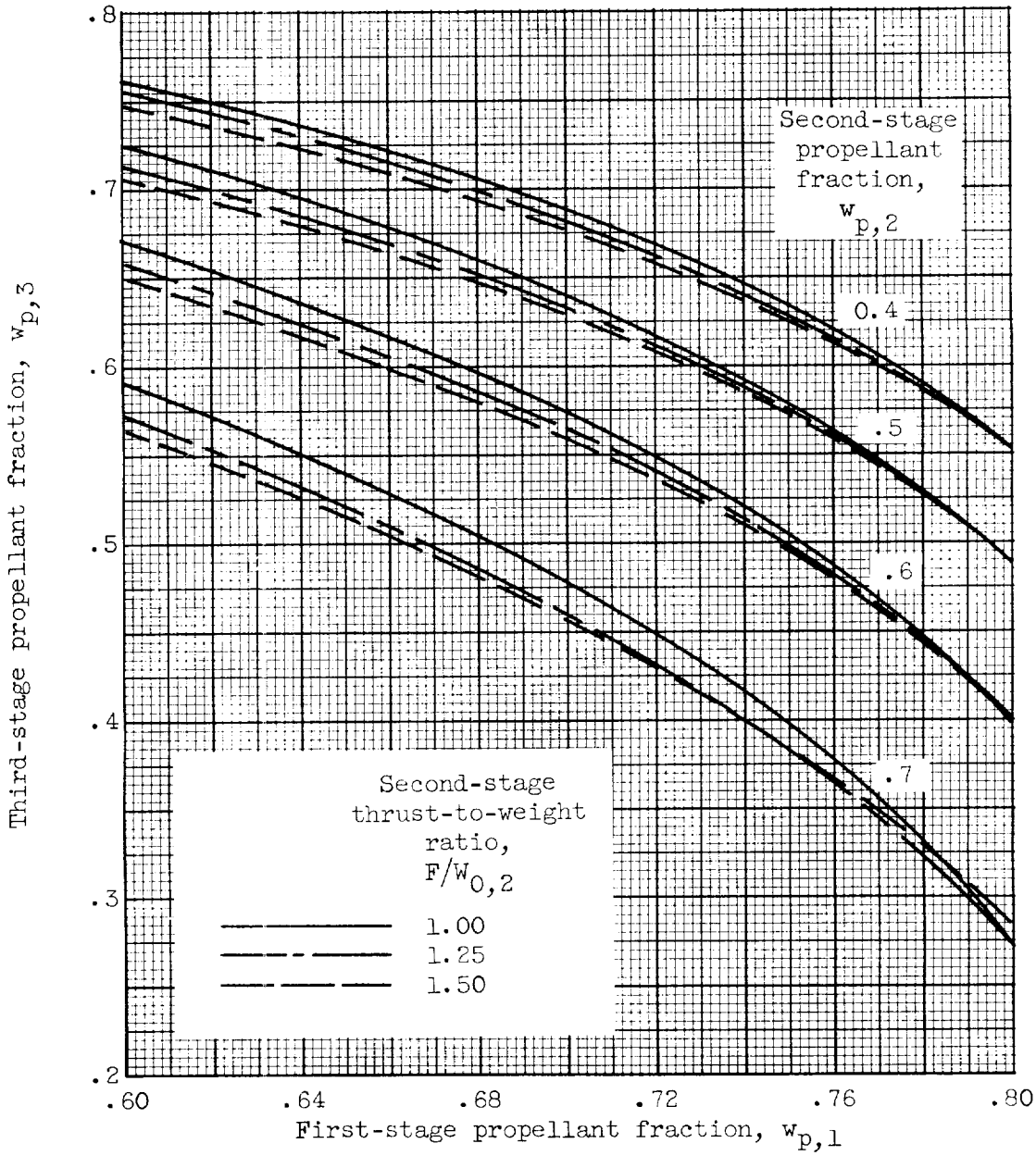

(b) $F/W_{0,1} = 1.20$; $F/W_{0,3} = 1.00$.

Figure 8. - Continued. Three-stage propellant-loading chart. 150-Nautical-mile orbit; $I_1 = 292$ (av.); $I_2 = 305$; $I_3 = 425$.

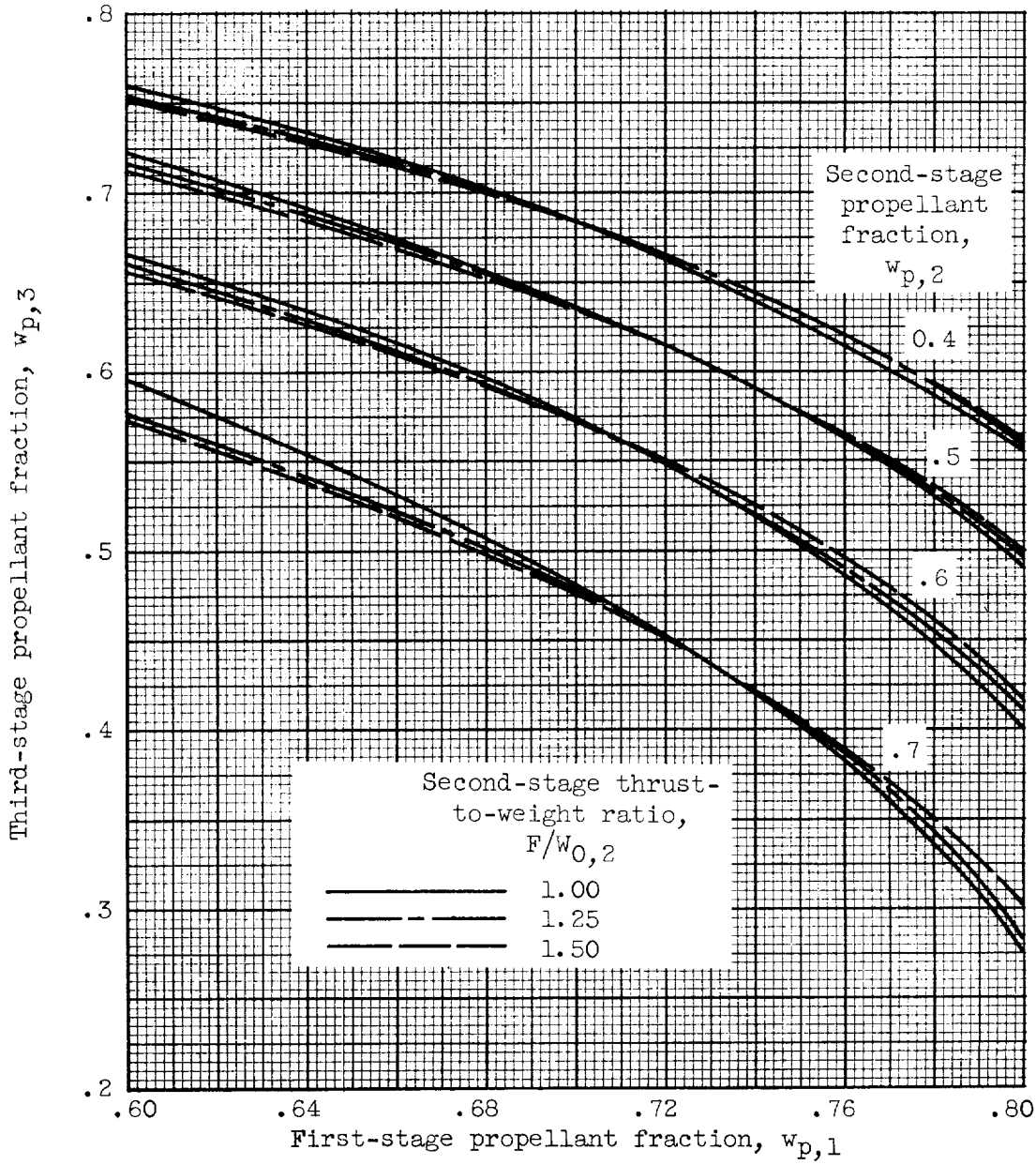

(c) $F/W_{0,1} = 1.20$; $F/W_{0,3} = 1.50$.

Figure 8. - Continued. Three-stage propellant-loading chart. 150-Nautical-mile orbit; $I_1 = 292$ (av.); $I_2 = 305$; $I_3 = 425$.

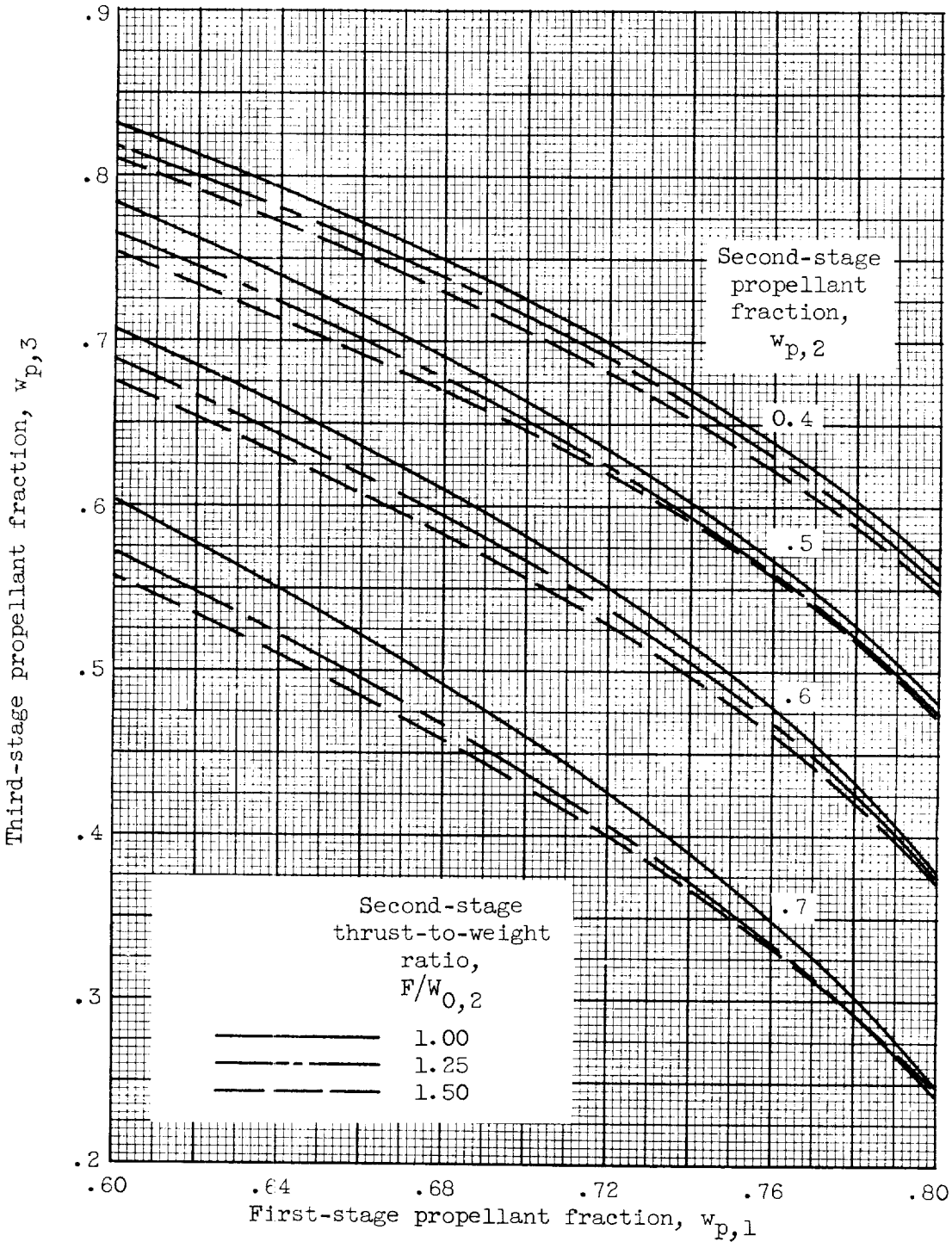

(d) $F/W_{0,1} = 1.30$; $F/W_{0,3} = 0.50$.

Figure 8. - Continued. Three-stage propellant-loading chart. 150-Nautical-mile orbit; $I_1 = 292$ (av.); $I_2 = 305$; $I_3 = 425$.

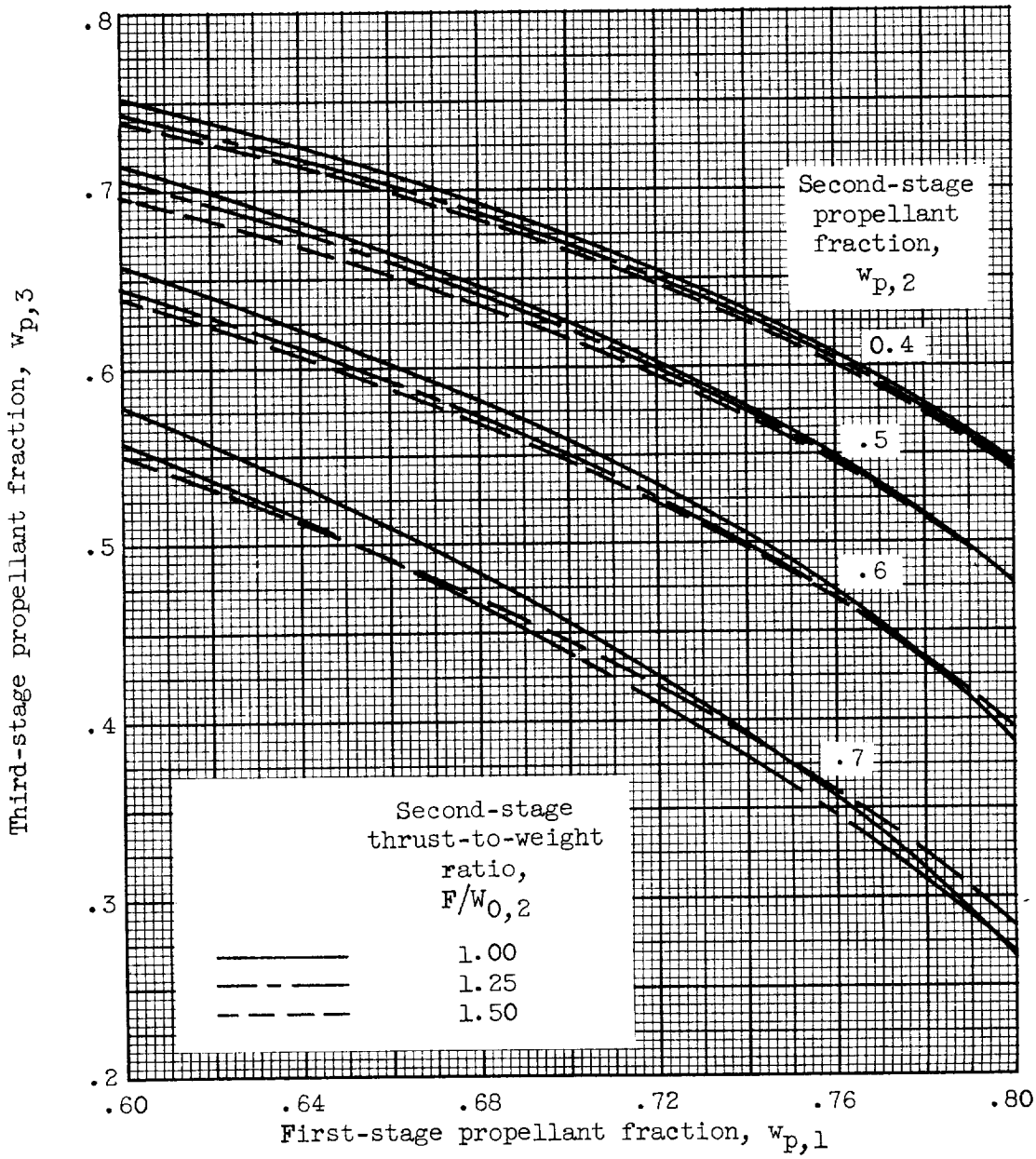

(e) $F/W_{0,1} = 1.30$; $F/W_{0,3} = 1.00$.

Figure 8. - Continued. Three-stage propellant-loading chart. 150-Nautical-mile orbit; $I_1 = 292$ (av.); $I_2 = 305$; $I_3 = 425$.

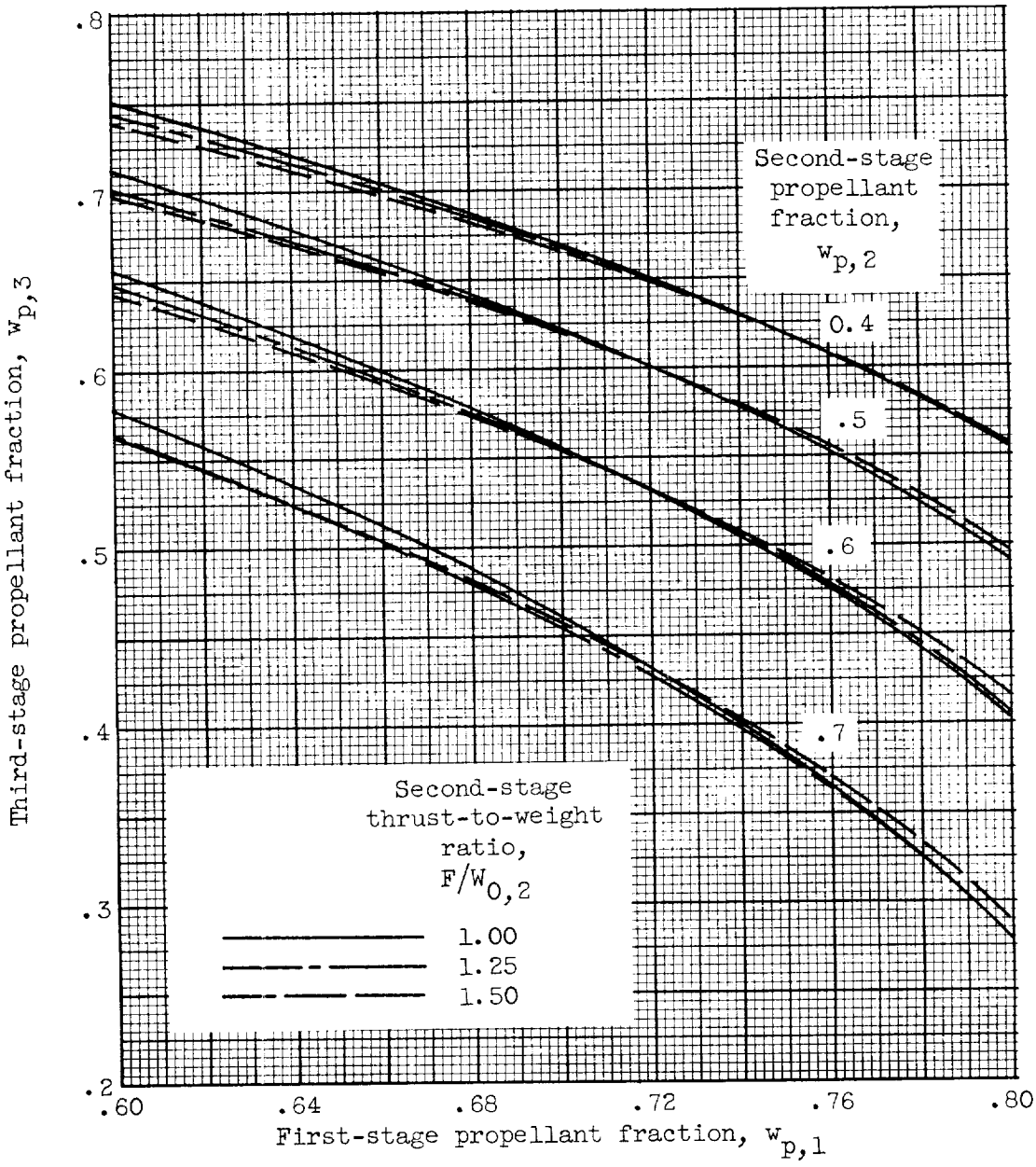

(f) $F/W_{0,1} = 1.30$; $F/W_{0,3} = 1.50$.

Figure 8. - Continued. Three-stage propellant-loading chart. 150-Nautical-mile orbit; $I_1 = 292$ (av.); $I_2 = 305$; $I_3 = 425$.

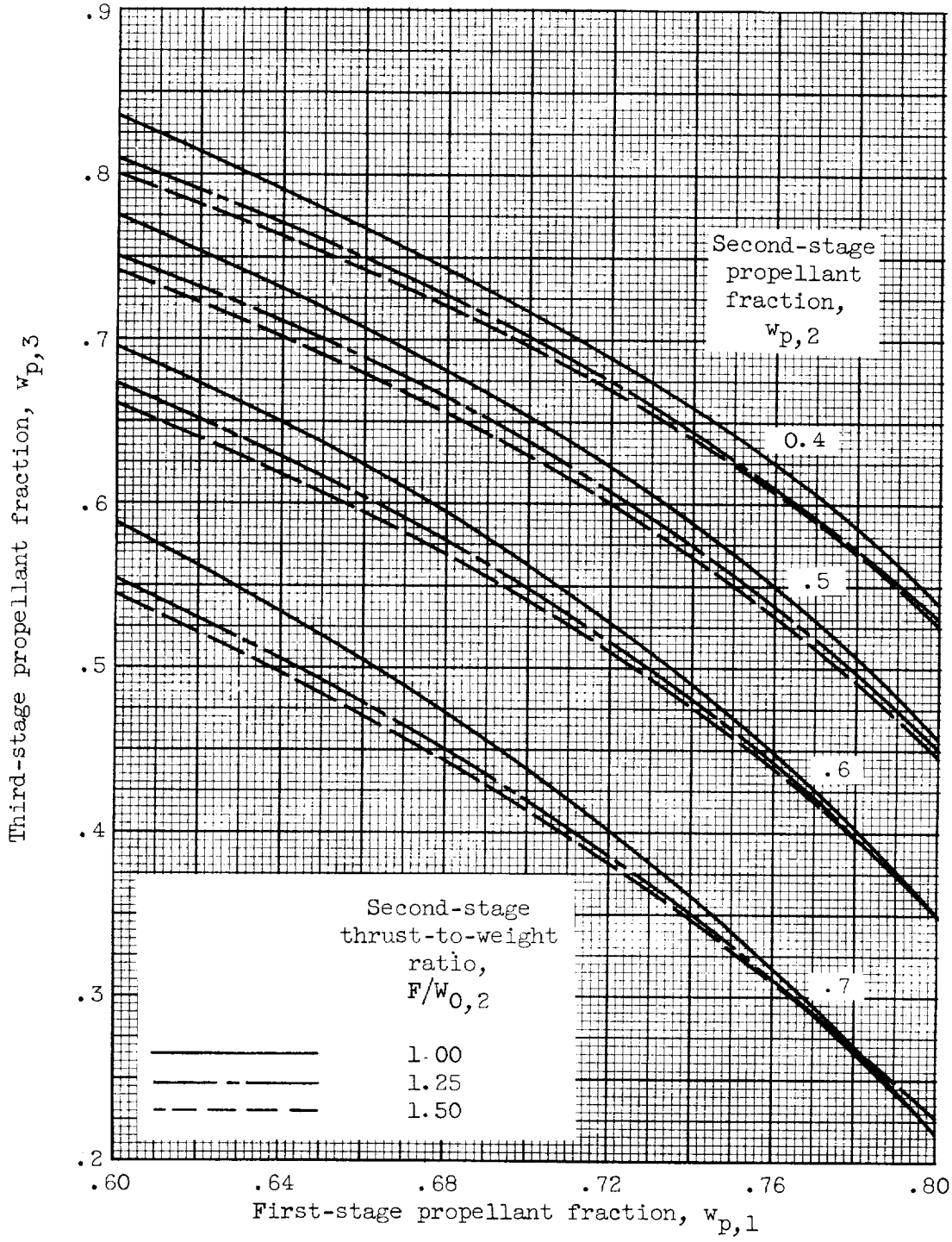

(g) $F/W_{0,1} = 1.40$; $F/W_{0,3} = 0.50$.

Figure 8. - Continued. Three-stage propellant-loading chart. 150-Nautical-mile orbit; $I_1 = 292$ (av.); $I_2 = 305$; $I_3 = 425$.

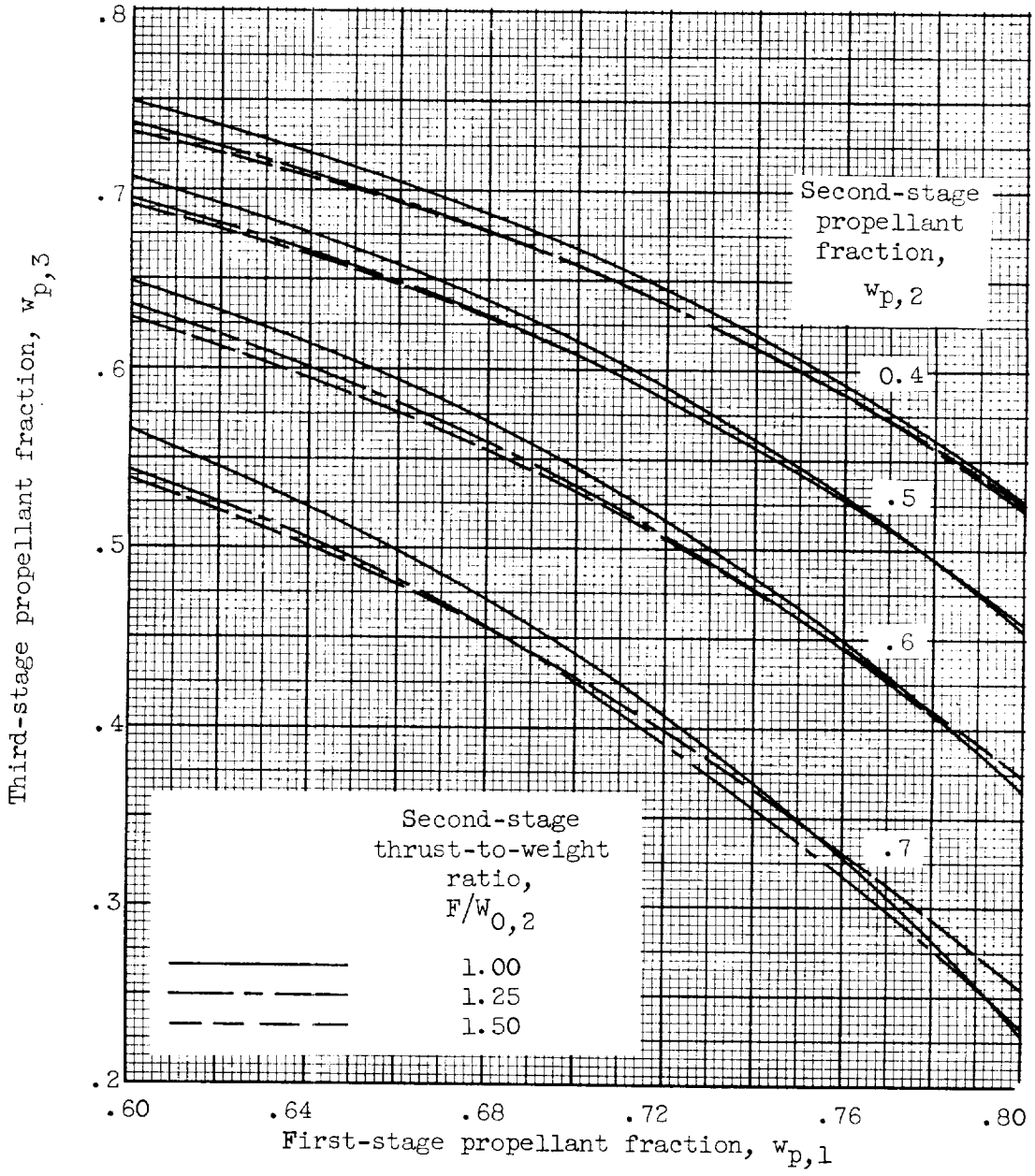

(h) $F/W_{0,1} = 1.40$; $F/W_{0,3} = 1.00$.

Figure 8. - Continued. Three-stage propellant-loading chart. 150-Nautical-mile orbit; $I_1 = 292$ (av.); $I_2 = 305$; $I_3 = 425$.

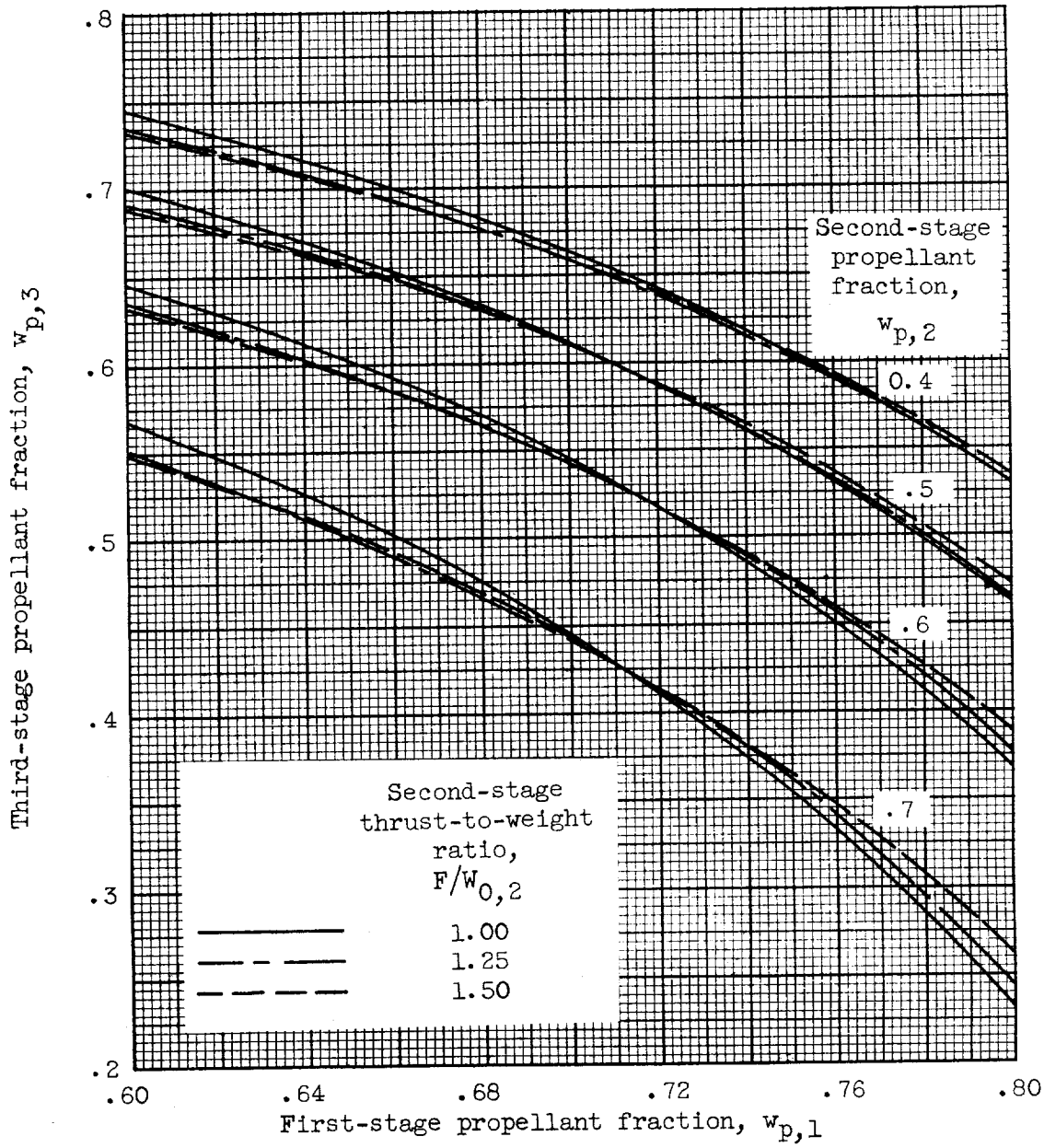

(i) $F/W_{0,1} = 1.40$; $F/W_{0,3} = 1.50$.

Figure 8. - Concluded. Three-stage propellant-loading chart. 150-Nautical-mile orbit; $I_1 = 292$ (av.); $I_2 = 305$; $I_3 = 425$.

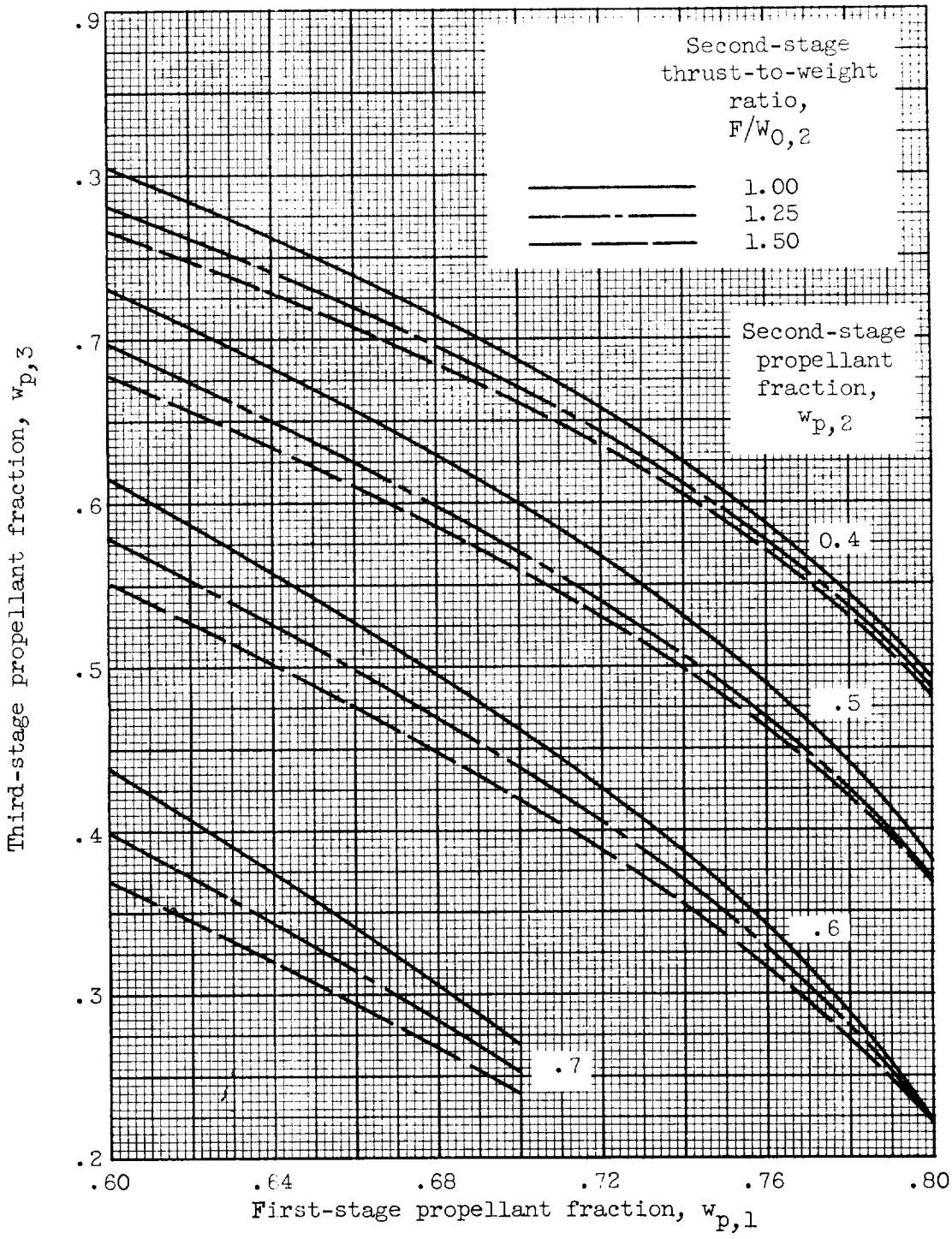

(a) $F/W_{0,1} = 1.20$; $F/W_{0,3} = 0.50$.

Figure 9. - Three-stage propellant-loading chart. 150-Nautical-mile orbit; $I_1 = 292$ (av.); $I_2 = 425$; $I_3 = 425$.

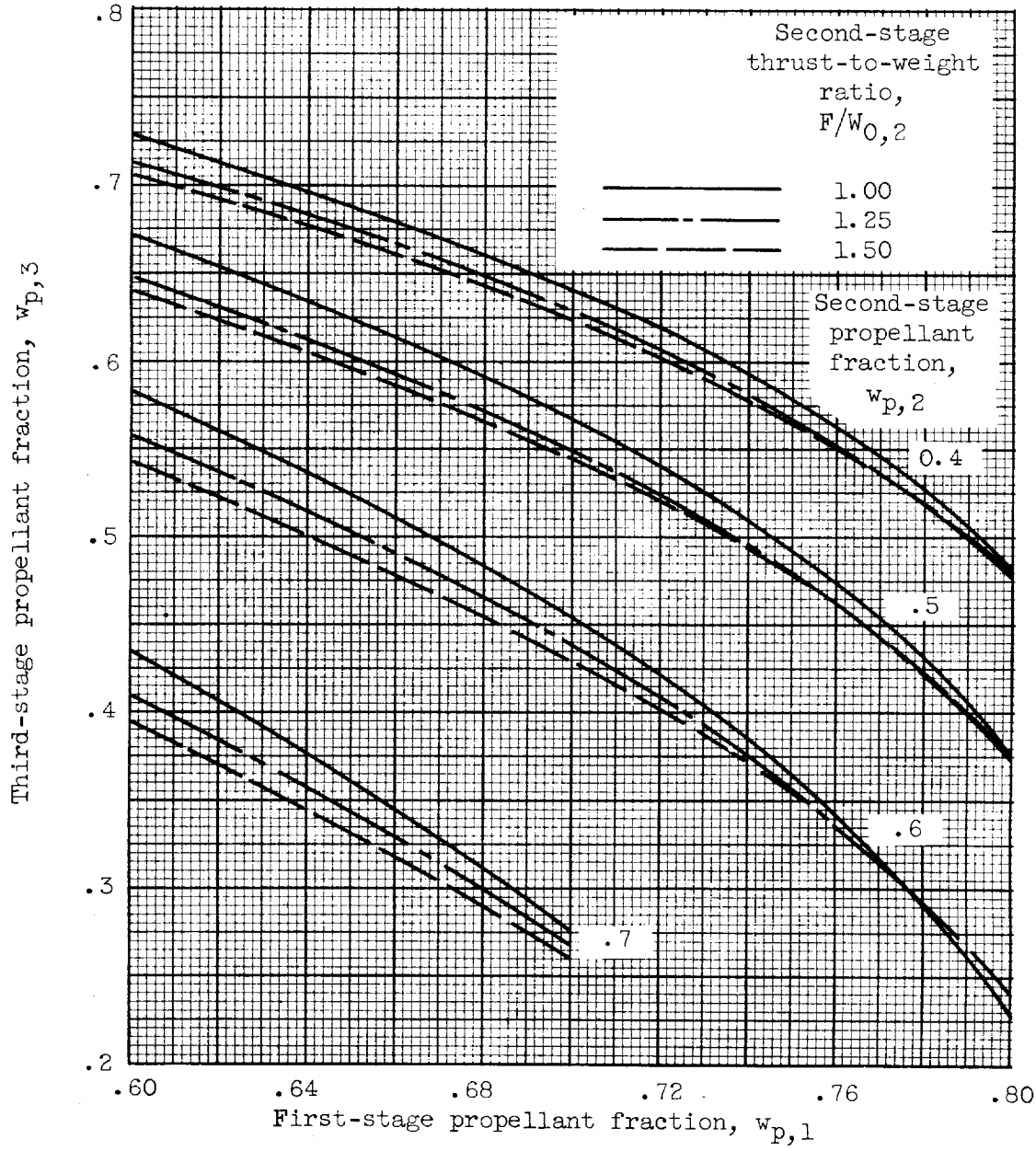

(b) $F/W_{0,1} = 1.20$; $F/W_{0,3} = 1.00$.

Figure 9. - Continued. Three-stage propellant-loading chart. 150-Nautical-mile orbit; $I_1 = 292$ (av.); $I_2 = 425$; $I_3 = 425$.

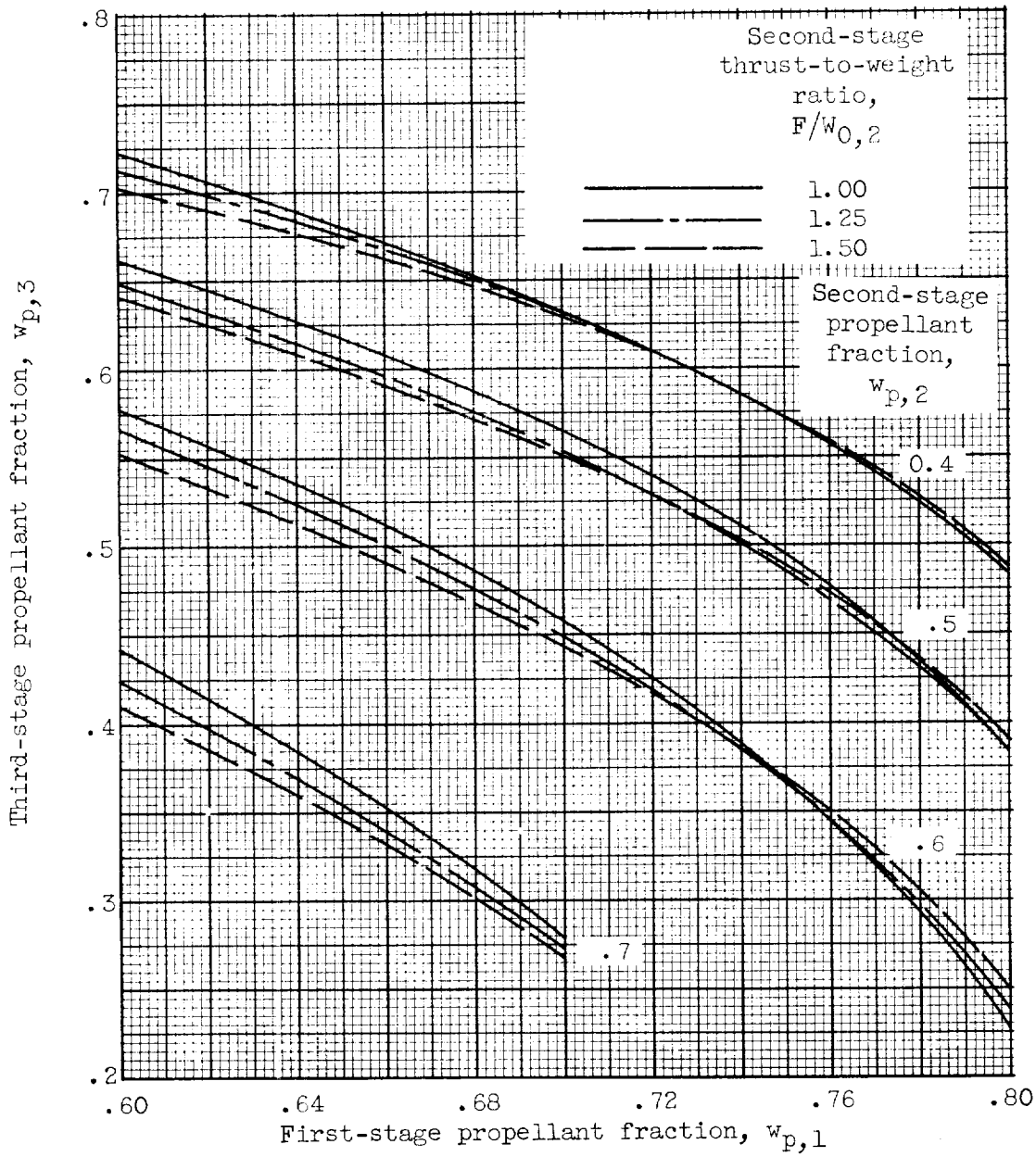

(c) $F/W_{0,1} = 1.20$; $F/W_{0,3} = 1.50$.

Figure 9. - Continued. Three-stage propellant-loading chart. 150-Nautical-mile orbit; $I_1 = 292$ (av.); $I_2 = 425$; $I_3 = 425$.

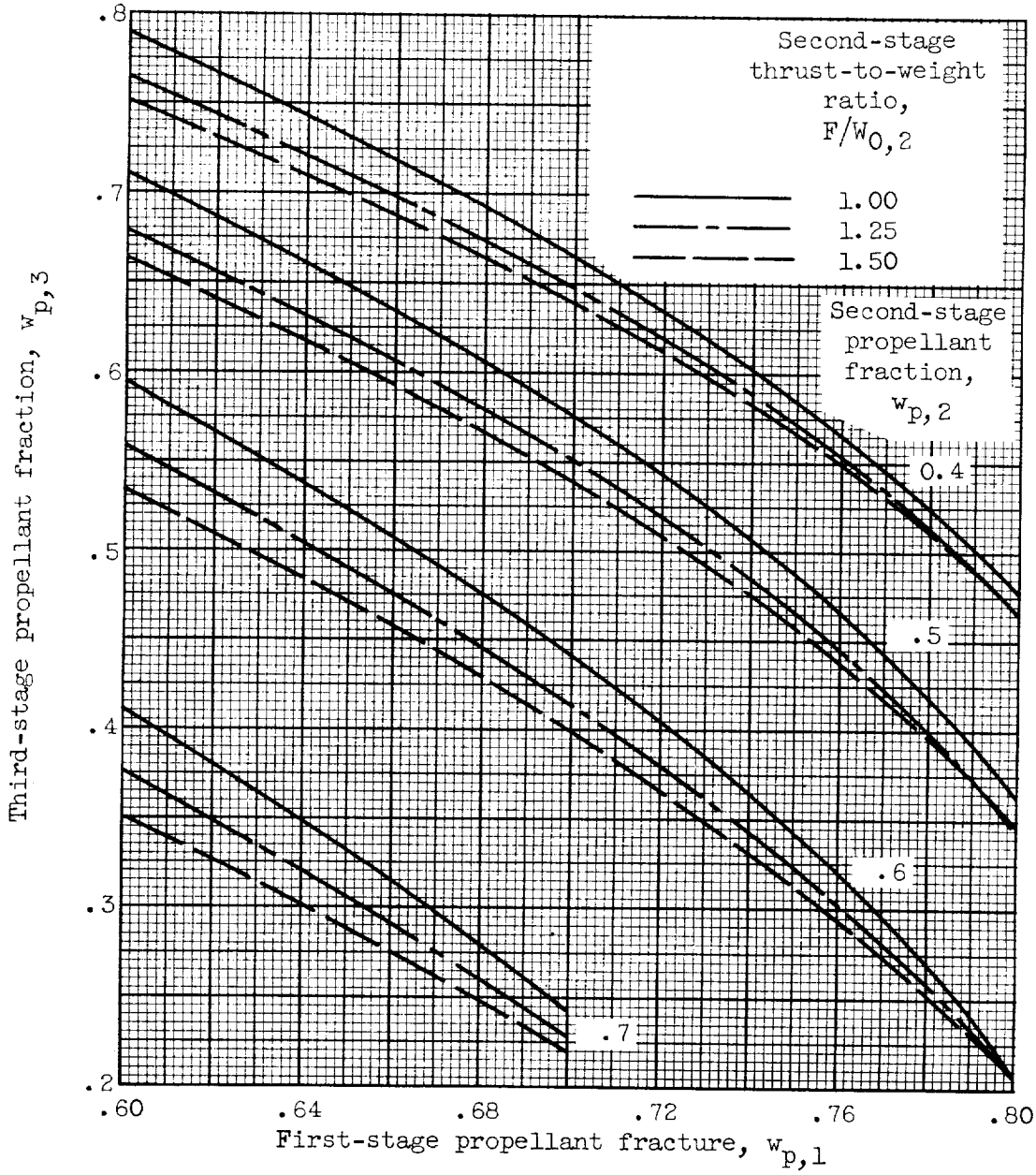

(d) $F/W_{0,1} = 1.30$; $F/W_{0,3} = 0.50$.

Figure 9. - Continued. Three-stage propellant-loading chart. 150-Nautical-mile orbit; $I_1 = 292$ (av.); $I_2 = 425$; $I_3 = 425$.

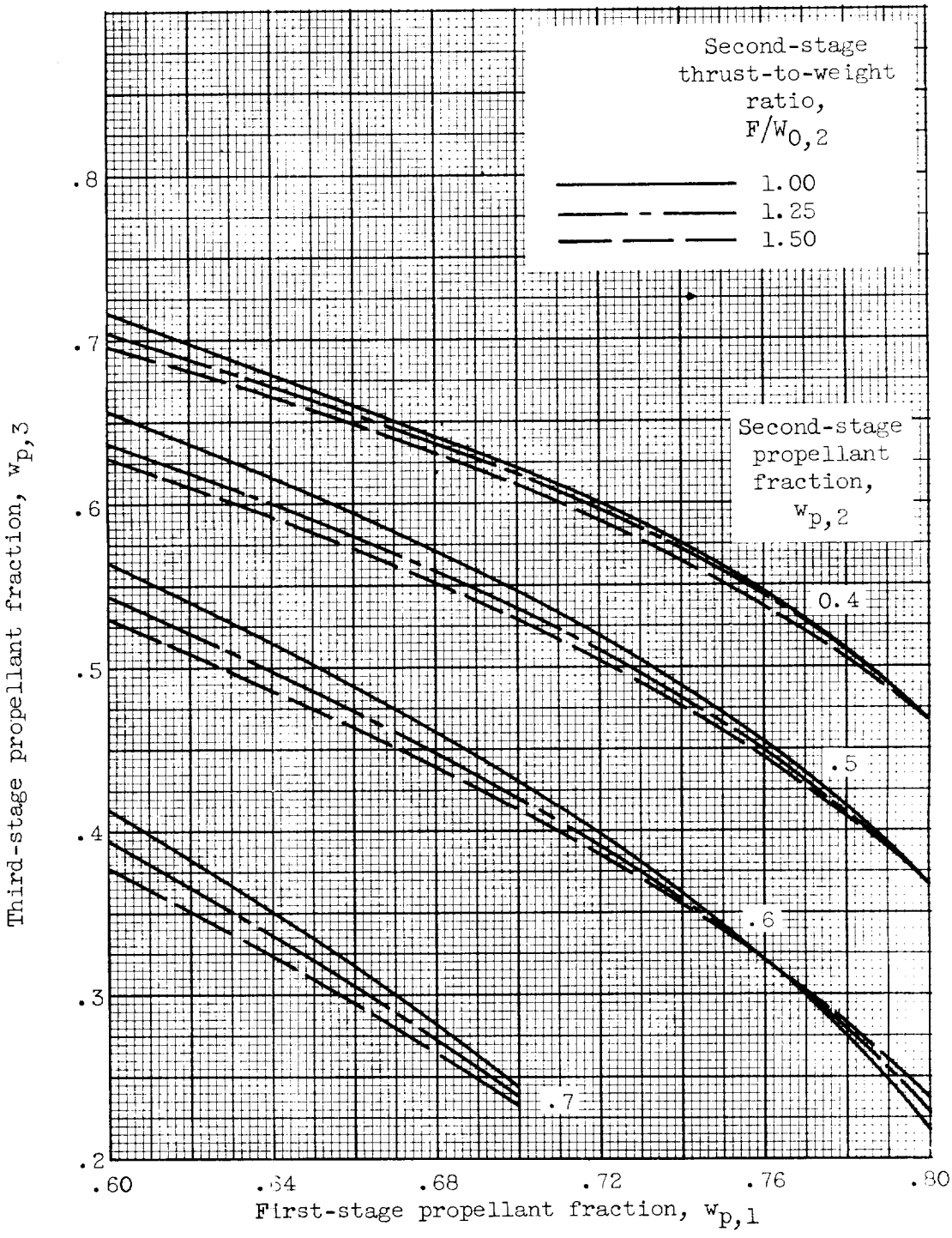

(e) $F/W_{0,1} = 1.30$; $F/W_{0,3} = 1.00$.

Figure 9. - Continued. Three-stage propellant-loading chart. 150-Nautical-mile orbit; $I_1 = 292$ (av.); $I_2 = 425$; $I_3 = 425$.

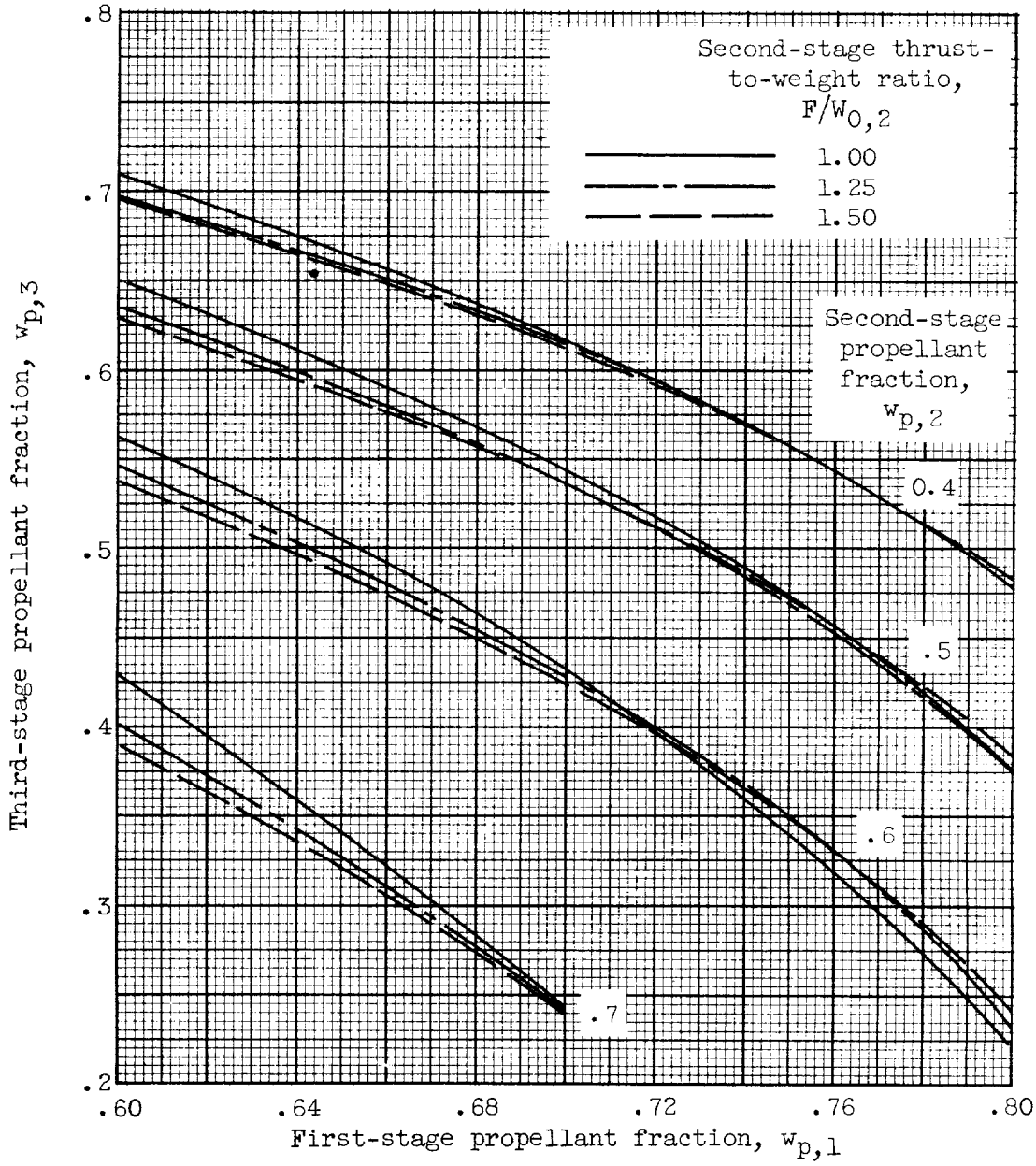

(f) $F/W_{0,1} = 1.30$; $F/W_{0,3} = 1.50$.

Figure 9. - Continued. Three-stage propellant-loading chart. 150-Nautical-mile orbit; $I_1 = 292$ (av.); $I_2 = 425$; $I_3 = 425$.

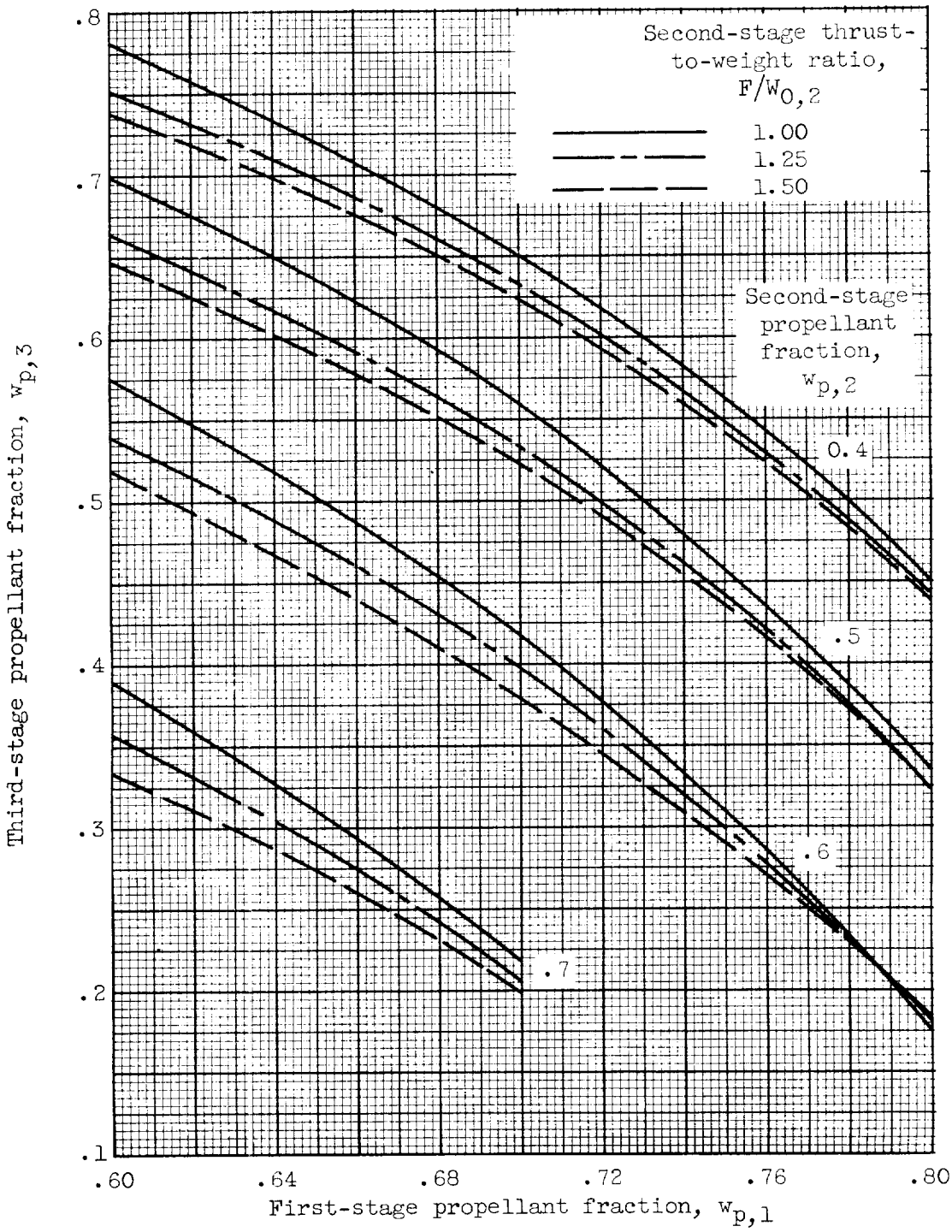

(g) $F/W_{0,1} = 1.40$; $F/W_{0,3} = 0.50$.

Figure 9. - Continued. Three-stage propellant-loading chart. 150-Nautical-mile orbit; $I_1 = 292$ (av.); $I_2 = 425$; $I_3 = 425$.

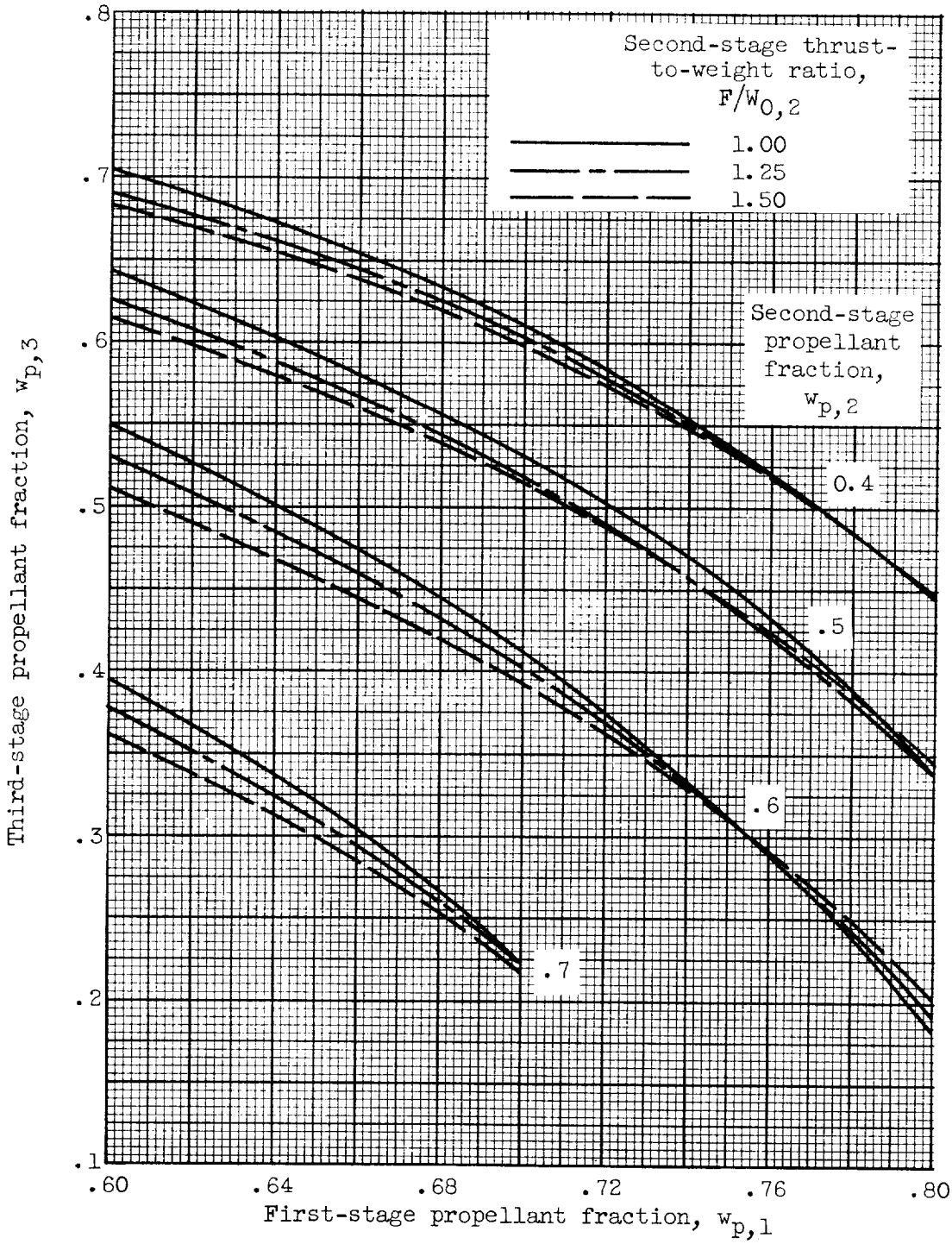

(h) $F/W_{0,1} = 1.40$; $F/W_{0,3} = 1.00$.

Figure 9. - Continued. Three-stage propellant-loading chart. 150-Nautical-mile orbit; $I_1 = 292$ (av.); $I_2 = 425$; $I_3 = 425$.

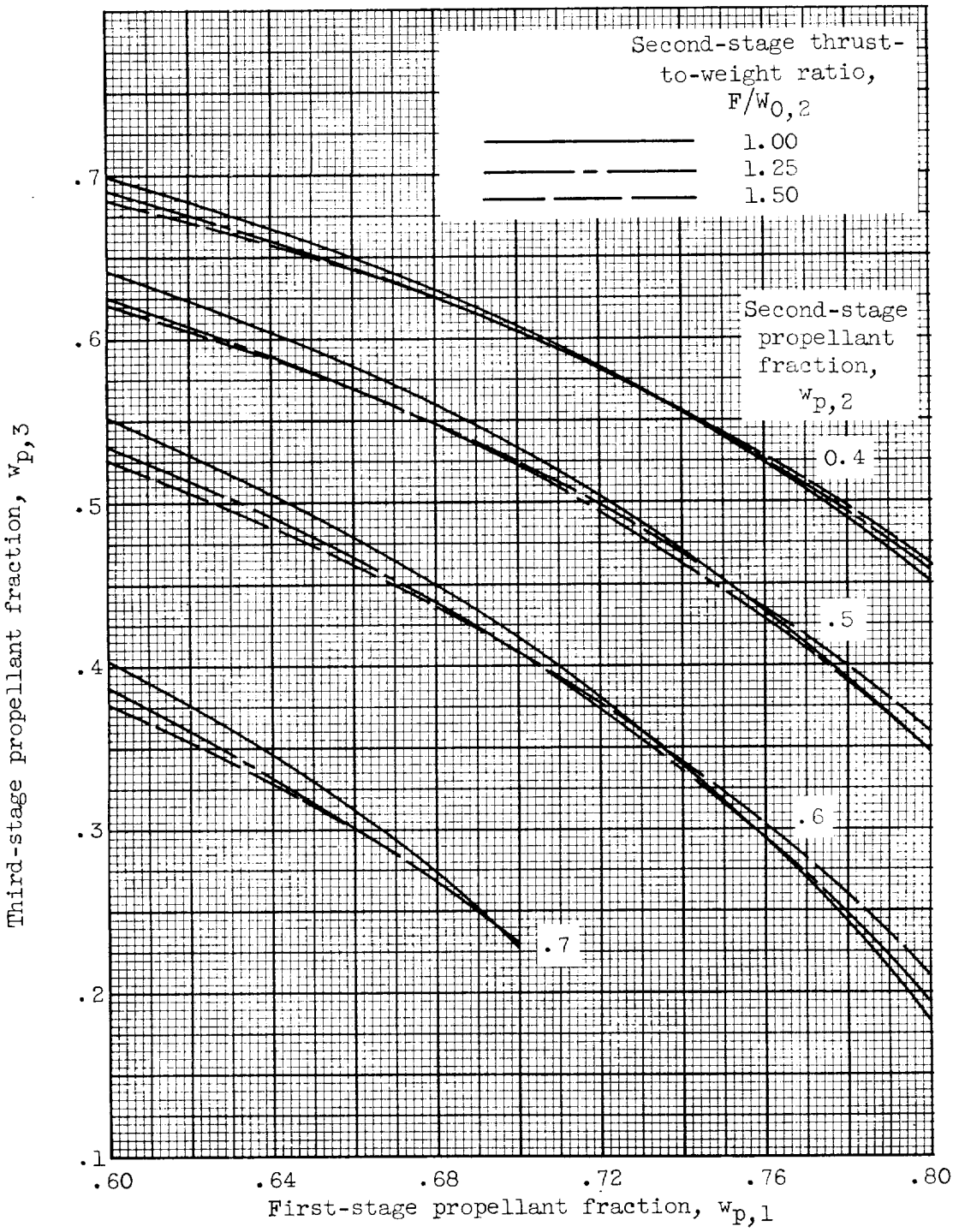

(i) $F/W_{0,1} = 1.40$; $F/W_{0,3} = 1.50$.

Figure 9. - Concluded. Three-stage propellant-loading chart. 150-Nautical-mile orbit; $I_1 = 292$ (av.); $I_2 = 425$; $I_3 = 425$.

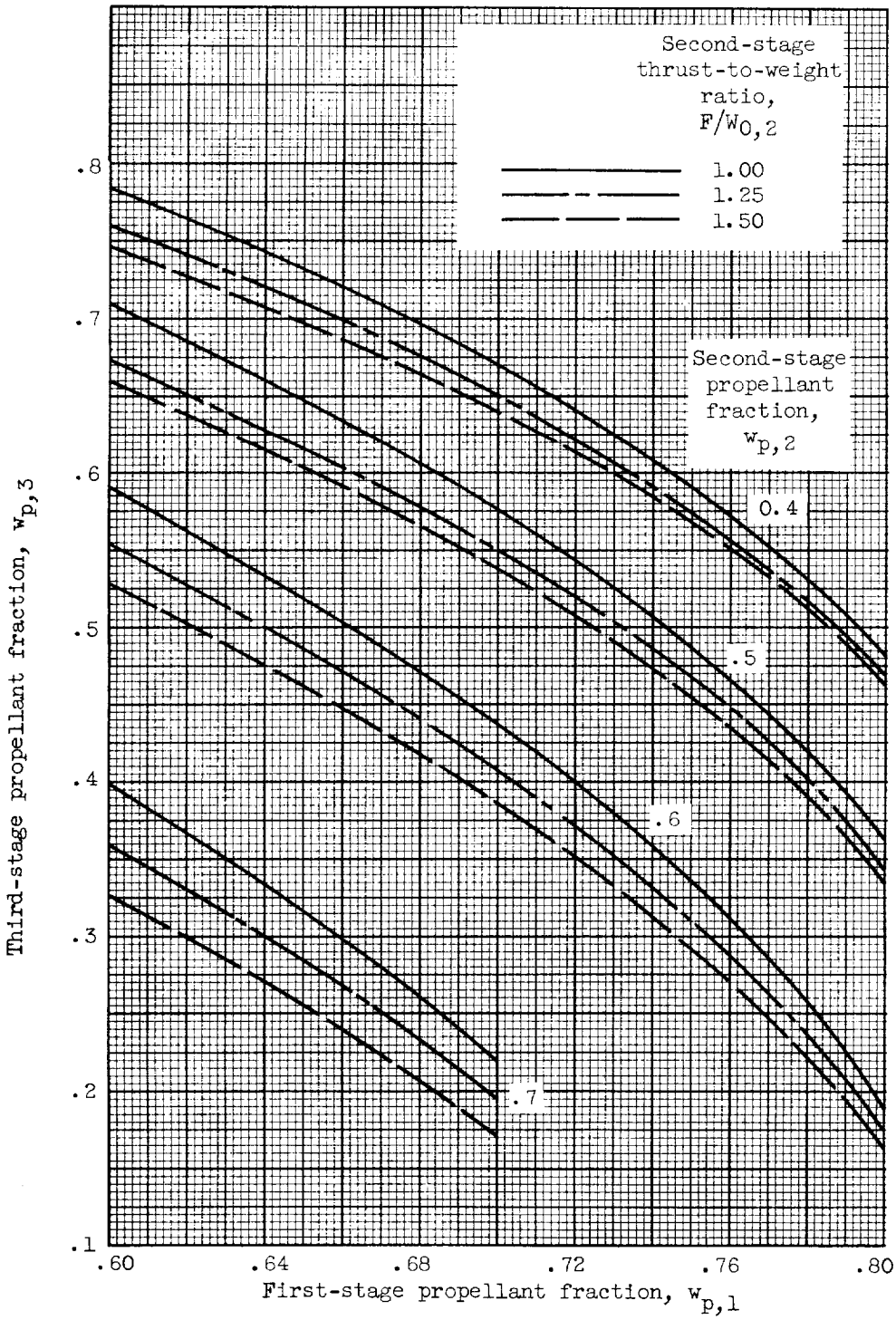

(a) $F/W_{0,1} = 1.20$; $F/W_{0,3} = 0.50$.

Figure 10. - Three-stage propellant-loading chart. 75-Nautical-mile orbit; $I_1 = 292$ (av.); $I_2 = 425$; $I_3 = 425$.

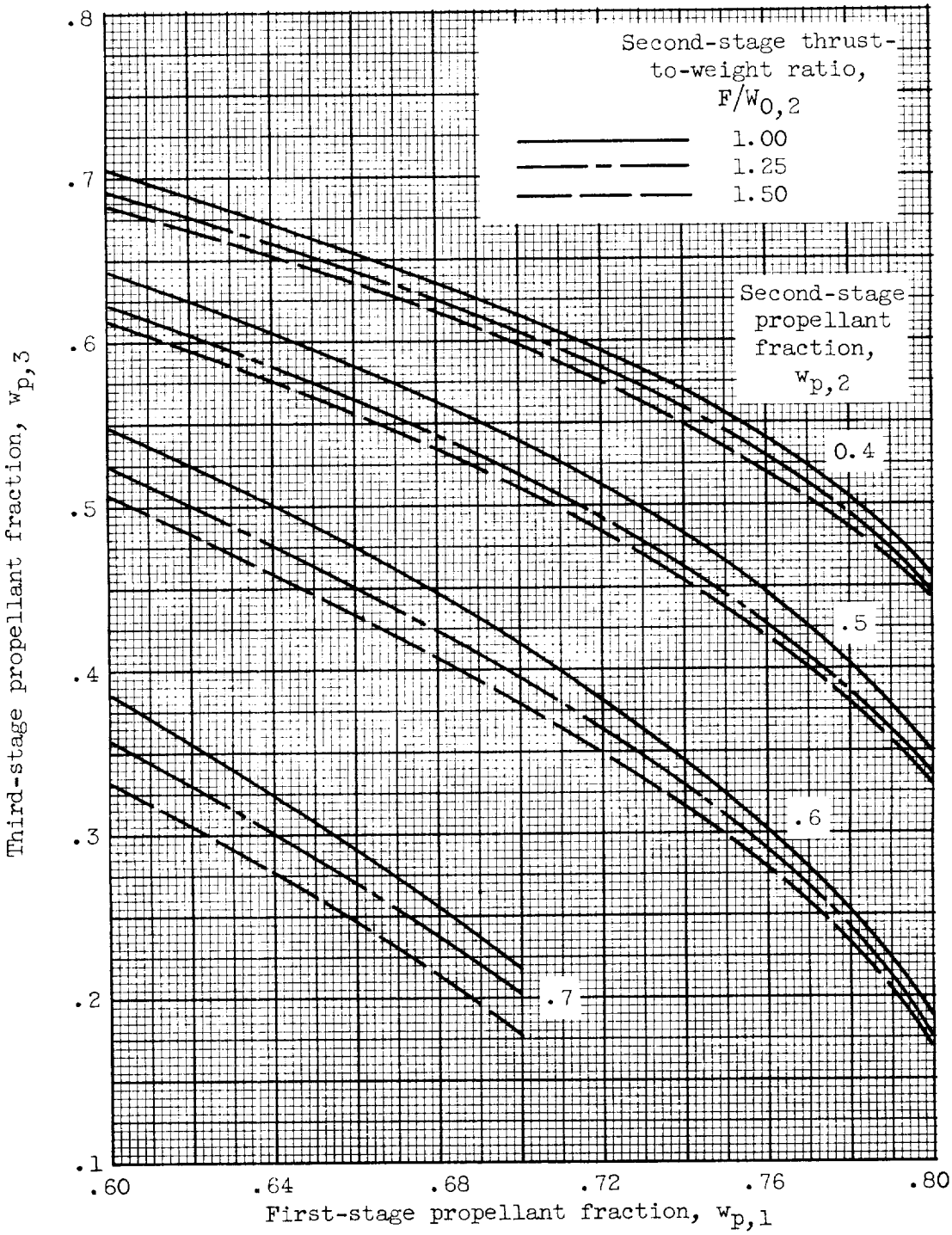

(b) $F/W_{0,1} = 1.20$; $F/W_{0,3} = 1.00$.

Figure 10. - Continued. Three-stage propellant-loading chart. 75-Nautical-mile orbit; $I_1 = 292$ (av.); $I_2 = 425$; $I_3 = 425$.

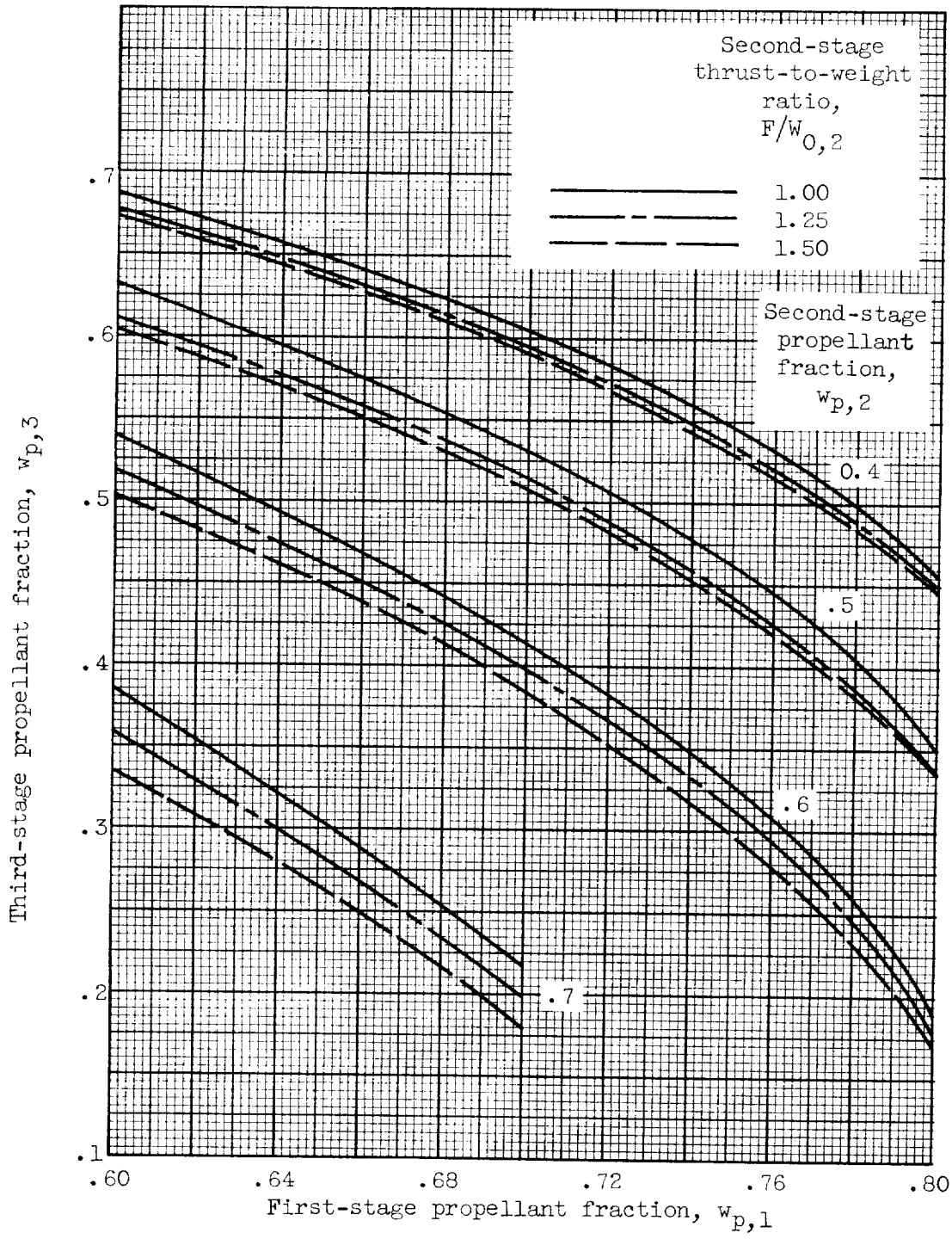

(c) $F/W_{0,1} = 1.20$; $F/W_{0,3} = 1.50$.

Figure 10. - Continued. Three-stage propellant-loading chart. 75-Nautical-mile orbit; $I_1 = 292$ (av.); $I_2 = 425$; $I_3 = 425$.

E-799

CE-10 back

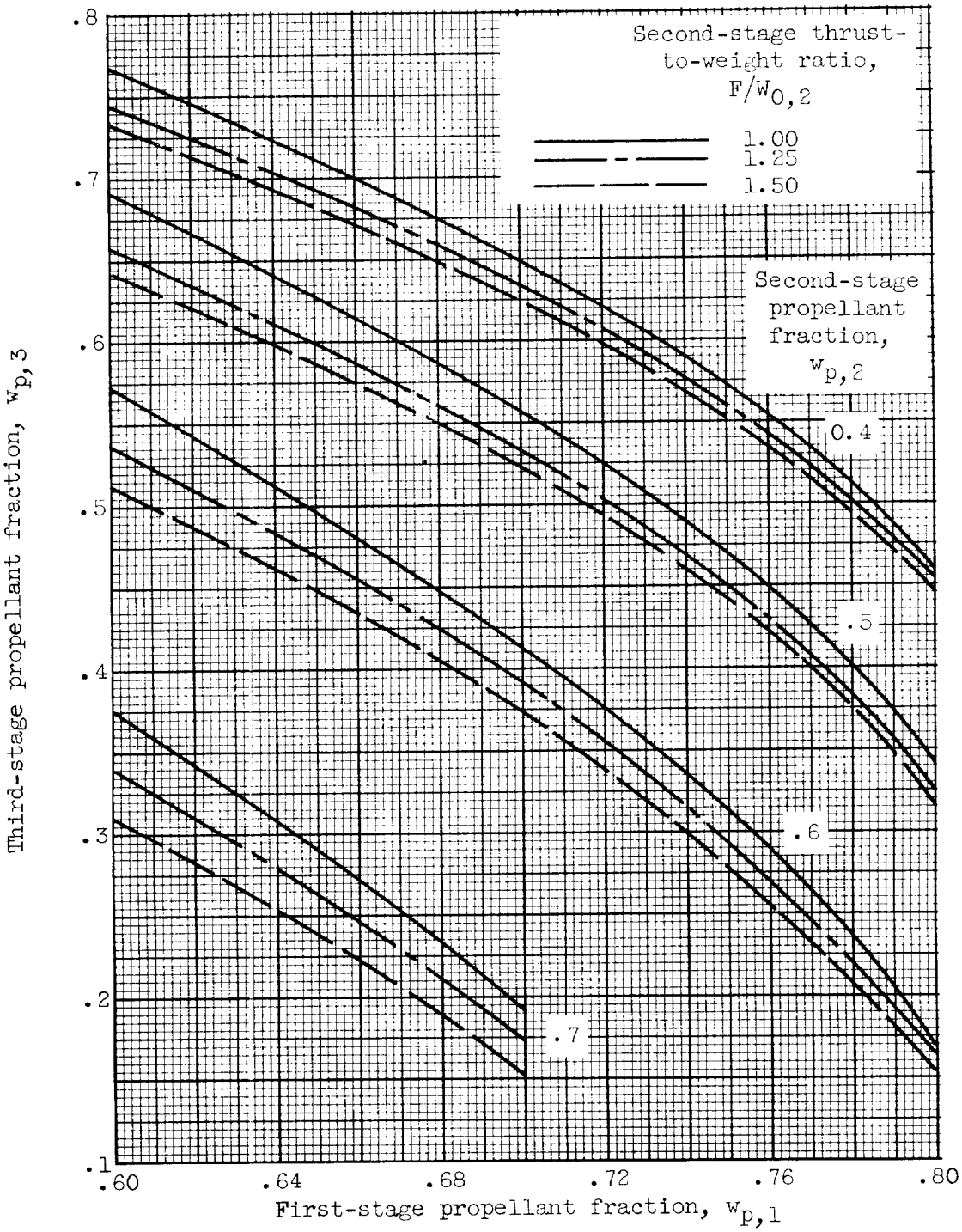

(d) $F/W_{0,1} = 1.30$; $F/W_{0,3} = 0.50$.

Figure 10. - Continued. Three-stage propellant-loading chart. 75-Nautical-mile orbit; $I_1 = 292$ (av.); $I_2 = 425$; $I_3 = 425$.

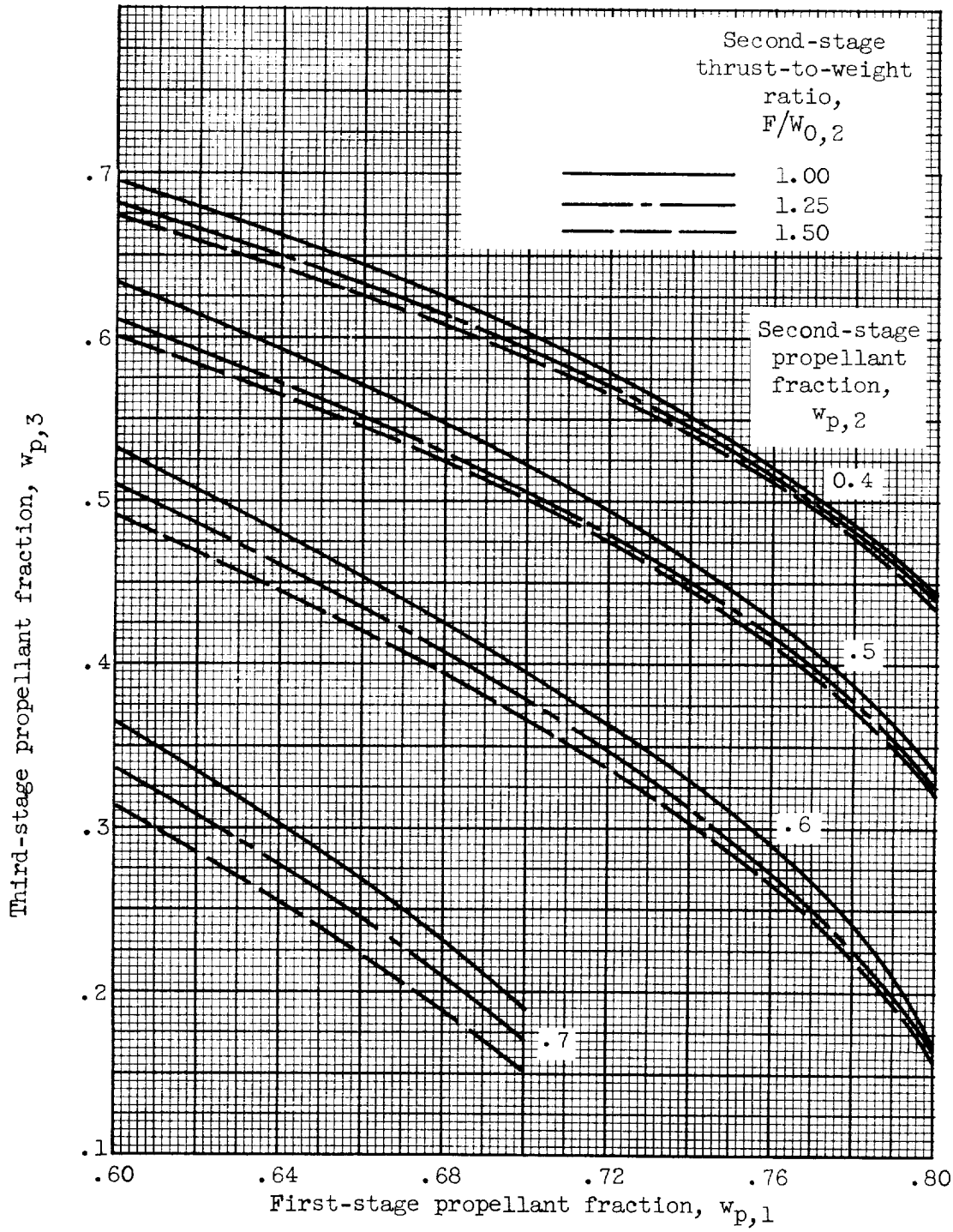

(e) $F/W_{0,1} = 1.30$; $F/W_{0,3} = 1.00$.

Figure 10. - Continued. Three-stage propellant-loading chart. 75-Nautical-mile orbit; $I_1 = 292$ (av.); $I_2 = 425$; $I_3 = 425$.

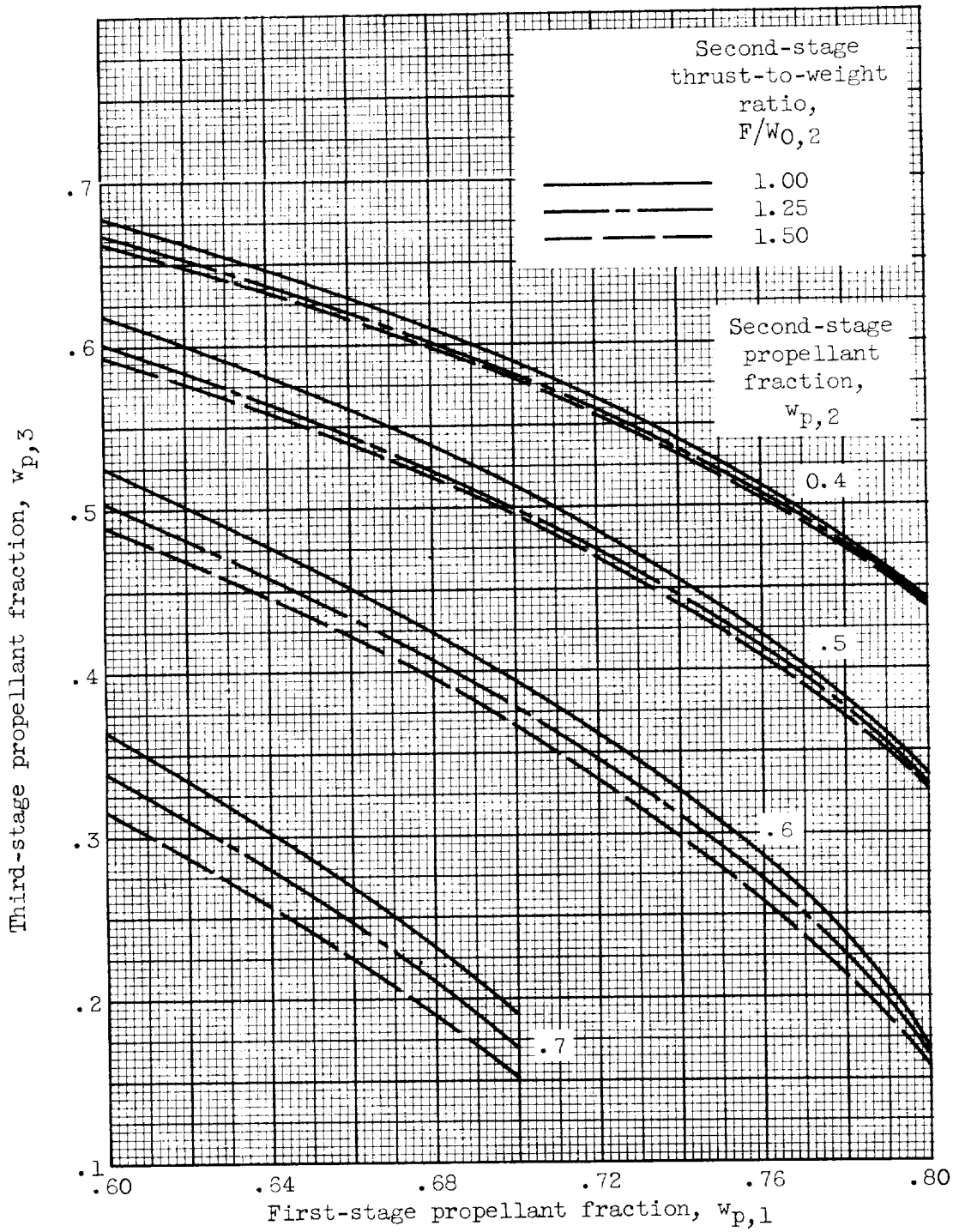

(f) $F/W_{0,1} = 1.30$; $F/W_{0,3} = 1.50$.

Figure 10. - Continued. Three-stage propellant-loading chart. 75-Nautical-mile orbit; $I_1 = 292$ (av.); $I_2 = 425$; $I_3 = 425$.

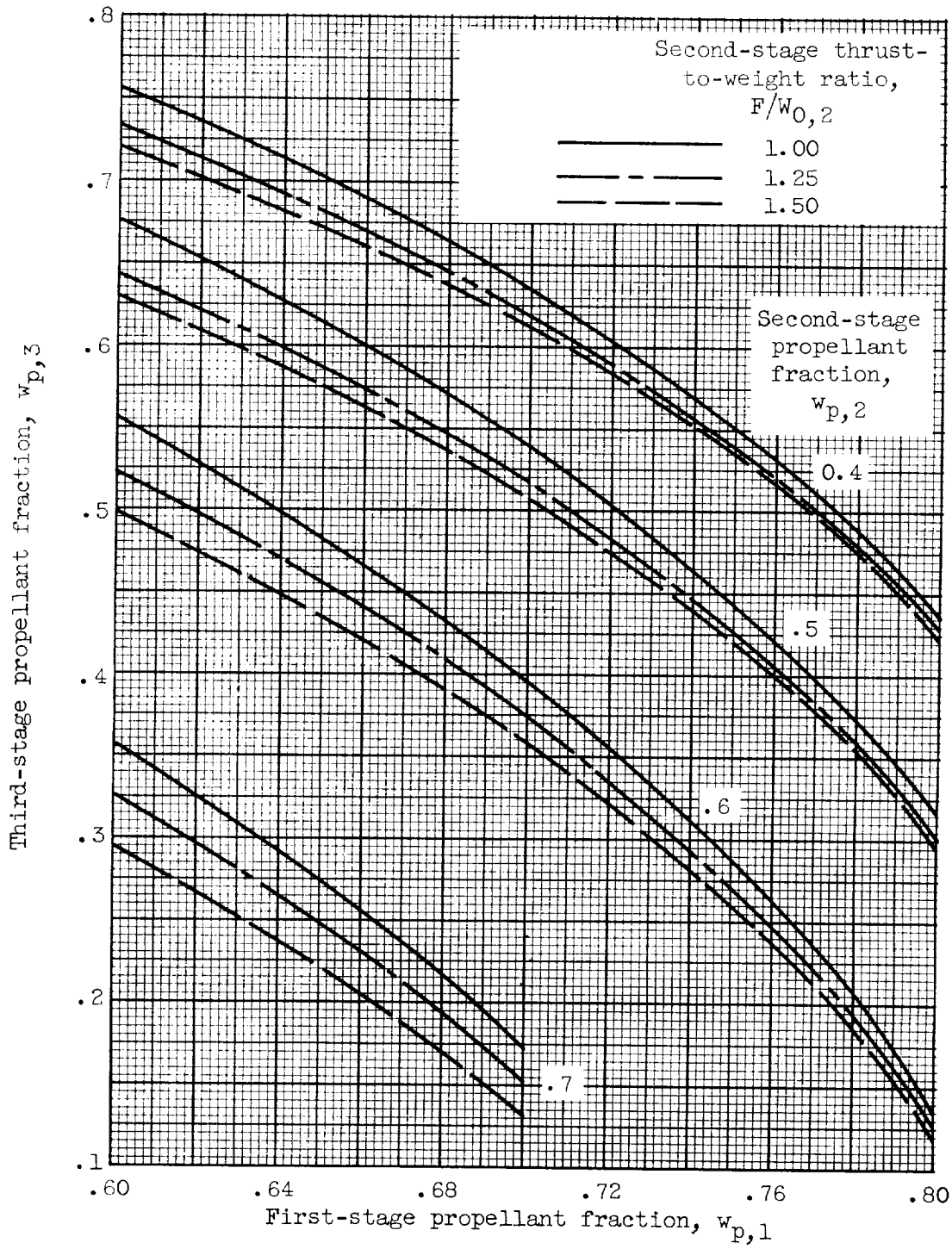

(g) $F/W_{0,1} = 1.40$; $F/W_{0,3} = 0.50$.

Figure 10. - Continued. Three-stage propellant-loading chart. 75-Nautical-mile orbit; $I_1 = 292$ (av.); $I_2 = 425$; $I_3 = 425$.

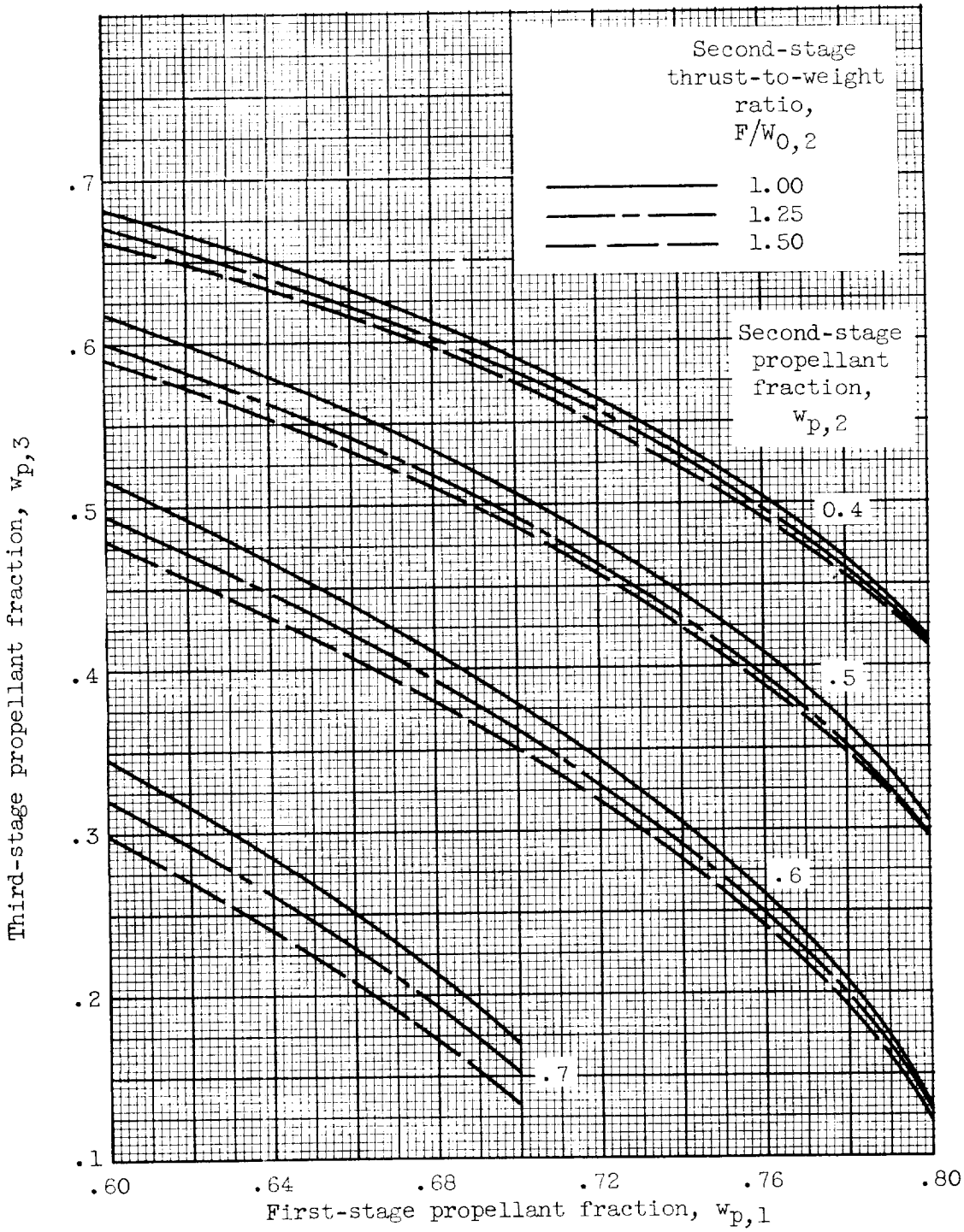

(h) $F/W_{0,1} = 1.40$; $F/W_{0,3} = 1.00$.

Figure 10. - Continued. Three-stage propellant-loading chart. 75-Nautical-mile orbit; $I_1 = 292$ (av.); $I_2 = 425$; $I_3 = 425$.

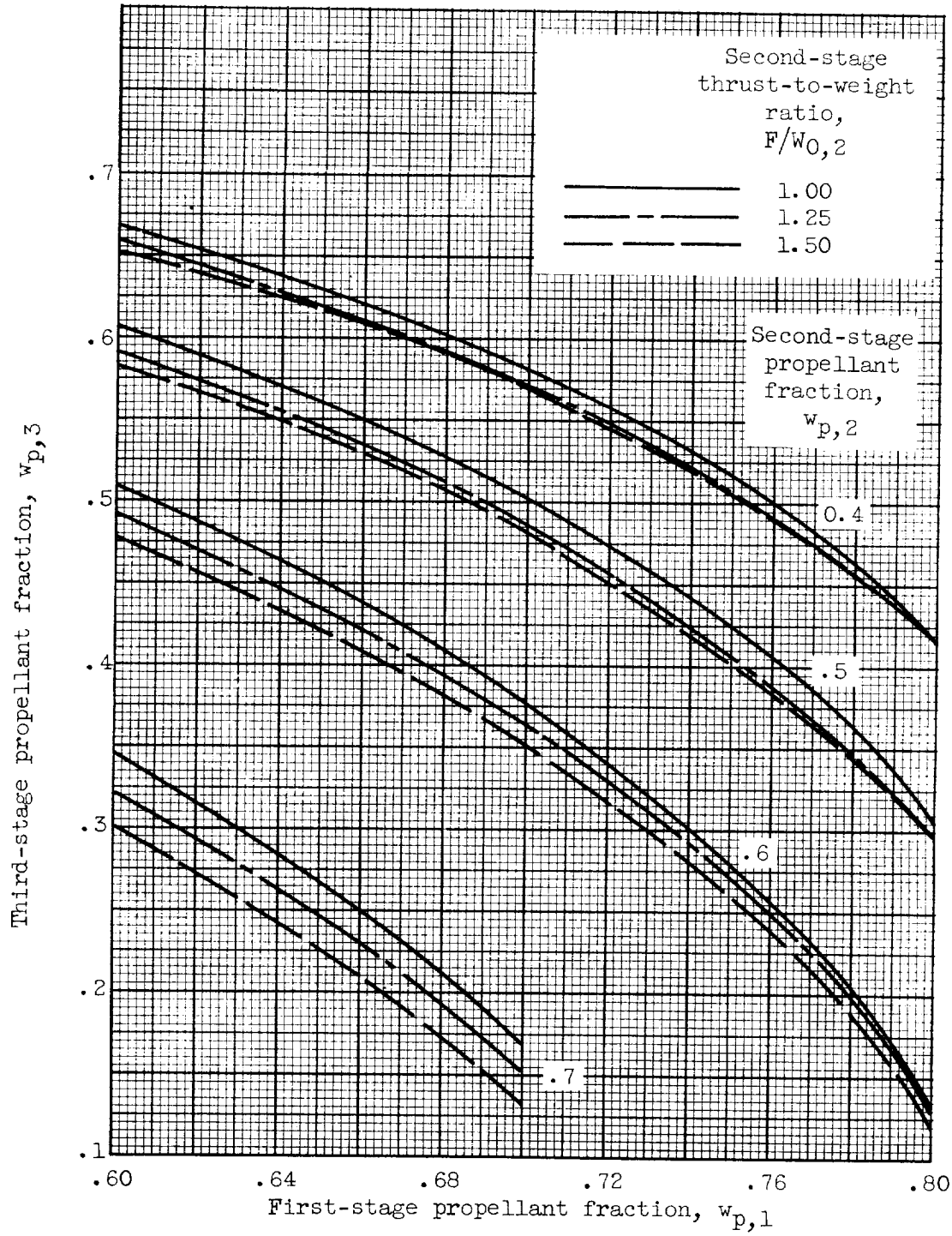

(i) $F/W_{0,1} = 1.40$; $F/W_{0,3} = 1.50$.

Figure 10. - Concluded. Three-stage propellant-loading chart. 75-Nautical-mile orbit; $I_1 = 292$ (av.); $I_2 = 425$; $I_3 = 425$.

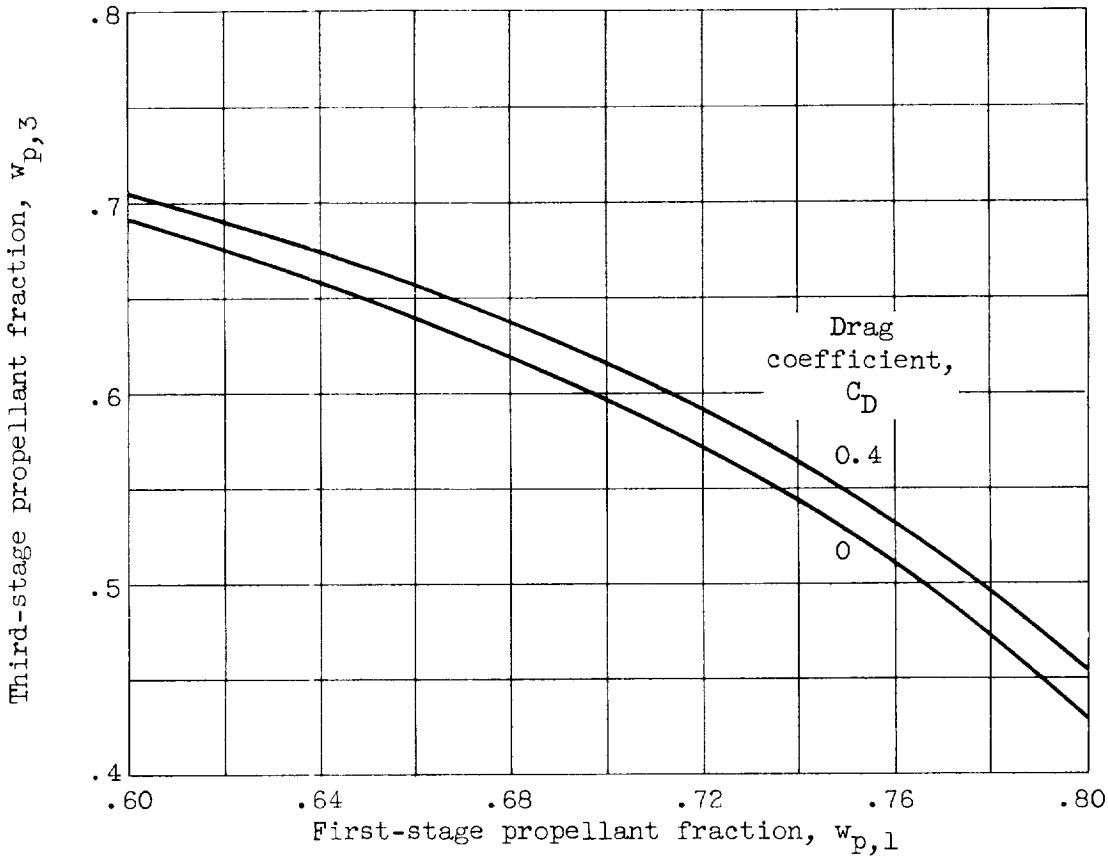

Figure 11. - Effect of drag on third-stage propellant fraction for various first-stage propellant fractions. $w_{p,2} = 0.50$; $F/W_{0,1} = 1.4$; $F/W_{0,2} = 1.0$; $F/W_{0,3} = 1.0$; $I_1 = 292$ (av.); $I_2 = 305$; $I_3 = 425$; 150-nautical-mile orbit.

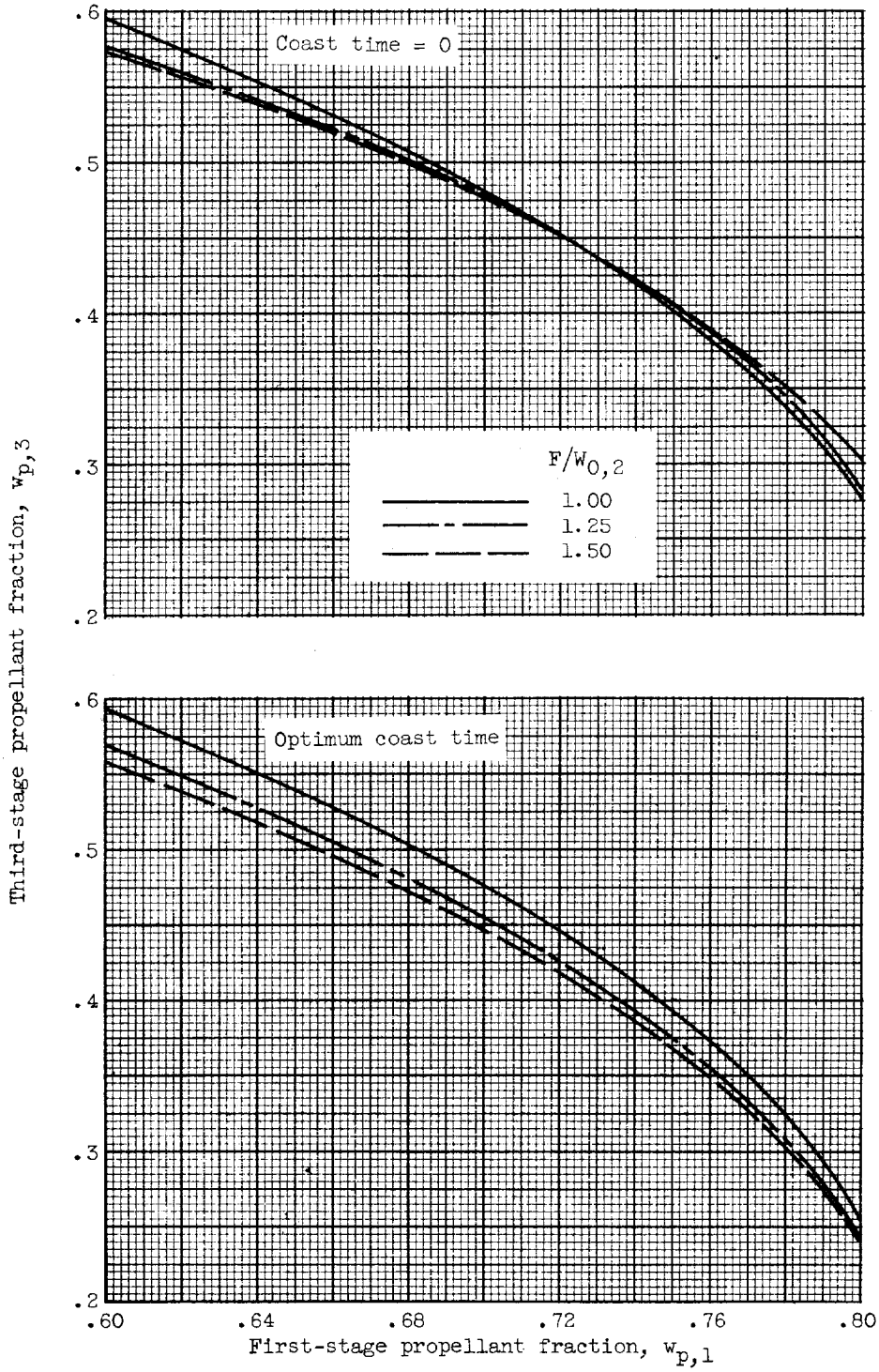

Figure 12. - Comparison of continuous-burning ascent to 150-nautical-mile orbit with use of optimum coast period between second and third stages. $F/W_{0,1} = 1.20$; $F/W_{0,3} = 1.50$; $w_{p,2} = 0.70$; $I_1 = 292$ (av.); $I_2 = 305$; $I_3 = 425$.

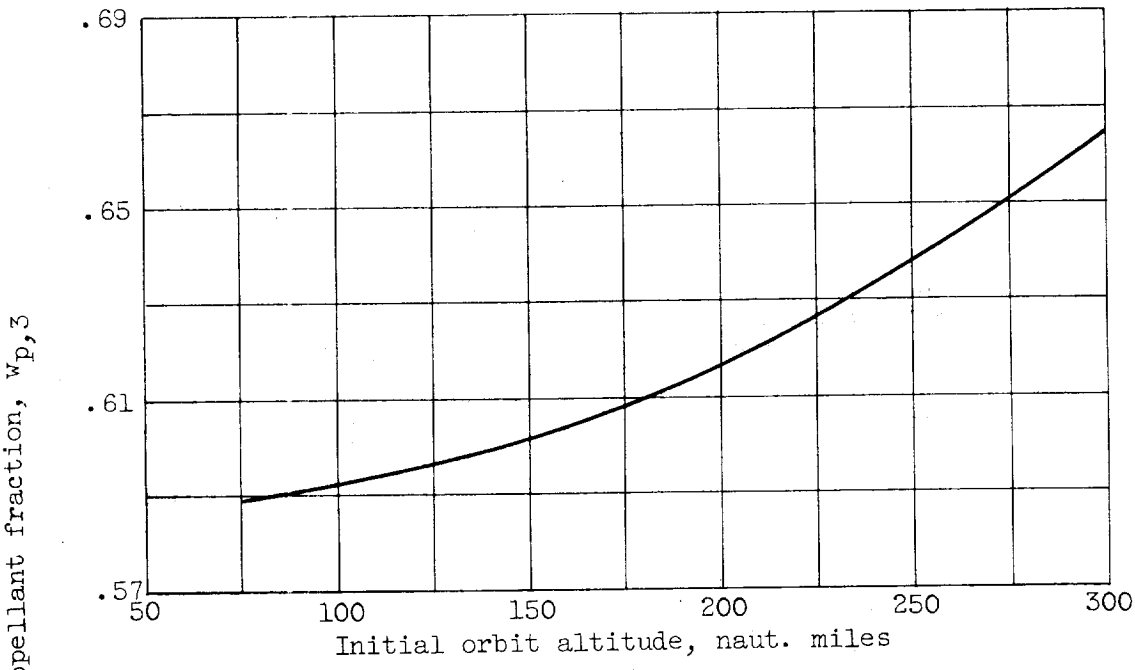

(a) Transfer to 500-nautical-mile circular orbit.

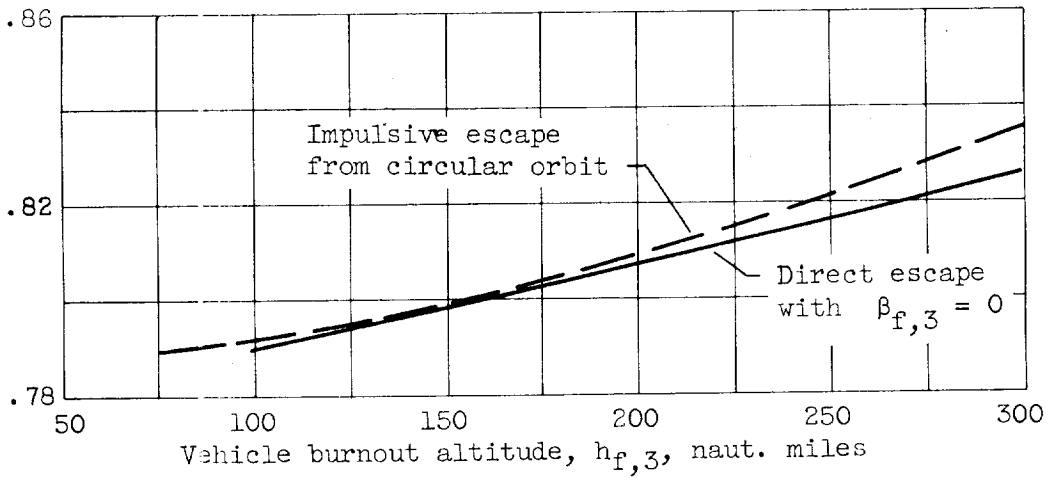

(b) Escape missions.

Figure 13. - Effects of impulsive thrust assumption and initial orbit altitude. $F/W_{0,1} = 1.40$; $F/W_{0,2} = 1.00$; $F/W_{0,3} = 1.00$; $w_{p,1} = 0.60$; $w_{p,2} = 0.70$; $I_1 = 292$ (av.); $I_2 = 305$; $I_3 = 425$.

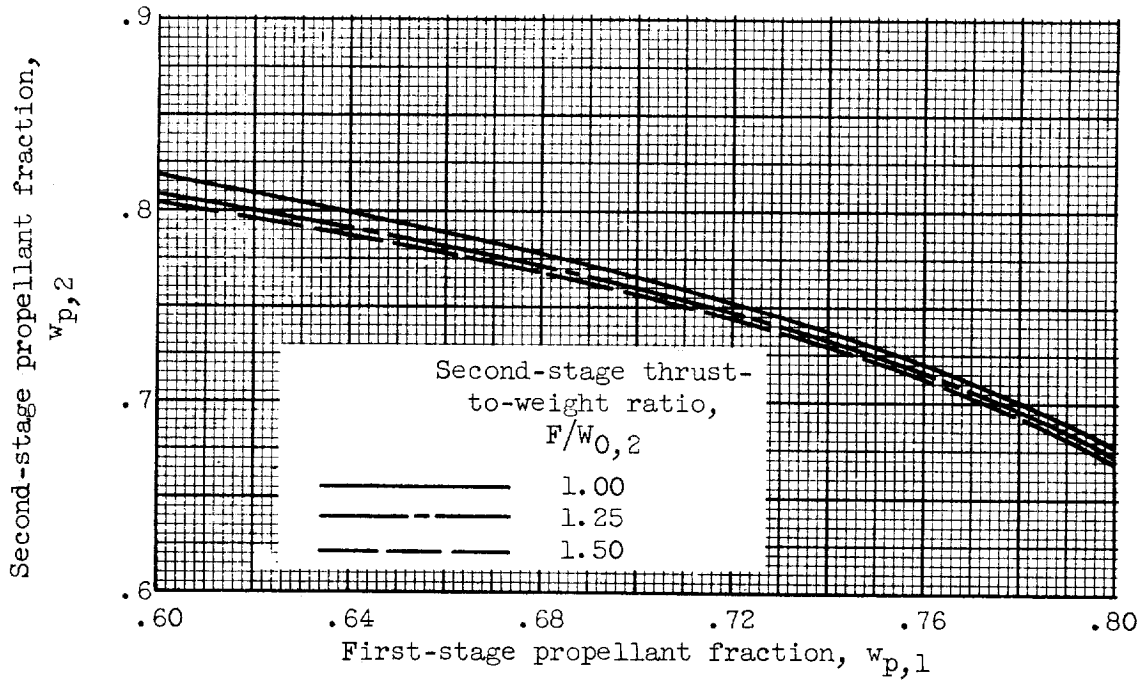

(a) $F/W_{0,1} = 1.20$.

Figure 14. - Two-stage propellant-loading chart. 75-Nautical-mile orbit; $I_1 = 292$ (av.); $I_2 = 425$.

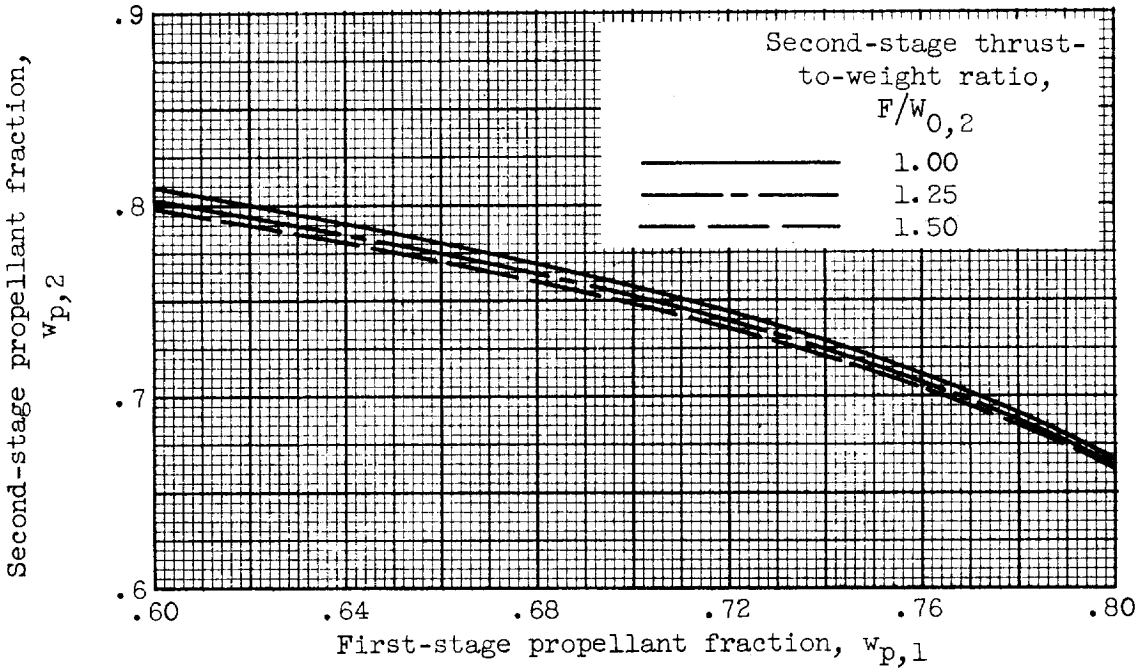

(b) $F/W_{0,1} = 1.30$.

Figure 14. - Continued. Two-stage propellant-loading chart. 75-Nautical-mile orbit; $I_1 = 292$ (av.); $I_2 = 425$.

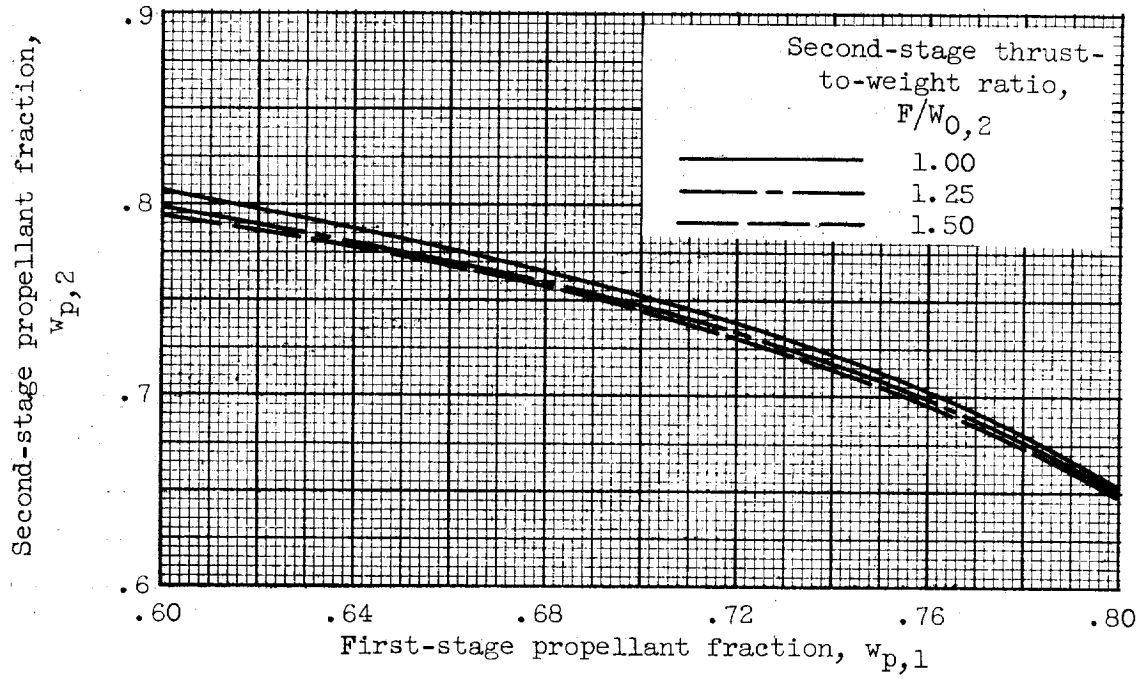

(c) $F/W_{0,1} = 1.40$.

Figure 14. - Concluded. Two-stage propellant-loading chart. 75-Nautical-mile orbit; $I_1 = 292$ (av.); $I_2 = 425$.

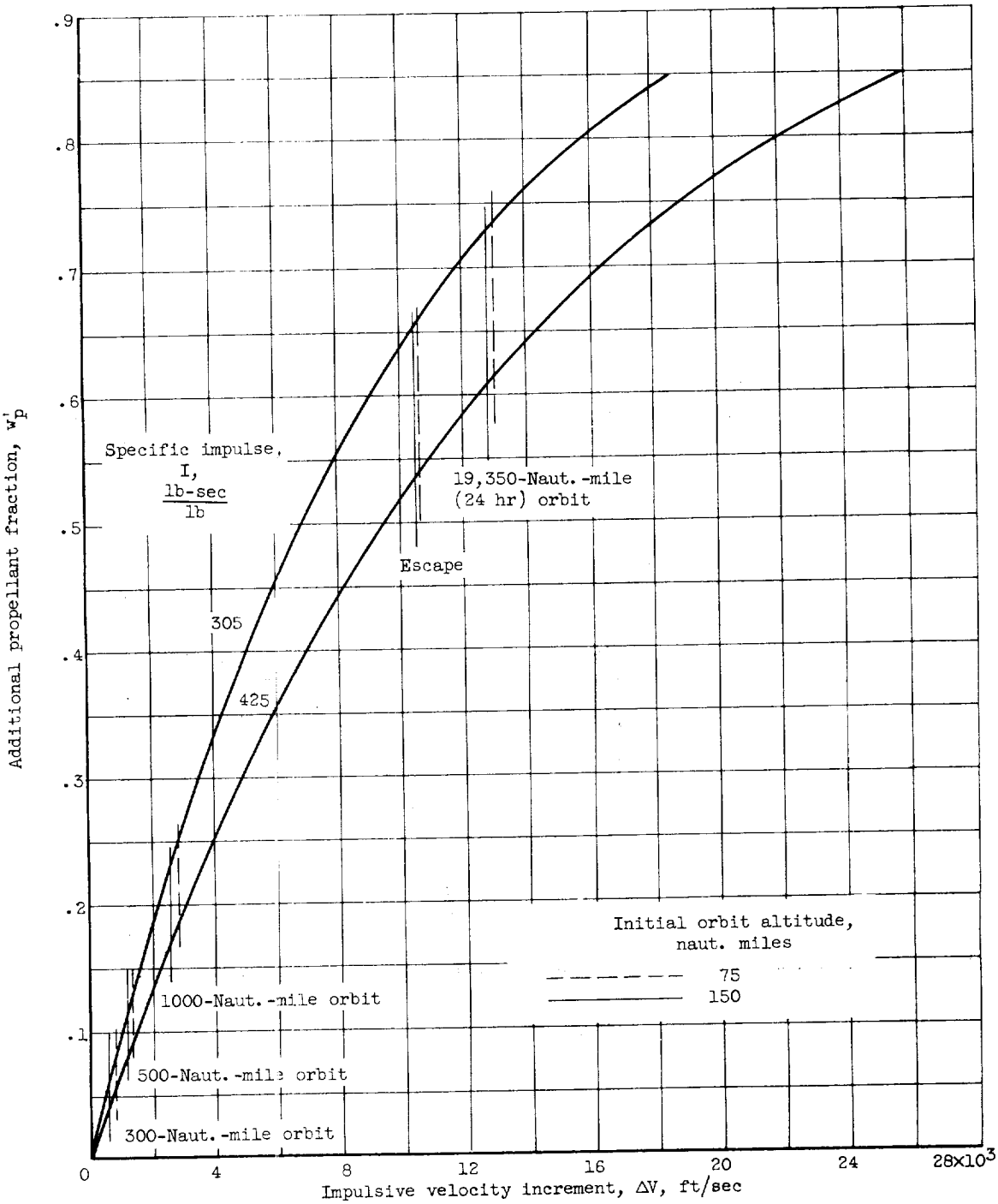

Figure 15. - Energy addition beyond orbit; nonrotating earth.

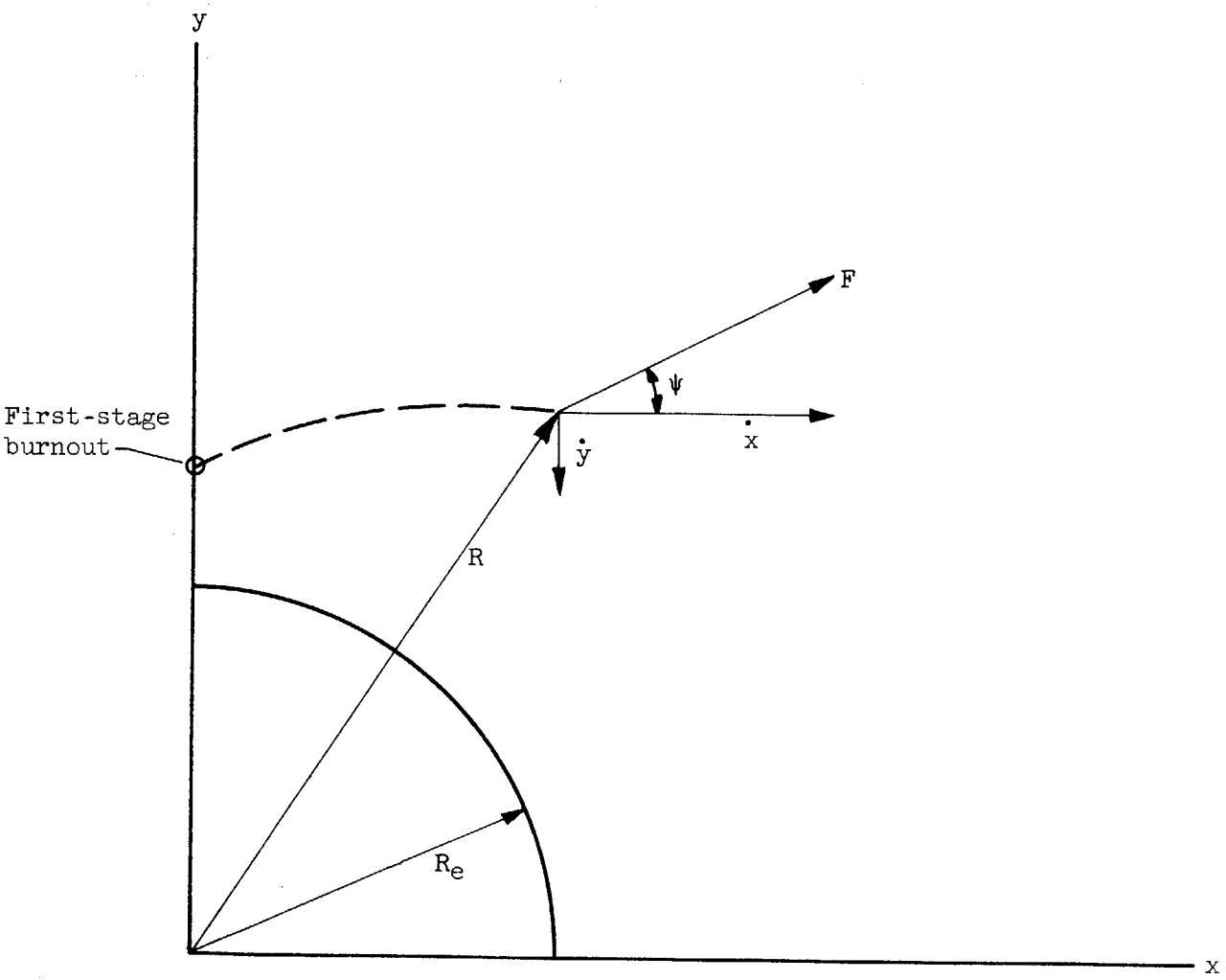

Figure 16. - Earth-centered, nonrotating (inertial) coordinate system.

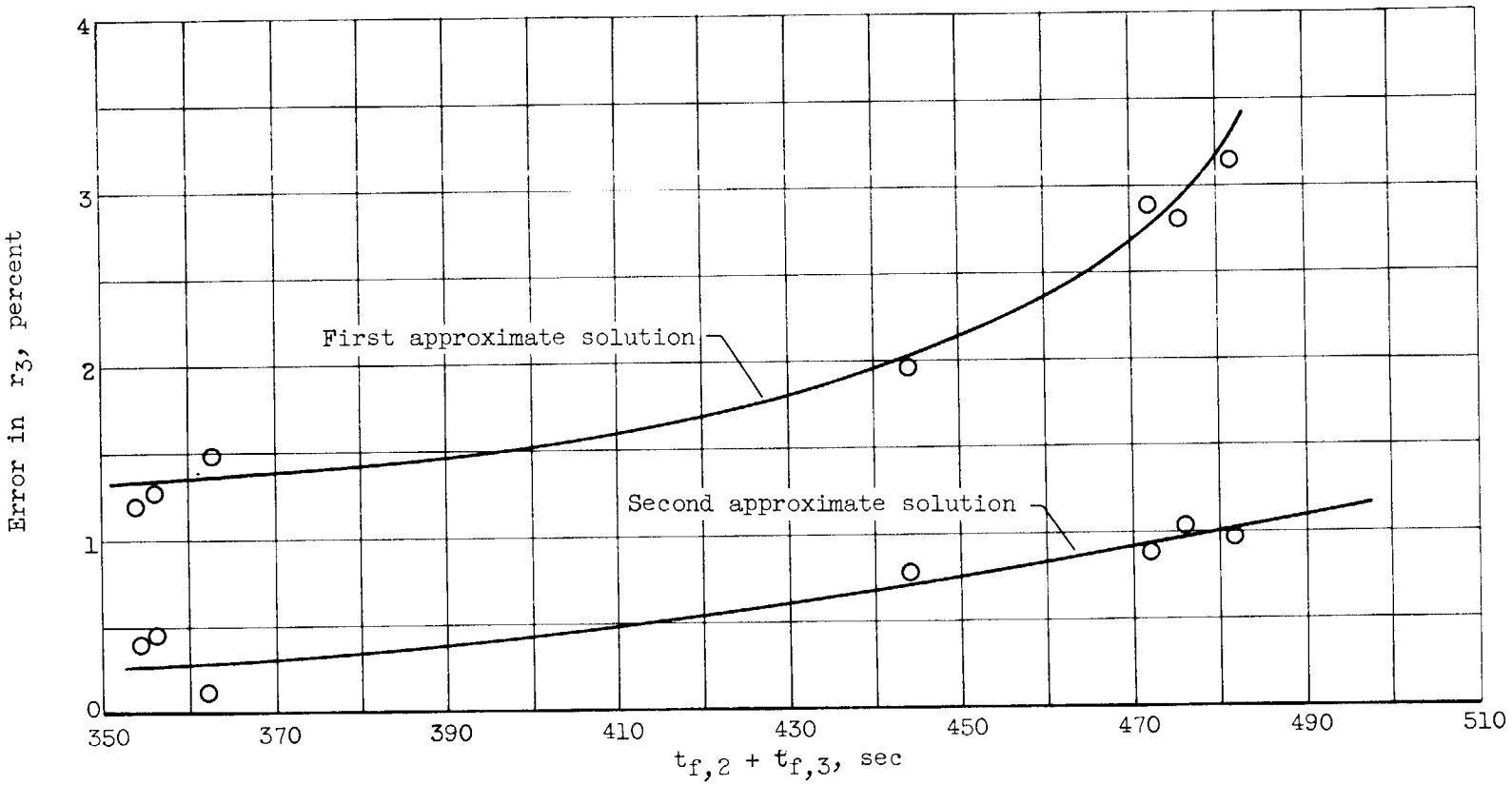

Figure 17. - Variation of third-stage weight-ratio error with total upper-stage burning time for satellite boosting vehicles. 150-Nautical-mile orbit.

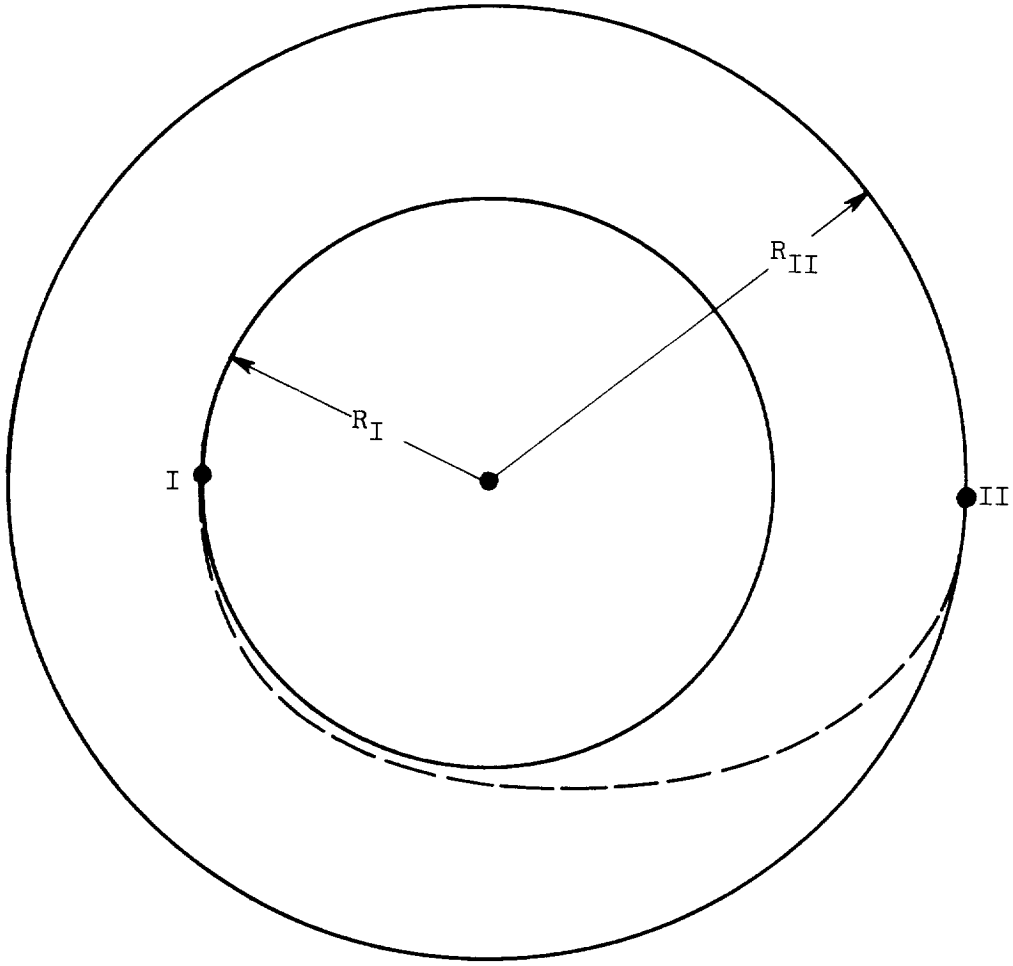

Figure 18. - Hohmann transfer.